Stellingen behorende bij het proefschrift:
An Instrument for Positron Micro-analysis
(Een Instrument voor Positronen Micro-analyse)

1 Het optimale aantal remoderatiestappen voor de helderheidsverbetering van een
   positronenbundel wordt bepaald door de kwaliteit van de probevormende lens van het
   analyse-instrument.
   Dit proefschrift hoofdstuk 4

2 Helderheidsverhoging van de positronenbundel door middel van remoderatie ten
   behoeve van analyse op micrometerschaal is altijd noodzakelijk voor het verkrijgen
   van een zo groot mogelijke stroom, wanneer een positronenbron gebruikt wordt die
   werkt op basis van een radioactief vervalproces.

3 De helderheid van alkali-ionenbundels kan door middel van remoderatie in wolfraam-
   folies worden verhoogd, waarbij de helderheidsverhoging wordt gecontroleerd door de
   hoge temperatuur van de remoderator en de bedekking met onzuiverheden.
   E.G. Overbosch, B. Rasser, A.D. Tenner, and J. Los in Surf. Sci. 92, 310 (1980)

4 Bij het verhogen van het meettempo bij positron-geïnduceerde Auger-elektron-
   spectroscopie verdient het toepassen van een parallelle detector de voorkeur boven een
   actievere positronen bron.
   *H.Q. Zhou, S. Yang, E. Jung, and A.H. Weiss, 10th International Conference on
   Positron Annihilation (1994)*

5 Positron-geïnduceerde Auger-elektron-spectroscopie is nuttig voor het opnemen van
   ijkspectra bij lage-energie Auger-overgangen, maar zal met het beschikbaar komen van
   intensere en helderdere positronenbronnen ondergeschikt blijven aan conventionele
   Auger-elektron-spectroscopie.

6 De relatief hoge waarde van de S-parameter bij 5 keV gemeten met een variabele
   energie positronenbundel door Asoka-Kamur *et al.* voor MOS-systemen met Al-contact
   kan ook verklaard worden door ballistisch transport van de positronen naar het Al-
   SiO$_2$-grensvlak veroorzaakt door het potentiaalveld in het oxide.
   P. Asoka-Kamur, K.G. Lynn, and D.O. Welch in J. Appl. Phys. 79, 4935, (1994)

7 Een ionen-optisch systeem wordt niet gelimiteerd door Coulomb-interacties wanneer
   een zeer hoge dan wel zeer lage resolutie behaald wordt.

8 Met de huidige toename van de rekenkracht moeten computerprogramma's, ontwikkeld ten behoeve van de deeltjesoptica, voor de gebruiker minder specialistisch worden.

9 De verandering in de spelling van het woord positon in positron in 'Van Dale groot woordenboek der Nederlandse taal' is onlogisch.
Van Dale groot woordenboek der Nederlandse taal, 11e editie 1984, 12e editie 1992, C.D. Anderson in Phys. Rev. 43, 491, (1933)

<div align="right">
Léon J. Seijbel
9 mei 1995
</div>

An Instrument for Positron Micro-analysis

(Een Instrument voor Positronen Micro-analyse)

An Instrument for Positron Micro-analysis

Proefschrift

ter verkrijging van de graad van doctor
aan de Technische Universiteit Delft,
op gezag van de Rector Magnificus Prof. ir. K.F. Wakker,
in het openbaar te verdedigen ten overstaan van een commissie,
door het College van Dekanen aan gewezen,
op dinsdag 9 mei 1995 te 16.00 uur

door

Leendert Joost SEIJBEL

materiaalkundig ingenieur
geboren te Middelburg

Dit proefschrift is goedgekeurd door de promotoren:
Prof. dr. ir. P. Kruit
Prof. dr. A. van Veen
Prof. dr. ir. H. van Dam

Samenstelling promotiecommissie:

Rector Magnificus, voorzitter
Prof. dr. ir. P. Kruit, TU Delft, promotor
Prof. dr. A. van Veen, RU Groningen, promotor
Prof. dr. ir. H. van Dam, TU Delft, promotor
Prof. dr. ir. A. van den Beukel, TU Delft
Prof. dr. ir. C.W.E. van Eijk, TU Delft
Ir. C.J. Rakels, Philips Electron Optics BV

Contents

1 Introduction to positron micro-analysis

Summary
In this chapter an introduction to positron micro-analysis is given. Positron micro-analysis is useful to detect small defects in semi-conductor structures. Compared to other techniques it has the advantage that it is not destructive, has a fairly good lateral resolution, combined with a good depth resolution, and can be used to examine all kinds of materials without any restrictions. A positron microbeam can be made only if the brightness of the positron source is high enough, or the beam is remoderated. An introduction to the remoderation principle is also given.

1.1 Introduction

For many years positron beams have proven to be very useful probes for materials analysis. Positrons are particles with the same mass as an electron, but with opposite charge; this means that positrons belong to the group of anti-matter. Their positive charge makes them very sensitive for changes in the electron density in materials. Many material properties are related to the defects that exist in its structure. Since the electron density and momentum distribution in these defects is different from those for a perfect crystal, positrons can be used to detect these defects. Positrons have been used to detect defects for many years in all kinds of materials like metals and polymers. Lately an increasing number of positron studies on semiconductors have been performed. To be able to analyze not only semiconductor bulk materials, but also structures made in these materials, an analyzing technique with a lateral resolution of the order of the size of these structures has become necessary. Positron micro-analysis will be able to fulfill this need.

In general anti-matter is very rare in nature. In some nuclear decay reactions positrons are produced e.g. $^{22}Na \rightarrow ^{22}Ne + \beta^+$. Using one of these reactions is one of the possibilities to produce positrons. The other possibility is to stop photons of sufficient high energy ($E >> 1.22MeV$) in a dense material; in this reaction both an electron and a positron are produced by pair formation.

A problem in advancing the use of positrons for materials analysis is that it is difficult to produce a mono-energetic, high brightness beam of positrons. For

performing materials analysis with high lateral resolution the positron beam must be focussed. To focus a beam of charged particles is not a difficulty; all that is needed is a number of electrostatic or magnetic lenses and apertures. In electron and ion optics those lenses are often used, for instance in a scanning electron microscope. Complications arise because the number of positrons in the beam is small. Focusing the beam into a small spot, of say 0.1 μm, implies the use of apertures that will intercept most of the positrons somewhere down the beam line.

This chapter describes the tools needed for doing positron micro-analysis, focusing especially on the annihilation of positrons and electrons, on the optics required to make a narrow beam, and on other modern positron techniques. Furthermore competitive and complementary techniques for detection of defects in materials are described.

In the next chapters of this thesis the setup of the Delft intense positron beam are described. Chapter 2 describes the total set up of the beam, followed by the chapter in which the properties of the remoderation foils are reported. From these properties the number of remoderation steps, necessary to enable positron micro-analysis, can be obtained. A way to calculate this number is presented in Chapter 4. The optics needed for this remoderation are treated in Chapter 5, followed by the mechanical description of this section. As probe forming system a scanning electron microscope is used. The optics needed to get the positron beam on the optical axis of this microscope are described in Chapter 7. The last chapter will be devoted to the computer control of the positron micro-analysis facility.

1.2 Positron physics

1.2.1 Positrons

Since positrons are anti-matter they are not stable in the vicinity of their anti-particles, electrons. In materials, where many electrons are available, positrons have a lifetime of only a few hundreds of picoseconds (10^{-10} s). In vacuum where no other particles are present, positrons are stable, with a mean lifetime of more than 2×10^{21} s [1].

The transformation of positrons and their anti-particles (electrons) into photons is called annihilation. There are several ways for positrons and electrons to annihilate. The most important annihilation process in materials is the process in which two photons are involved. In this reaction between an electron and a positron two gamma rays are emitted:

$$e^+ + e^- \rightarrow 2\gamma. \tag{1.1}$$

If both the electron and the positron are at rest at the time the annihilation takes place, the energy of the photons can be calculated from the rest masses m_0 of the positron and electron via $E = m_0c^2 = 511$ keV. In that case the two gamma rays would be emitted in exactly opposite directions. If the positron-electron pair is not at rest (they have a momentum p relative to the laboratory frame) the total energy of the two emitted photons will be slightly different, there will also be an angle between the rays as illustrated in Figure 1.1 and there will be a spreading of the energy around 511 keV.
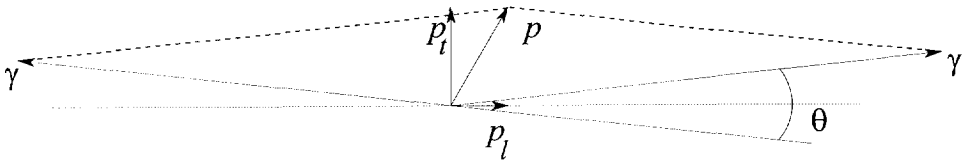
Figure 1.1   The two photons arising from the annihilation process if the annihilation pair has a momentum p. θ is the angle between the real direction and exactly opposite.

The angle θ can be calculated from the transverse term of the momentum p_t,

$$\theta = \frac{p_t}{m_0 c}. \tag{1.2}$$

Typical electron momenta are of the order of 10^{-24} kg m s^{-1}, and so the angle between the two gamma rays is of the order of a few milliradians. The shift in energy ΔE from 511 keV can be calculated from the longitudinal component of the momentum p_l,

$$\Delta E = \frac{cp_l}{2} \tag{1.3}$$

With the same momentum the shift in energy of the photons is of the order of 1 keV. These shifts can be measured with modern solid state detectors that have an energy resolution of the order of 1 keV. Due to this shift there is a distribution of energies. This distribution ranges from 511 keV-ΔE to 511 keV+ΔE.
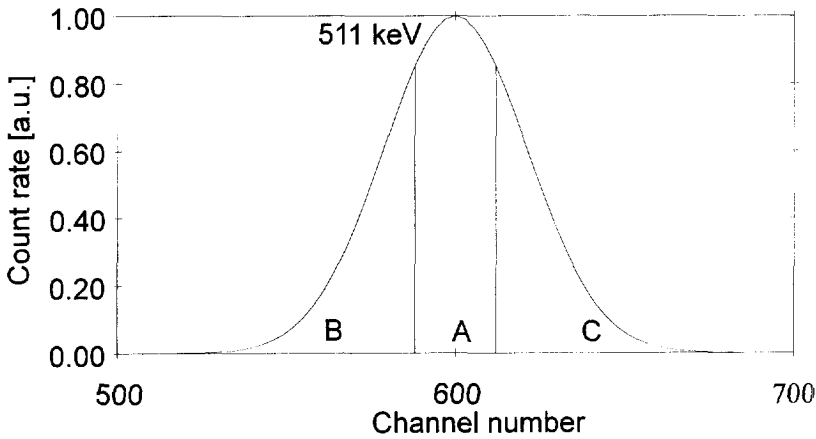
Figure 1.2   Photon energy distribution peak. The S parameter is defined as the area A divided by the total area A+B+C

For quantifying this distribution, McKenzie et al.[2] introduced the Doppler broadening parameter also called the S-parameter. This parameter describes the broadening of the energy distribution. It is defined by the ratio of the area of the central part of the energy distribution peak to the total area of the peak as has been depicted in Figure 1.2. The absolute value of S is of no physical meaning, since it is dependent on the resolution of the used detector and the chosen areas. An often used solution to overcome this problem is not to use the S parameter but to use the relative change in S with the S of the bulk material as a reference[3].

Since the energy of the positrons is lower in a defect, the positron will be trapped by this defect. A consequence is that when defects are present in the material, positrons will tend to diffuse to these defects. The importance of the

S-parameter is that it describes the electrons in the material. In the material the implanted positrons have been slowed down to thermal kinetic energies. In that case the contribution of the positrons to the momentum is small compared to the contribution of the electrons. Measuring the energy shift or the angle is measuring the momentum of the electrons. Since core electrons have a higher momentum than outer electrons, the core electrons will give larger deviations from the 511 keV. If relatively more core electrons annihilate with the positrons, the photon peak will be broader. On the other hand in defects there will be more annihilation events with the outer electrons, resulting in a smaller energy shift. This will result in a more narrow peak and thus a smaller S.

Besides the energy and the angle of the photons, a third property can be measured: the lifetime of the positrons in materials. The lifetime of a positron depends on the material in which they are implanted. When measuring the lifetime of positrons, the annihilation photons are used for detection of the annihilation of the positron. The creation of a positron can be detected by using a pulsed beam or a radioactive isotope that gives a photon, with an energy different from 511 keV. This photon can be used to start a clock.

1.2.2 Positron implantation

In the case of slow positron beams, the positrons are implanted in the material having kinetic energies in the order of a few hundreds of eV's to a few tens of keV's. In view of the short lifetimes of positrons in matter it is important to know how fast the positrons have been thermalized to reach average energy of $3k_bT/2$.

The first slowing down to a few tenths of an eV is mainly due to electron interactions. The time it takes to get at this energy is of the order of 1 ps. From this energy to thermalization, phonon excitations are the most important. Since the energy transfer in this case is much lower, the stopping times are much longer. Typical stopping times are in the order of 10 ps.

When the positrons all have been thermalized, it is possible to calculate the implantation profiles. These profiles have been obtained from Monte Carlo studies by Jensen et al.[4,5] and by Valkealahti and Nieminen[6,7] and can be

parameterized by a so-called Makhovian profile, given by:

$$P(E,z) = \frac{mz^{m-1}}{z_0^m} \exp\left(-\left(\frac{z}{z_0}\right)^m\right) , \tag{1.4}$$

in which $P(E,z)\,dz$ is defined as the fraction of the positrons with energy E that is stopped between z and $z+dz$. The parameter z_0 can be related to the mean implantation depth $\bar{z}$ by:

$$\bar{z} = \frac{\sqrt{\pi}}{2} z_0 . \tag{1.5}$$

It is assumed that the mean implantation depth is given by:

$$\bar{z} = \frac{\alpha}{\rho} E^n , \tag{1.6}$$

in which α and n are material independent constants and ρ is the density of the material. In a recent paper Ghosh et al.[8] show that the Makhovian implantation profiles give a too low positron concentration near the surface. A better parameterization is also given by Ghosh in a more recent paper[9], in which she reports the constants α and n of Eq. (1.6) to be material dependent.

After the implantation the positron can diffuse through the material. This diffusion is stopped when the positron annihilates with an electron or when it is trapped by an inhomogeneity in the material. This last case is the most important for positron analysis. It can be illustrated for the case of a vacancy in a metal. In a perfect crystal the potential energy of the positrons is periodic with the periodicity of the lattice. The positron wave functions are Bloch functions. They describe a positron probability distribution that possesses this same periodicity. Removal of an atom and a redistribution of the electrons results in a local lowering of the positron potential energy. In most metals the potential well is deep and broad enough to ensure at least one bound state for positrons.

An example of a positron trapped in such a bound state is shown in Figure 1.3. The positron wave function was calculated by Gupta and Siegel[10] for a positron diffusing in a bcc tungsten crystal. In the left-hand side figure, the positron wave function follows the periodicity of the positron potential energy of the perfect crystal. For a crystal with a defect, as shown at the right-hand side, the

positron is trapped in the potential well that was formed by the removal of one of the tungsten atoms from the perfect crystal. The number of atoms in the calculations was 25.
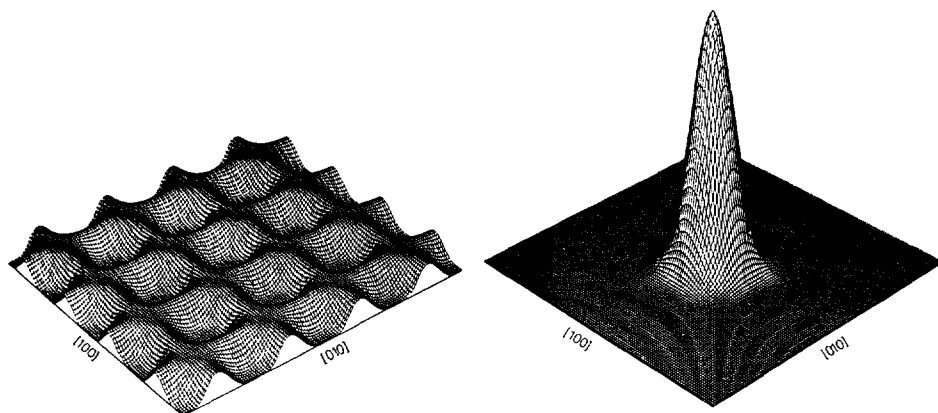
Figure 1.3   Wave function of a delocalized positron in a perfect bcc tungsten lattice (left) and of a localized positron in a vacancy in a tungsten crystal (right). From Gupta and Siegel.

1.2.3 Positronium

In some cases the positron can be bound to an electron to form a so-called positronium atom (Ps). The binding energy of such an atom is 6.8 eV. This atom can exist in two states. The singlet $^1S_0$ state (para-positronium or p-Ps) is the less stable form, it has a total spin zero. In vacuum it has a lifetime of approximately 125 picoseconds. As a rule, a p-Ps atom decays into two photons of about 511 keV.

The more stable form of positronium is the triplet $^3S_1$ state (ortho-positronium or o-Ps), its total spin S equals 1. In vacuum it has a lifetime of approximately 142 ns. It decays nearly always into three photons. The energy distribution of these photons is continuously increasing from 0 to 511 keV, while the sum of the three photons amounts to 1022 keV. The relative amount of p-Ps:o-Ps is 1:3, provided that it is formed in the absence of external disturbances.

The total amount of positronium formed depends on the electron density in the material. In metals and semi-conductors the density is too high to form a reasonable amount of positronium. Nevertheless positronium is also for metals and semiconductors important, since it can be formed at the surface of the specimen. This is especially important when using low energy positrons.

1.2.4 Positron generation

The two ways to create positrons are pair production and by the nuclear decay of some nuclei. A linear electron accelerator (LINAC) can be used to create positrons using pair production.

Radioactive positron emitters are e.g. ^{22}Na, ^{58}Co, and ^{64}Cu. ^{64}Cu has a short half-life of only 12.8 hours. The other isotopes have longer lifetimes, 2.6 years and 71 days respectively. The short lifetime of the ^{64}Cu-source demands that supply of this source is available from a nearby nuclear reactor. The neutrons from the reactor have to activate the ^{63}Cu more or less continuously, whereby ^{64}Cu is formed[11]. The sodium isotope can be used over years without having too much loss in current. This source is frequently used in low intensity beams. Plans to create Co-sources with strengths up to 100 kCi are developed at the reactor of the Idaho National Engineering Laboratory[12].

In the case of a LINAC, a pulsed electron beam is stopped in a high mass material. Out of the resulting bremsstrahlung positron-electron pairs are created. The consequence of the pulsed electron beam in the LINAC is that the positron beam also will be pulsed.

1.3 Positron analysis techniques

From the 80's new developments in positron physics have been numerous. Recent reviews were written by Schultz and Lynn[13] and by Seeger and Banhart[14]. One of the first developments is the variable-energy positron beam (VEP), consisting of positrons being emitted by a radioactive source. In Delft the design of such a beam was started in 1984. The construction of it was realized in 1986 after which it came into operation[15]. One of the advantages of

a VEP is that it provides mono-energetic positrons. Usually, sources emit positrons with a continuous energy distribution from zero to a few MeV's. Most positron beams use negative work function metals to moderate the positrons after which the positrons are emitted with energies varying from 1 to 4 eV. The fraction of positrons emitted varies from 10^{-4} to 10^{-3}. After moderation, the positron beam is accelerated and guided with electrostatic or magnetic fields to the specimen. There is no focusing of the beam onto the specimen. Hence the lateral resolution of a VEP is low. Nowadays there are many positron beams all around the world[16,17,18]. Most of these beams are used for defect profiling like the Delft VEP is[19]. A few of these beams are used for atomic physics experiments.

Another recent positron technique is Positron annihilation induced Auger Electron Spectroscopy (PAES)[20], in which a positron annihilates with an electron in one of the inner shells of an atom. When an electron of one of the outer shells of the atom falls inward, energy is released. This energy is used for Auger electrons to be emitted. By measuring the energy of the Auger electrons, information on the composition of the material can be obtained. This technique can be used with focused and non-focused beams. The advantage of PAES over conventional auger spectroscopy is that the spectrum does not contain any backscattered or secondary electron in the background.

Another recent technique is Low Energy Positron Diffraction (LEPD)[21], in which a moderated beam of positrons with energies typically lower than 200 eV is focussed upon a specimen. The low energy positrons have a probability of being elastically backscattered into the vacuum before experiencing an inelastic collision. By measuring the diffracted intensities, the precise coordinates of the atoms in the few upper layers can be found. A description of this technique is given by Duke[22]. The differences between LEPD and low energy electron diffraction (LEED) are small. LEED and LEPD studies on two component semiconductors show structures within the error estimates of the two techniques. New measurements and a refining of the used models have to be made to make the techniques more accurate. More recently Ito et al.[23] have observed Reflection High Energy Positron Diffraction (RHEPD) patterns. In RHEPD an incident positron beam having an energy of several keV's is diffracted at the sample surface.

An imaging technique is the Positron Re-emission Microscope (PRM) technique as proposed by Hulett et al.[24]. This technique was the first technique to get relatively high resolution information with the help of positrons. Van House and Rich[25] have done surface investigations with a PRM and obtained a resolution of 4 μm. An intense positron beam is focussed into a small spot on a specimen, which will re-emit positrons. Through a system of lenses the image of the re-emitted positrons is enlarged on a phosphor screen. Not all places on the specimen re-emit the same number of positrons, so contrast in the image can be obtained in this way. Due to the low brightness of the used beams, the time it takes to get an image can be longer then several hours. Due to the large affinity for defects in the material, PRM can be useful to detect defects just under the surface of negative positron affinity materials[26].

The newest developments are the Scanning Positron Micro beams (SPM). In this thesis the Delft design for such a beam will be described. Another design for such a SPM is being built at the Universität der Bundeswehr in Munich[27,28]. This beam is a pulsed beam with a minimum spot size of 1 μm. The pulsing of the beam enables to do positron lifetime spectroscopy with a high lateral resolution. Another high resolution positron beam is being built in Michigan[29]. This machine combines analysis techniques like Auger electron spectroscopy, scanning electron microscopy and scanning positron micro-analysis in one apparatus.

1.4 Positron optics

To focus a beam of charged particles one or more lenses are needed. Unlike in the field of light optics, these lenses can not be made of glass or a synthetic material. Lenses in particle optics are electrostatic or magnetic fields with certain shapes. Magnetic fields can be created simply by letting a current run through a coil. By placing magnetic material around the coil, a lens can be obtained. An electrostatic lens can be obtained just by arranging a number of electrodes and applying the right potentials on these electrodes. The difficulty of making a lens is to keep aberrations as low as possible. Every optical system has its own optical demands on aberrations. Therefore the solution for every optical problem is different. Sometimes minimization of the spherical aberration is needed, in other cases the chromatic aberration is more important.

One of the most important properties of a focussed beam is its reduced brightness. This brightness B_r is defined by the current I divided by the area $\pi/4 \; d^2$ times the solid angle Ω times the energy of the particles in the beam E:

$$B_r = \frac{I}{\frac{\pi}{4}d^2\Omega\,E}. \tag{1.7}$$

This brightness is a conserved quantity in the absence of non-conservative fields. It can easily be seen that the brightness does not change by accelerating, decelerating, (de)magnifying, or by stopping part of the beam on an aperture. For instance, accelerating the beam changes the energy of the particles, on the other hand the opening angle decreases the same factor as the energy increased. By demagnifying, the spot size becomes smaller at the cost of a larger opening angle, and since the angular magnification is equal to 1 over the magnification, the brightness does not change. The last possibility of stopping the beam gives a reduction in opening angle of the beam, but at the cost of loosing current, and again in the same amount, so the brightness does not change.

Aberrations of the lens system can cause a reduction in the current density of the beam. Although the volume in phase space does not change, the shape is not the easy to handle rectangle. The most important aberrations of lenses for positrons are the third order geometrical aberrations: These aberrations depend on combinations of the opening angle and the size of the positron source to third power. Chromatic aberrations are in general not important since the energy differences between the positrons are small.

The consequence of a low brightness is that the number of positrons in a probe of a certain size is very low. For a normal positron beam this yields a current of less than one positron per second, if it would be focused into a spot of 100 nm given a reasonable energy. With conservative fields like magnetic and electrostatic fields, it is not possible to get more particles in the probe, so a special trick has to be used.

A nowadays often used way to enhance the brightness of a positron beam was found by Mills[30]. When a beam of positrons is focused upon a material, the positrons will enter the material and will loose their kinetic energy rapidly and become thermal. Since most materials have a negative work function for

positrons, it follows that the positrons are thrown out of the material with a kinetic energy as large as the absolute value of this work function. This process is called remoderation. What happens during remoderation is that the energy of the particles is reduced to the value of the work function, thus the brightness of the beam has been enhanced. A more extensive description of remoderation will be given in Chapter 4.

In this way it would be possible to enhance the brightness of the beam in a single step to the desired value just by increasing the energy of the primary beam by a factor equal to the quotient between the desired brightness and the current brightness. However for this to work, the other terms in Equation(1.7) should not change with the energy. Unfortunately the number of positrons that is re-emitted depends on the energy and can be much smaller than 100%. Furthermore the change is in all the other terms in the unfavorable direction. There is only a current of thermalized positrons out of the remoderation material if the accelerating energy is in the order of a few keV's. When the positrons are inside the material, they can annihilate with the electrons in the material. The annihilation takes place in most cases in defects in the material like vacancies, dislocations and grain boundaries. Therefore the best remoderation materials are defect-free mono-crystalline materials.

Another demand is that the surface of the crystal is clean; it must be placed in an ultra high vacuum system with a pressure in the order of 10^{-10} mbar. The clean surface is needed because contaminated atoms on the surface can cause a trapping of the positrons and the creation of positronium, both resulting in a decrease of free positrons.

However, despite all these measures not all positrons will be re-emitted; at least 65% of the positrons will annihilate in the material. This optimum has been measured by Poulsen et al.[31] for a positron accelerating energy of 4 keV. From this it can be calculated that the best brightness enhancement is about 1000 times.

Remoderation is possible for positrons, but since the work function for electrons is positive, it is easy to see that the brightness of an electron beam cannot be enhanced by remoderation; the electrons would be bound to the remoderation material.

As Canter et al.[32] show, the microprobe resolution limit is a probe size of 100 nm. Information from smaller probes can not be obtained since the positrons will diffuse over a distance of that same order of magnitude. They describe the electrostatic optics needed to use the reflection geometry for remoderation. The Delft design is based on the transmission geometry and is discussed in Chapter 5 of this thesis.

1.5 Other defect probing techniques

1.5.1 General

Techniques that are able to localize and characterize defects are important in materials science, since defects can influence the properties of a material to a great extent. For instance defects in a semiconductor will cause different electrical properties of this device. Sometimes devices have to be stable under radiation, for instance if they are used in space or other radiation environments.

The most important effects of defects in MOS devices occur at the interface between a SiO_2- and a Si-layer. These defects determine the properties of the semiconductor, they can be present in the layer from the fabrication of the layer or they can be formed during operation of the device. Presently the defect studies that have been done are mainly in large specimens of silicon with a silicon oxide layer on it. With a positron microbeam it might be possible to investigate defects in small semiconductor structures.

The defects that exist are due to the fact that the lattice of the oxide layer does not fit with the silicon layer. To be electrically neutral, each silicon atom must be bound to four oxygen atoms, where each oxygen atom must be bonded to two silicon atoms. If not all the atoms are bonded, some electrically active positions in the crystal lattice are present, giving changes to the semiconductor properties. In these defects electrons can be trapped resulting in a lowering of the conductivity of the interface. As a result of the two different layers a misfit between the two layers may occur. The misfit between the two layers can give a strain between the two layers, that may be relaxed by the incorporation of strange atoms like hydrogen.

To detect these kinds of defects positrons can be used in many types of materials. The best way to do defect studies is to combine it with another tool. In the next paragraphs three different defect localizing techniques are described: first the transmission electron microscope, second thermal desorption spectrometry and finally deep level transient spectrometry.

1.5.2 Transmission electron microscopy

The best known technique for making defects visible is the high resolution transmission electron microscope (HRTEM). The advantages of HRTEM are that the technique is widely used, that the images made by HRTEM are relatively easy to interpret, and that the defects are very well localized. Disadvantages are the destructive type of research, only very thin specimen can be used. Another disadvantage is that the defects cannot be too small, where positron defect probing is sensitive in a range from single vacancies up to voids of several nanometers. HRTEM is especially useful in imaging of 2-d defects like grain boundaries. Line defects like dislocations are more difficult to image, where only few point defect studies have been done by using HRTEM. A more extensive description on this subject has been given by Smith and Barry[33].

Another technique in the transmission electron microscope is Electron Loss Near Edge fine Structure (ELNES). A recent overview is given by Egerton[34]. With this technique the electron excitation from core level states can be measured. The energy loss spectrum contains a fine structure that depends on the chemical environment of the atoms. When a foreign atom or a vacancy is neighboring the atom, the density of the electrons is changed. By looking at the small changes in the energy loss spectrum, the chemical composition can be found.

1.5.3 Thermal helium desorption spectrometry

Another technique to detect defects is thermal helium desorption spectrometry (THDS) as introduced by Kornelsen[35]. A helium ion is implanted at room temperature in a specimen. If defects are present in the material, the He-atom can diffuse to these defects. If the potential well caused by the defect is deep enough, the He-atom can be trapped by this defect. When the specimen is

subsequently heated to about two third of its melting temperature, the noble gas atoms are desorbed. By measuring the temperature where the gas is released, the binding energy of the gas atom to the defect can be measured. Since different defects have different binding energies, the defect type can be found. With this technique especially point defects and small defect complexes in both metals and semiconductors can be detected as can be seen in a recent review by van Veen[36]. Disadvantages of this technique are that there is no lateral resolution, and that it can be destructive.

1.5.4 Scanning deep level transient spectroscopy

Deep level transient spectroscopy, introduced by Lang[37], is a technique with which it is possible to detect point defects in semiconductors. The strength of this technique is that it is able to detect all types of deep level point defects. Later, Petroff and Lang[38] used this technique in a SEM, to combine the technique with the high lateral resolution of the SEM calling this technique scanning deep level transient spectroscopy (SDLTS). A recent review of the technique is given by Breitenstein and Heydenreich[39]. During the measurements three phases of the semiconductor can be distinguished. The example is given for a hole trap of a space charge region (SCR) of an n-type Schottky barrier. First, there is thermal equilibrium, the traps are typically ionized by holes. If minority carriers are generated by the action of an electron beam, holes flow through the SCR causing trap filling. After switching off the electron beam, the filled traps thermally ionize and the carriers are swept away by the electric field. This process is associated with a measurable transient current and change in transient capacitance. The simplest way to do SDLTS is by measuring the current or capacitance as a function of the time, resulting in a thermal emission time constant. By plotting this constant as a function of temperature, a spectrum can be created, in which the different traps give peaks at different temperatures.

1.6 Conclusions

Positron analysis is a strong technique to do defect studies. The positive charge of the positron makes it extremely sensitive to point defects. The positron studies until now make it clear that a positron microbeam can be extremely

useful in the understanding of properties of small structure semiconductor components as well in other materials. Compared to other techniques, positron micro-analysis has its own specific advantages. It can be used to detect point defects in all kinds of materials with a resolution of 100 nm. To use it in combination with other defect probing techniques will give a good insight into the properties of materials.

References

1.   E.M. Belotti, M. Corti, E. Fiorini, C. Liguori, A. Sarracino, P. Sverzellati, and L. Zanotti, Phys. Lett. B **124**, 435, (1983)

2.   I.K. McKenzie, J.A. Cadly, and R.R. Gingerich, Phys. Lett. A **33**, 279, (1970)

3.   A. Dupasquier, and G. Ottaviani, Lecture at International School of Physics "Enrico Fermi", course "Positron Spectroscopy of Solids", (1993)

4.   K.O. Jensen, A.B. Walker, and N. Bouarissa, *Positron Beams for Solids and Surfaces*, eds. P.J. Schultz, G. Massoumi, and P.J. Simpson, (AIP, New York, 1990) p.17

5.   K.O. Jensen, and A.B. Walker, Surf. Sci. **292**, 83, (1983)

6.   S. Valkealahti, and R.M. Nieminen, Appl. Phys. A **32**, 95, (1983)

7.   S. Valkealahti, and R.M. Nieminen, Appl. Phys. A **35**, 51, (1984)

8.   V.J. Ghosh, D.O. Welch, and K.G. Lynn, Proceedings of the 5th International Workshop of Slow-Positron Beams and Techniques for Solids and Surfaces, eds. E.H. Ottewitte, and A.H. Weiss, (AIP, New York, 1994), p. 37

9.   V.J. Ghosh, Appl. Surf. Sci. **85**, 187, (1995)

10.   R.P. Gupta, and R.W. Siegel, J. Phys. F **10**, L7, (1980)

11.   A. van Veen, H. Schut, P.E. Mijnarends, L.J. Seijbel, and P. Kruit, Proceedings of the 5th International Workshop of Slow-Positron Beams and Techniques for Solids and Surfaces, eds. E.H. Ottewitte, and A.H. Weiss, (AIP, New York, 1994), p. 354

12.   B.L. Brown, A. Denison, H. Makowitz, D.W. Gidley, W.E. Frieze, H.C. Griffin, and P. Encarnacion, Proceedings of the 5th International Workshop of Slow-Positron beams and Techniques for Solids and Surfaces, eds. E.H. Ottewitte, and A.H. Weiss, (AIP, New York, 1994), p. 289

13.   P.J. Schultz, and K.G. Lynn, Rev. Modern Phys. **60**, 701, (1988)

14.   A. Seeger, and F. Banhart, Helv. Phys. Acta **63**, 403, (1990)

15.   H. Schut, PhD. dissertation, Delft University of Technology, (1990)

16.   S. Tanigawa, Helv. Phys. Acta **63**, 385, (1990)

17.   A.A. Manuel, and M. Peter, Helv. Phys. Acta **63**, 397, (1990)

18.   K.G.Lynn, M. Weber, L.O. Roellig, A.P. Mills Jr., and A.R. Moodenbach in *Atomic Physics with Positrons*, eds. J.W. Humberston, and E.G.A. Armour, (Plenum, New York, 1987), p. 161

19.   R.A. Hakvoort, PhD. dissertation, Delft University of Technology, (1993)

20.   A. Weiss, R. Mayer, M. Jibaly, C. Lei, D. Mehl, and K.G. Lynn, Phys. Rev. Lett. **61**, 2245, (1988)

21.   R. Mayer, and K.G. Lynn, Phys. Rev. B **33**, 2507, (1986)

22.   C.B. Duke, Lecture at International School of Physics "Enrico Fermi", course "Positron Spectroscopy of Solids", (1993)

23.   Y. Ito, M. Hirose, I. Kanazawa, O. Sueoka, and S. Takamura, Mat. Sci. Forum **105-110**, 1893, (1992)

24.   L.D. Hulett, J.M. Dale, and S. Pendyala, Mat. Sci. Forum **2**, 133, (1984)

25.   J. Van House, and A. Rich, Phys. Rev. Lett. **61**, 488, (1988)

26.   K.F. Canter, Lecture at International School of Physics "Enrico Fermi", course "Positron Spectroscopy of Solids", (1993)

27.   P. Willutzki, P. Sperr, D.T. Britton, G. Kögel, R. Steindl, and W. Triftshäuser, Mat. Sci. Forum **105-110**, 2009, (1992)

28.   W. Triftshäuser, G. Kögel, K. Schreckenbach, and B. Krusche, Helv. Phys. Acta **63**, 378, (1990)

29.   D.W. Gidley, W.E. Frieze, T.L. Dull, G.B. DeMaggio, E.Y. Yu, H.C. Griffin, M. Skalsey, R.S. Vallery, and B.D. Wissman, Proceedings of the 5th International Workshop of Slow-Positron Beams and Techniques for Solids and Surfaces, edited by E.H. Ottewitte, and A.H. Weiss, (AIP, New York, 1994), p. 391

30.   A.P. Mills Jr., Appl. Phys. **23**, 189 (1980)

31.   M.R. Poulsen, M. Charlton, J.Chevallier, B.I. Deutch, F.M. Jacobsen, and G. Laricchia in *Positron Annihilation*, Proc. of the 8th Int. Conf. on Positron Annihilation, eds. L. Dorikens-Vanpraet, M.Dorikens, and D. Segers, (World

Scientific, Singapore, 1989), p. 597

32.   K.F. Canter, G.R. Brandes, T.M. Roach, A.P. Mills Jr., Solid State Phen. **28&29**, 341, (1993)

33.   D.J. Smith, and J.C. Barry, in *High-Resolution Transmission Electron Microscopy and Associated Techniques*, eds. P.R. Buseck, J.M. Cowley, and L. Eyring, (Oxford University Press, New York, 1988), p. 477

34.   R.F. Egerton, in *Quantitative microbeam analysis*, eds. A.G. Fitzgerald, B.E. Storey, and D. Fabian, (IOP, London, 1993), p. 145

35.   E.V. Kornelsen, Can. J. Phys. **42**, 364, (1964)

36.   A. van Veen in *Fundamental Aspects of Inert Gases in Solids*, eds. S.E. Donelly, and J.H. Evans, (Plenum Press, New York, 1991), p. 41

37.   D.V. Lang, J. of Appl. Phys. **45**, 3023, (1974)

38.   P.M. Petroff, and D.V. Lang, Appl. Phys. Lett. **31**, 60, (1977)

39.   O. Breitenstein, and J. Heydenreich in *SEM Microcharacterization of Semiconductors*, eds. D.B. Holt, and D.C. Joy, (Academic Press, London, 1989), p. 339

2 The intense positron beam facility at the Delft nuclear reactor

Summary

This chapter summarizes the design and realization of the intense positron facility at the Delft nuclear reactor and introduces the setup for the microbeam system. The facility will deliver an intense positron beam (> 10^8 e^+ s^{-1}) that is highly mono-energetic. The positron beam will be used for positron micro-analysis and angular correlation measurements. The positron source consists of small cylinders of copper with thin tungsten foils on the inner surfaces of the cylinders. The positrons can be moderated in the tungsten. From this source the positrons are transported out of the reactor by a low axial magnetic field. After leaving the magnetic field, the positrons undergo their first remoderation. At that position the positrons can be used to do 2D ACAR. After transportation more remoderation steps are performed to do positron micro-analysis. After the remoderation the bright positron beam is introduced in a scanning electron microscope via transport optics and a deflector.

2.1 Introduction

This chapter describes the overall design of the Delft positron beam at the research reactor. There are several possibilities to create intense positron beams as already discussed in Chapter 1. Normally, making use of ^{22}Na or ^{58}Co sources will not result in intense beams. With LINAC-based beams it is possible to have intensities a factor of 100 higher[1]. This kind of beam often has the disadvantage that the positrons come in short pulses that will result in a saturation of the detector. Making use of a beam stretcher has shown to be of help to solve this problem. The highest intensity beams are the beams in which reactors are used. Both the activation of copper by neutron capture, and pair production via high energetic γ-radiation will result in high intensity beams[2].

A few years ago plans were developed at Delft University of Technology to use the research reactor for generating an intense positron beam. Continuously activated copper foils positioned close to the reactor core would act as the primary positron source[3,4]. The basic idea was to neutron activate ^{64}Cu in copper foils and to use moderation in tungsten to generate slow

positrons. Due to the moderate neutron flux at the reactor a large source had to be used to get a large amount of positrons.

The positron beam will be equipped with two different positron analysis techniques. First the Doppler broadening technique at a sub-micrometer scale, and second the two-dimensional angular correlation of annihilation radiation (2D ACAR). Both techniques will be used for defect analysis.

The equipment to be connected to the beam for measuring 2D-ACAR spectra consists of a vacuum chamber in which the specimen can be rotated in all possible directions, and two large area so-called Anger cameras[5]. An Anger camera is a scintillation crystal, with an array of phototubes behind it. This setup will be accommodated in the experimental hall to be built north of the reactor hall.

Brightness enhancement by remoderation in tungsten foils will be applied repeatedly to convert the large diameter primary beam into a narrow parallel microbeam[6,7]. This beam will be introduced into a converted Philips scanning electron microscope SEM 535 and guided toward the specimen along the same optical path as the electrons and focused to a probe size of about 100 nm. This micro-analysis setup is subject of the next chapters.

In the next section an overview of the positron beam setup will be given. This will be followed by an overview of the microbeam setup. Design considerations will be given in this part of the thesis. The next chapters in this thesis will deal with the elaboration of the microbeam.

2.2 Setup of the positron beam facility at the Delft research reactor

2.2.1 System overview

The positron facility, called POSH: positrons at the HOR-reactor (Hoger Onderwijs Reactor), is schematically shown in Figure 2.1. The facility consists of the following parts:

A)   The vacuum tube. This tube is made of aluminum, and has a diameter of 160 mm. The tube houses the positron source and the coils for the
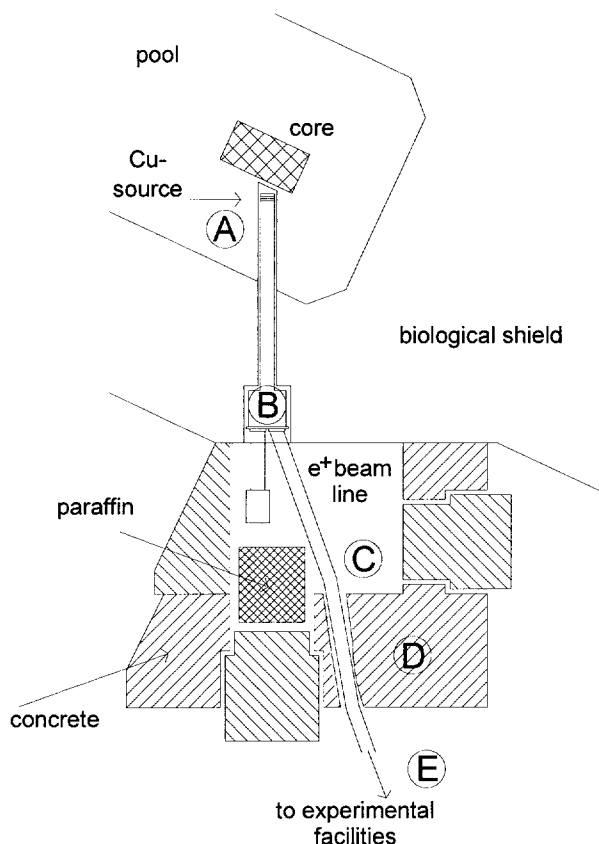
Figure 2.1   Schematic diagram of the positron beam at the Delft nuclear reactor. For explanation of the parts A through E refer to the text.

magnetic transport. This source is made of copper and tungsten. Since the specimen for positron analysis is at ground potential, the source must be operated at high voltage. The highest possible voltage in the tube for the source and the inner tube is 45 kV.

B)   Deflection part of the positron beam. The beam is deflected over 19° to be able to remove the neutrons and gamma rays.

C)   A section made of stainless steel for further guiding and bending of the positron beam. In this section it is possible to monitor the beam via a microchannel plate and a phosphorous screen equipped with a video camera.

D)   A small blockhouse for biological shielding of neutron and gamma radiation, which can now be seen through the opening in which the vacuum tube has been positioned.

E)   Experimental area where the positron beam is guided to the micro-analysis apparatus or the 2D ACAR setup.

The total beam system is constructed according to ultra high vacuum standards. The beam will be pumped by internal getter material, ion getter pumps, and titanium sublimation pumps. At the end of section C a turbo-molecular pump will be installed.

2.2.2 Positron production at the core of the nuclear reactor

Activation of copper

When copper is chosen as the positron generating material via the reaction $^{63}Cu(n,\gamma)^{64}Cu$ (half-life of 12.8 h), a maximum positron activity per unit of volume $I = 1.8 \times 10^{11}$ e$^+$cm^{-3}s^{-1} is attained after approximately 48 h[3]. This figure is based on the use of natural Cu (69% ^{63}Cu) and a thermal neutron flux of 8×10^{12} n cm^{-2}s^{-1}. The yield of slow positrons from a copper surface is derived with the aid of a yield factor Y, which represents the number of re-emitted slow positrons per positron arriving at the Cu surface by diffusion, and the diffusion length $L = (D\tau)^{1/2}$, where D is the diffusion coefficient and τ the positron lifetime in Cu. With $Y = 0.55$ and $L = 104$ nm (for defect-free Cu) one finds

$$e^+_{yield} = Y \times I \times L = 1.03 \times 10^6 \, cm^{-2}s^{-1}. \qquad (2.1)$$

It is clear that for a high e$^+$ yield a large emitting surface area is required. Assuming an area of 1000 cm^3, a total yield of 1.03×10^9 should be feasible. To maximize the emitting area, four arrays of small copper cylinders have been made. In Figure 2.2 the setup is shown. The diameter of the small copper cylinders is about 9 mm. The thickness of the copper is 0.127 mm; the thin tungsten foils inside the cylinders are 7 μm thick. The cylinders have been arranged in a hexagon with a cross section of 92 mm.
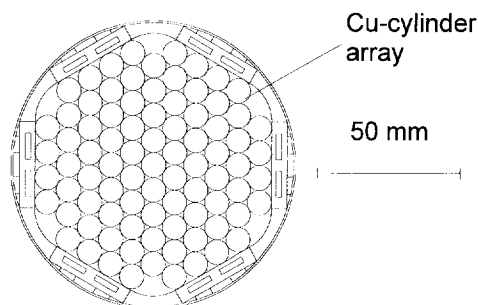
Figure 2.2   Setup of the positron source. Small copper cylinders form an array to maximize the number of positrons. Four of these arrays will be used.

The above calculation assumes that only the positrons generated within a distance L from the surface contribute to the yield. Comparison with more exact yield calculations[8] shows that this calculation method predicts a yield with 20% accuracy. A design requirement following from maximizing the yield is that foils should be thicker than the mean penetration range (30 μm) of the fast positrons emitted by ^{64}Cu, or else a part of the generated positrons will leak from the source region without contributing to the positron concentration in the foils.

The copper surfaces can be covered with thin foils of tungsten so that one profits from the better moderating properties of tungsten in case the Cu surfaces become covered with impurities as a result of deterioration of the vacuum. If 3 μm tungsten foils are used the yield will only drop to 80% of the value for uncovered copper. Furthermore, the extraction geometry should be optimized to extract the positrons with high efficiency from the source area.

Extraction efficiency
In Figure 2.3 results of trajectory calculations, performed by Mokiem[9], are shown for positrons emitted by the surfaces of the small cylinders which form the elements of the source array. The emitting area of the back plane is 78 cm^2 and the area of each plane of cylinders is 352 cm^2. On the basis of these calculations estimates have been made of the transmission efficiencies of positrons emitted from the back surface and from the cylinder surfaces 1 through 4. These estimates have been listed in Table 2.1 (from Mokiem[9]). It
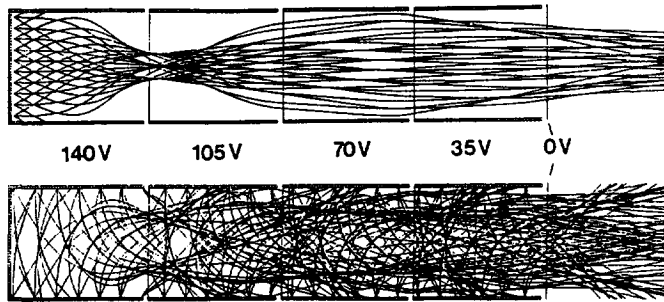
Figure 2.3   Calculated trajectories for positrons emitted by a: the surface of the
              cylinders, and b: the back surface

follows that the overall efficiency amounts to 67%. Thus, from a total
positron emitting surface area of $1500 \, cm^2$, $1000 \, cm^2$ is effectively
delivering positrons at the focusing part of the source. The focusing part is
shown in Figure 2.4. Positrons emerging from the last cylindrical section can
be brought together in a beam with a waist of 2.2 cm diameter. Note that
positrons consist of different energy groups, since the four discs with
cylinders are at different potentials.

Subsequently, the positrons are injected into the magnetic guiding system
consisting of a long solenoid generating a 0.02 T axial field. During focusing
some additional 20% of the beam is lost. The transmission of the beam
through the solenoid will be close to 100%. The beam is transported at a
kinetic energy of about 5 keV in an electrically floating internal tube that is
kept at a potential of -5 kV with respect to the positron source.

The positron current expected at the exit of the solenoid is of the order of
$1 \times 10^9 \, e^+ s^{-1}$. Together with the large opening angle and source size, it
follows that the brightness of this beam is very low. The brightness of this
beam must be enhanced by remoderation in a tungsten or nickel foil. After
one remoderation we expect to have a parallel beam of 1 cm diameter with a
five times reduced intensity of $2 \times 10^8 \, e^+ s^{-1}$. The brightness of the beam is at
that position about $2 \times 10^{-6} A \, sr^{-1} m^{-2} eV^{-1}$, 10^{10} times lower than a tungsten
hair pin electron source. Further remoderation, as described in the next
chapters, will bring the brightness to a value of about $2 \, A \, sr^{-1} m^{-2} eV^{-1}$.

Table 2.1 Extraction efficiency of the positron source.

total transmission[a] through disk j of positrons originating in disk i[b]						effective surface area[c]	
						3	4 disks
i =	0	1	2	3	4		
j = 0	1.	0.91	0.9	0.91	0.91	71 (52)	71 (46)
1		0.96	1	0.56	0.56	198 (144)	198 (130)
2			0.5	0.56	0.56	198 (160)	198 (144)
3			6	0.96	0.56	338 (304)	198 (160)
4			0.9		0.96		338 (304)
			6				
effective area						805 (660)	1003 (784) cm^2
area						1134	1486 cm^2
transmission						0.71 (0.58)	0.67 (0.53)
intensity (10^8e$^+$s^{-1})						8.8 (7.2)	11. (8.7)

a) on the basis of trajectory calculations
b) i,j = 0 corresponds to the back plane of the first disk
c) figures for 100% (90%) transmission of the grids between the disks
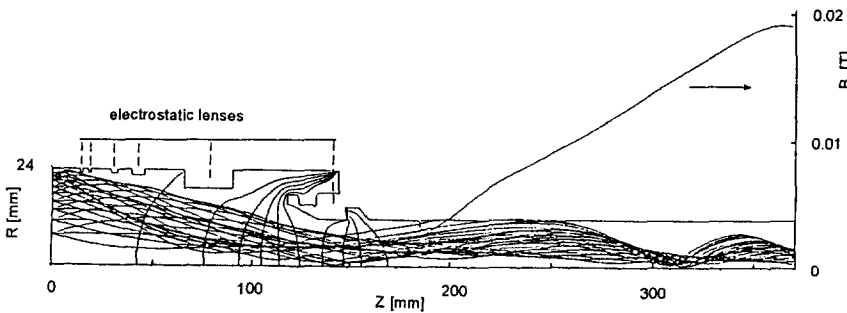
Figure 2.4   Calculated trajectories for positrons entering the focusing part of the positron source. The positrons move to the solenoid on the right hand.

The first remoderation to reduce the beam size will take place at the point at which the beam leaves the concrete blockhouse. After this remoderation the maximum beam energy will be 40 keV. Remoderation occurs in a zone where the magnetic field has been reduced to nearly zero. Further transport

to the micro-analysis setup will be performed electrostatically. For transport over longer distances, e.g. to serve the 2D ACAR equipment, the beam will be re-introduced into a magnetic guiding system. At two locations a beam monitor will be installed to observe the beam size and beam quality. A chevron assembly of microchannel plates and a phosphor screen can be moved into a beam section. Via a mirror and a video camera the cross section of the beam can be recorded.

The magnetic field will be terminated by a magnetic screen of about 1 m^2 with a hole of about 35 mm diameter. Using this termination the magnetic field of 0.01 T drops to 0.001 T within 25 mm. When leaving the magnetic field, the positrons will loose the same amount of transverse energy as they had gained when entering the magnetic field[10]. Electrostatic lenses are used to focus the beam on the first remoderator into a spot of 10 mm. Since the remoderator will be positioned at a few tens of cm's behind the magnetic screen, the magnetic field at that position will be almost zero. After this first remoderation the beam becomes mono-energetic. Since from this point on the beam parameters are better known than in the previous sections, the positron beam is much easier to guide. After this point, a beam switch will be introduced to guide the beam either to the 2D-ACAR setup or to the microbeam facility.

2.2.3 Radiation shielding aspects

It can be calculated that one of the problems encountered in the design of the POSH facility concerns the leakage of the neutron and gamma radiation through the straight cylindrical duct in the shielding wall of the nuclear reactor. Without any measures taken, the primary neutron and γ flux densities just outside the biological shield would reach levels of the order of 10^8 n cm^{-2}s^{-1} and 10^9 γ cm^{-2}s^{-1}, respectively, at a reactor power of 2 MW thermal. In addition, one is faced with the production of secondary γ's due to the capture of thermal neutrons in the POSH construction materials such as flanges and other vacuum components. Capture γ rays emerge also from the boron doped paraffin used for thermalization and absorption of neutrons. Several computer codes such as neutron transport codes, point kernel gamma shielding codes, and neutron activation codes were used by Havranek et al.[11]

to calculate a design for a shielding geometry capable of reducing the neutron and gamma dose rates below a level of 5 μSv/h. This has resulted in a concrete block house (thickness of walls and ceiling approx. 1 m) adjacent to the biological shield of the reactor. Inside this block house the positron beam is bent horizontally over 19° before it penetrates the wall of the block house. In order to attenuate the primary neutron beam, a boron doped paraffin beam stop (length 80 cm, diameter 60 cm) is provided.

2.2.4 Other intense positron facilities

In the world several positron projects have been started. The list discussed below is not a complete one, but gives an overview of different possibilities. The examples used are the high intensity beam at the Brookhaven reactor[8], the high brightness beam at Brandeis University[12], the Michigan positron microscope program[13] and the scanning positron microscope in Munich[14].

Brookhaven National Laboratory
The source of positrons that is used in the Brookhaven positron beam is ^{64}Cu. It is produced in the high flux beam reactor at Brookhaven by means of the same reaction as used in the Delft design. The difference is that the source must be used outside the reactor. Due to the short lifetime of the ^{64}Cu, the beam needs a daily renewal of the source. With the high thermal neutron flux of 8.3×10^{14} n/cm^{2}s a positron current of 1×10^8 e$^+$/s could be measured. The magnetically guided beam has been equipped with several techniques such as ACAR and a positronium beam.

Brandeis University
At Brandeis University a ^{58}Co source has been used over the past years to generate positrons. Before remoderation the positron beam is deflected over 90 degrees. Hereafter, the mono-energetic positron beam is remoderated twice in a backward re-emission configuration. The positron beam at Brandeis has been mainly used as a positron re-emission microscope with a resolution of 10 nm. The two-stage remoderation section is the basis of other positron beam designs e.g. by Goodyear and Coleman[15].

University of Michigan
The setup of the Michigan positron facility consists of several scanning positron techniques combined with electron techniques such as scanning electron microscopy and Auger electron spectroscopy. The source that will be used is a 1 Ci ^{58}Co 3 mm diameter disk. In collaboration with the Idaho National Engineering Laboratory new plans on the construction of a 10^5 Ci source are being developed. The beam is designed with three remoderators, one in reflection mode and two in transmission mode.

Universität der Bundeswehr Munich
In collaboration with the University of Trento, a scanning positron microscope has been built in Munich. The design is based on their pulsed beam system[16]. The source consists of concentric rings of tungsten and cadmium. In cadmium thermal neutrons are implanted resulting in high energy gamma-radiation. The photons are stopped in the tungsten foils (25 μm) resulting in the production of positron-electron pairs. Using one remoderation step it is possible to focus the positron beam to a 1 μm probe. The positron microscope gives information on defects and defect structures on near surface microscopic regions by measuring characteristic lifetimes.

2.3 Setup of the positron microbeam analysis

2.3.1 Instrumentation for microanalysis

In the first sections of this chapter the design of the intense beam was already discussed. This is the starting position of the design of the microbeam. The positron beam coming to the microbeam setup has been remoderated once. With this beam it is not possible to do analysis with a (sub-) micrometer range lateral resolution without loosing too many positrons.

The positron analysis will take place in a converted Philips scanning electron microscope 535-M (SEM). The reason for using a SEM is that this instrument is already equipped with a probe forming system, and that it is possible to pre-examine the specimen with a high resolution electron beam. A schematic overview of the setup is given in Figure 2.5. The figure shows the remoderation section, consisting of a number of remoderators, a transport

electron   transport
source   optics   POSH-beam

90°-deflector

                                        remoderation section

SEM
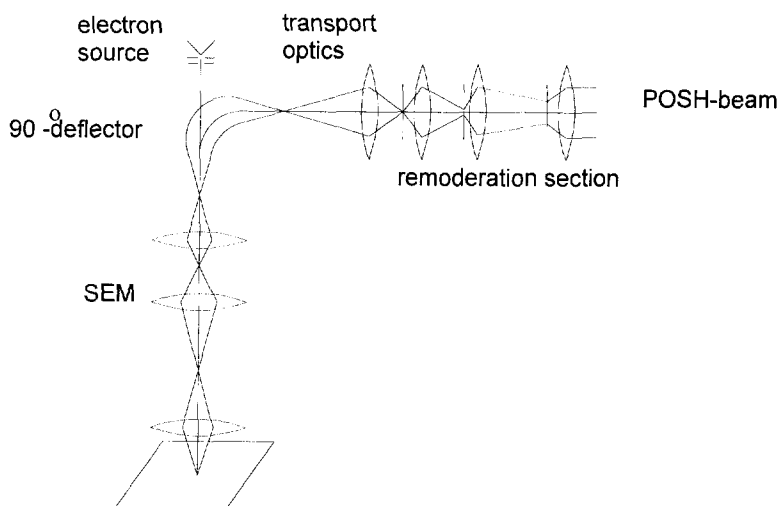
Figure 2.5   Schematic overview of the positron microbeam. This microbeam consists of
              a remoderation section, transport optics, a 90°-deflector, and a scanning
              electron microscope.

section, and the SEM. In the figure forward remoderation is shown, although
a choice between the two remoderation possibilities, forward and backward
re-emission, is possible. To get the beam on the optical axis of the
microscope, a 90°-deflector is necessary. The option to put the microscope in
a horizontal direction and let the electron beam come in from the side can
also be considered. But the more complex mechanical construction makes it
less opportune.

The way the positron microbeam will be used is by selecting first interesting
areas of the sample by means of the electron beam. In the SEM the deflector
can be switched off, and the electron beam is focused on the specimen. With
this microscope it is possible to make images of a specimen with a lateral
resolution of about 7 nm. The SEM is equipped with four different kinds of
detector, viz. a secondary electron detector, a backscatter detector, a cathode
luminescence detector, and a sensitive ammeter. To do the positron analysis,
the specimen chamber of the SEM will be equipped with a Ge-solid state
detector.

2.3.2 Positron measurement setup

The positron microbeam will be used to do Doppler broadening experiments on a (sub-)micrometer scale in the lateral direction. By changing the energy, and thus the mean implantation depth, a depth resolution can be obtained. Practical energies are in the range from 500 eV to 25 keV, so the beam will be operated in this range. The probe size is chosen to be about 100 nm, of the order of the diffusion length of positrons in many materials.

To do the Doppler experiments, a large number of annihilation photons are necessary. A number of 5×10^5 photons in the 511 keV peak are mostly used to do an accurate experiment. About 40% of the photons end up in the 511 keV-peak,[17] so it is clear that about one million photons must be measured by the detector. The detector has an efficiency for 511 keV photons of 25%. Combined with a possible distance of the detector to the specimen of 100 mm and the size of detector of 76 mm diameter, this results in an overall detector efficiency of about 1%. Knowing that each positron gives two photons, it can be concluded that about 10^8 positrons are necessary to measure a single point.

The number of positrons in a probe of a given size is determined by the brightness of the beam and the energy of the positrons. In the design of the positron microbeam it is not possible to vary the brightness of the beam during a measurement. Therefore it is not possible to do a depth (energy) scan with a constant positron current and probe size. Thus performing a depth scan, one can change the measuring time per energy or the probe size. A more detailed discussion is given in Chapter 4.

2.4 Discussion and conclusions

The success of a reactor based positron source depends largely on the vacuum and material conditions that can be achieved in the positron source tube. Radiation safety requires that the vacuum tube and other parts of the system consist mainly of low-activation materials, in our case aluminum and alumina. Aluminum UHV systems have proven to operate satisfactorily, but here we have to face the complication of an environment with rather intense

neutron and γ radiation. Thus far, it is unknown how much gas will be released by the high vacuum construction materials under radiation and how this will affect the positron re-emission properties of the copper or tungsten surfaces.

Although the reactor at Delft has a rather moderate neutron flux, radiation damage will eventually accumulate to a level where the diffusion length of the positrons is shortened considerably. The positron yield is proportional to the diffusion length and will therefore be reduced. A reduction by a factor of two is expected when the defect concentration for tungsten accumulates to a level of 10 appm. Trapping rates at simple defects (vacancies) in Cu are expected to be a factor of 50 higher than in W, since this material can be compared with molybdenum[18]. Therefore, in Cu reduction of the diffusion length should occur much earlier. However, at the working temperature of 100°C monovacancies anneal in Cu but not in tungsten. The epithermal neutrons (energy up to 1 MeV; flux $10^{12}\mathrm{cm}^{-2}\mathrm{s}^{-1}$) will create about 10^3 displacements per neutron. During one year of operation (250 days) the neutron fluence will be $2\times10^{19}\mathrm{n\,cm}^{-2}$, giving rise to about 2×10^{-2} displacements per atom. Frenkel pair recombination processes taking place at the ambient temperature will cause damage levels to be a factor of 10-100 lower. Thus, concentrations of surviving defects are expected to be of the order of 200-2000 appm. These concentrations can be reduced by periodic in-situ annealing.

The in-core slow positron beam is now under construction. The positrons are produced in a source with a large surface area. Information will have to be gained with respect to the behavior of the materials used in the source during one year of operation in a reactor environment. 2D-ACAR-equipment is now under development.

References

1. R.H. Howell, M.J. Fluss, I.J. Rosenberg, and P. Meyer, Nucl. Instr. & Meth. B **10**, 373, (1985)

2. W. Triftshäuser, G. Kögel, K. Schreckenbach, and B. Krusche, Helv. Phys. Acta **63**, 378, (1990)

3.   A. van Veen, POSH, Internal Report IRI-131-89-01, unpublished, (1989)

4.   A. van Veen, H. Schut, P.E. Mijnarends, L.J. Seijbel, and P. Kruit, Proceedings of the 5th International Workshop of Slow-Positron Beams and Techniques for Solids and Surfaces, eds. E.H. Ottewitte, and A.H. Weiss, (AIP, New York, 1994), p. 354

5.   H.O. Anger, Rev. of Scient. Instr. **29**, 27, (1958)

6.   L.J. Seijbel, P. Kruit, A. van Veen, H. Schut, Mat. Sci. Forum **105-110**, 1977, (1992)

7.   K.F. Canter, G.R. Brandes, T.N. Horskey, P.H. Lippel, and A.P. Mills jr., in *Atomic Physics with Positrons*, eds. J.W. Humberstone, and E.G.A. Armour, (Plenum, New York), p. 153

8.   K.G. Lynn, M. Weber, L.O. Roellig, A.P. Mills Jr., and A.R. Moodenbach in *Atomic Physics with Positrons*, eds. J.W. Humberstone, and E.G.A. Armour, (Plenum, New York), p. 161

9.   R. Mokiem, masters thesis Delft University of Technology, (1994), unpublished

10.   R.F.J. Neelissen, Internal report Department of Applied Physics, (1993), unpublished

11.   V. Havranek, H. Schut, A. van Veen, J.L. Kloosterman, and J.E. Hoogenboom, Internal report IRI-131-91-001, unpublished, (1991)

12.   K.F. Canter, T. Horskey, P.H. Lippel, W.S. Crane, and A.P. Mills Jr., in *Positron (Electron)-Gas Scattering*, eds. W.E. Kauppila, T.S. Stein, J.M. Wadehra, (World Scientific, Singapore, 1986), p. 202

13.   D.W. Gidley, W.E. Frieze, T.L. Dull, G.B. DeMaggio, E.Y. Yu, H.C. Griffin, M. Skalsey, R.S. Vallery, and B.D. Wissman, Proceedings of the 5th International Workshop of Slow-Positron Beams and Techniques for Solids and Surfaces, eds. E.H. Ottewitte, and A.H. Weiss, (AIP, New York, 1994), p. 391

14.   W. Triftshäuser, to be published in J. de Physique, (1995)

15.   A. Goodyear, and P.G. Coleman, Mat. Sci. Forum **105-110**, 1867, (1992)

16.   P. Willutzki, J. Störmer, G. Kögel, P. Sperr, D.T. Britton, R. Steindl, Meas. Sci. Technol. **5**, 548, (1994)

17.   H. Schut, PhD. dissertation, Delft University of Technology, (1990)

18.   R.M. Nieminen, and M.J. Manninen, in *Positrons in Solids*, ed. P. Hautojärvi, (Springer Verlag, Berlin, 1979), p. 145

3 Remoderation properties of tungsten foils

Summary
This chapter discusses the theory, measuring setup, and preliminary results on the re-emission properties of thin tungsten foils. With the setup of the measurements it is possible to measure the positrons that are transmitted by the foils. It is demonstrated that both slow thermalized positrons and fast positrons can be measured. The theory is used to describe the results of forward re-emission measurements of the tungsten foils.

3.1 Introduction

To be able to do positron micro-analysis, a high brightness positron beam is necessary. Since intrinsically high brightness positron sources are not available at this moment, the brightness of the source must be enhanced. In an earlier chapter and also in Chapter 4, the remoderation principle, proposed by Mills[1], has been discussed.

To be able to remoderate the beam in an efficient way, remoderators with a high re-emission yield are necessary. Two remoderation principles can be used in positron microbeams: viz. forward and backward remoderation. In the first case the positrons diffuse after implantation through a thin foil and are re-emitted at the other side of the foil. In the latter case, the positrons diffuse back to the side of implantation. In this case both thick crystals and thin foils can be used.

When the positron reaches the surface there are three possibilities for the positron. First, the positron can be trapped by the surface, second, the positron can be bound to an electron forming a positronium atom, and finally, the positron can be re-emitted as a free particle. The energy of the re-emitted positron is then equal to the absolute value of the negative work function. To be sure that all the positrons that reach the surface also leave the surface, a clean surface is needed. In this chapter results of positron re-emission yields are given as function of the heat treatment. The chance that a positron reaching the surface really is emitted, is called branching ratio for free positrons (ε_{e+}).

The first systematic results of forward and backward re-emission of positrons from thin tungsten foils were reported by Chen et al.[2]. They measured a maximum forward re-emission yield of 18% at an incident energy of 5 keV for a 100 nm thick tungsten foil; ε_{e+} was measured to be over 50%. Later Poulsen et al.[3] obtained a forward re-emission yield of 38% at an implantation energy of 4 keV for the same type of material but with a different treatment of the foils resulting in an ε_{e+} of over 75%.

The foils used in these experiments were purchased from the Thin Film Department of Arhus University in Arhus Denmark. The foils are mono-crystalline tungsten foils with (100)-orientation. The thickness of the foils is 100 nm. That is only a few hundred atom layers thick. The fabrication method of these foils is described by Mertler et al.[4].

For the Delft positron beam it is important to have a method to enable high re-emission yields with a cleaning procedure that can easily be performed. In this chapter first a theoretical basis is given for the re-emission properties, followed by the re-emission measurement setup in which different methods can be tested, after which preliminary results of the measurements are treated.

3.2 Theory of implantation and re-emission

3.2.1 Implantation

The implantation of positrons in materials has been subject of many studies. Recently Ghosh[5] fitted the implantation profiles found by Monte Carlo calculations[6] to the expression

$$P(z,E) = \frac{N_{lm}}{<z(E)>} \left(\frac{z}{C_{lm} <z(E)>} \right)^l \exp \left[-\left(\frac{z}{C_{lm} <z(E)>} \right)^m \right], \quad (3.1)$$

where l, m, C_{lm} are fitting parameters. Eq.(3.1) becomes an often used Makhovian implantation profile for l equals m-1. The normalizing constant N_{lm} is determined by requiring that

$$\int_{0}^{\infty} P(z,E)\,\mathrm{d}z = 1 \quad . \tag{3.2}$$

The mean implantation depth $<z(E)>$ can be fitted for positron energies between 1 and 12 keV with

$$<z(E)> = \frac{A}{\rho} E^{n} \quad , \tag{3.3}$$

where ρ is the material density and A and n are fitting parameters.

Figure 3.1   Positron implantation profile for a 4.5 keV positron beam in a 100 nm thick tungsten foil using the fitted parameters of Ghosh.
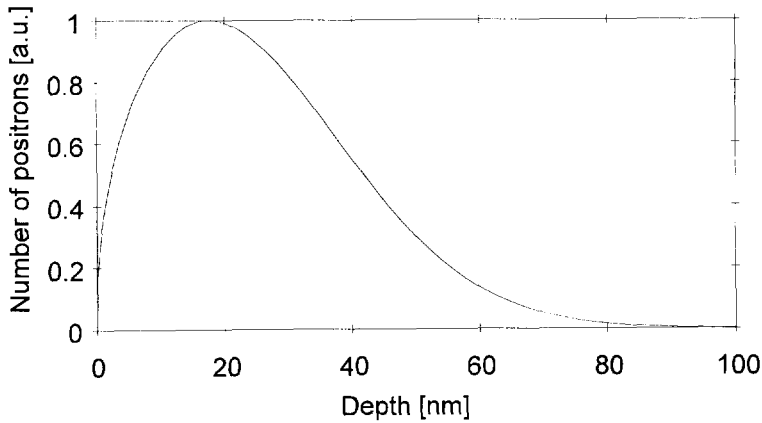
Figure 3.1 shows the implantation profile of a 4.5 keV positron beam in 100 nm thin tungsten foil using the fitting parameters of Ghosh. The assumption of Mills[7], that the implantation profile hardly changes in the case of a thin foil compared to a semi-infinite medium, has been used. The mean implantation depth is in this case equal to 26.1 nm.

3.2.2 Diffusion and trapping

For the case of a thin tungsten foil the diffusion equation is given by:

$$D_+\frac{d^2c(z)}{dz^2} - (\kappa + \lambda_b)\,c(z) + P(z) = 0 \ . \tag{3.4}$$

in which D_+ is the diffusivity, κ is the positron trapping rate, that is proportional to the defect concentration, and λ_b is the bulk annihilation rate. The sum of the rates κ and λ_b is equal to τ^{-1}, where τ is the positron lifetime in the material. For almost defect free mono-crystalline materials, the positron trapping rate is much smaller than the bulk annihilation rate. An important parameter, the positron diffusion length (L_+) can be found by using:

$$L_+ = \sqrt{D_+\tau} \ . \tag{3.5}$$

The diffusion equation can only be solved analytically for second order Makhovian implantation profiles i.e., $l=1$ and $m=2$. The boundary conditions

$$c(0) = L_a\frac{dc}{dz}\Big|_{z=0} \tag{3.6}$$

and

$$c(T) = L_a\frac{dc}{dz}\Big|_{z=T} \tag{3.7}$$

are the so called radiative boundary conditions, with L_a a parameter that can be considered to be a surface absorption length and T the thickness of the foil. From the solution it is possible to calculate the re-emission yields at both sides of the crystal, where in our case the forward re-emission is the most important.

3.2.3 Re-emission

The forward re-emission yield (η_f) is found by taking the first derivative at $z=T$ and the back re-emission yield (η_b) is found by taking this derivative at $z=0$, according to:

$$\eta_f = -\varepsilon_{e^+} + \frac{D_+}{J_0}\frac{dc}{dz}\bigg|_{z=T} \tag{3.8}$$

and

$$\eta_b = \varepsilon_{e^+} + \frac{D_+}{J_0}\frac{dc}{dz}\bigg|_{z=0} . \tag{3.9}$$

The solution of the diffusion equation for perfect absorbing boundaries ($L_a=0$) was found by Vehanen and Mäkinen[8]

$$\eta_f = \varepsilon_{e^+} + \left[\sinh\left(\frac{T}{L_+}\right)\right]^{-1}\int_0^T \sinh\left(\frac{z'}{L_+}\right) P(z')dz' . \tag{3.10}$$

Chen et al.[2] fitted the measured re-emission yields by using a Makhovian profile. The fitting parameters found are $n=1.80$, $A=51.0$ nm g/cm^3/keV$^{1.8}$, $m=1.14$, $L_+=138$ nm and $\varepsilon_{e+}=0.512$.

With the new parameterization of Ghosh[5] a better fit can not be found as seen in Figure 3.2. The parameters of Ghosh[5] for tungsten are $n=1.35$, $A=66.5$ nm g/cm^3/keV$^{1.35}$, $m=2.106$, $l=0.4395$, $C_{lm}=1.421$ and $N_{lm}=1.113$. The diffusion length could not be fitted to the measured profiles using reasonable lengths so the same diffusion length as Chen et al.[2] used, $L_+=138$ nm, has been used. The branching ratio ε_{e+} was found to be about 0.451. In the figure it can be seen that the parameters found by Ghosh[5] give worse results than the simple approximation of Chen et al.[2].
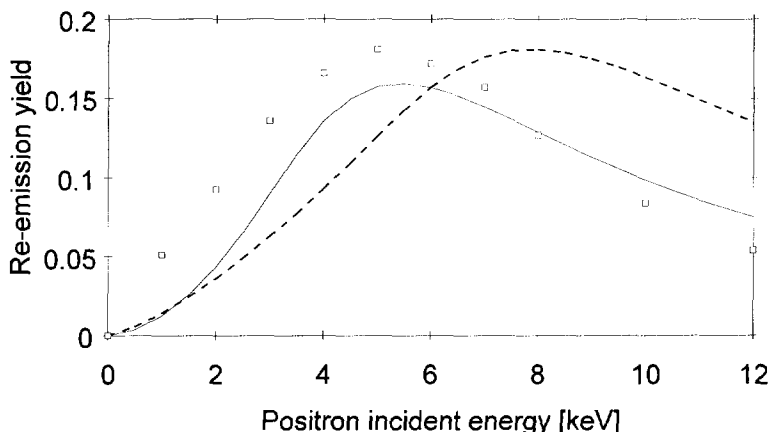
Figure 3.2   Fits to the re-emission yields measured by Chen et al. using the fitting
parameters of Chen et al. (solid line) and Ghosh (dotted line).

3.3 Setup of the measurements

3.3.1 Measurement method

The aim of the measurements is to determine the forward re-emission yield
(η_f). This yield can be found by dividing the transmitted positron current (I_f)
through the foil by the total current (I_t) as in:

$$\eta_f = \frac{I_f}{I_t} .$$

(3.11)

The positron currents can be found by measuring the annihilation photons
with a Ge-detector. Therefore the transmitted positrons must be stopped not
to close to the foil, since the positrons not transmitted also contribute to the
photon current. Therefore, a second Ge-detector has been used to measure
the number of photons originating from the foil. The positron currents can be
found by using

$$I_f = (N_{f1} - K N_{f2}) C$$

(3.12)

and

$$I_t = (N_{t1} - K N_{t2}) C \; , \tag{3.13}$$

in which K is a constant that determines the number of false counts i.e., photons originating from the foil that reach the detector at the stop, C a constant that is a measure for the efficiency of the detector, and $N_{(f,t),(1,2)}$ the number of photons through the foil or the hole on the two detectors respectively.

3.3.2 Setup of the beam

The measurements described in this chapter have been performed with the Variable Energy Positron beam (VEP) at the Interfaculty Reactor Institute (IRI). Therefore, the VEP has been extended with two more vacuum chambers. In the first chamber, the remoderation foil was installed, in the second chamber a positron beam stop was placed. Two Ge-detectors were installed at the two chambers looking to the side of the foil and the beam stop respectively. An overview of the setup is given in Figure 3.3. In this figure the two detectors can not be seen. Magnetic coils in a Helmholtz configuration are used to get all emitted positrons on the beam stop in the second vacuum chamber.

On a linear motion feedthrough a holder has been made to position foils and dummy foils. The dummy foil is a thick foil with a hole of the same size as the thin foil, so the transmitted positron current (I_t) can be measured.

A grid in front of the foil can be used to re-implant slow positrons and two grids behind the foil can be used to separate the slow from the fast positrons. The voltage on the first of these two grids can be positive with respect to the foil, so only the fast positrons are measured in this mode. The second grid is used to accelerate the positron beam. The acceleration voltage used is 50 V.
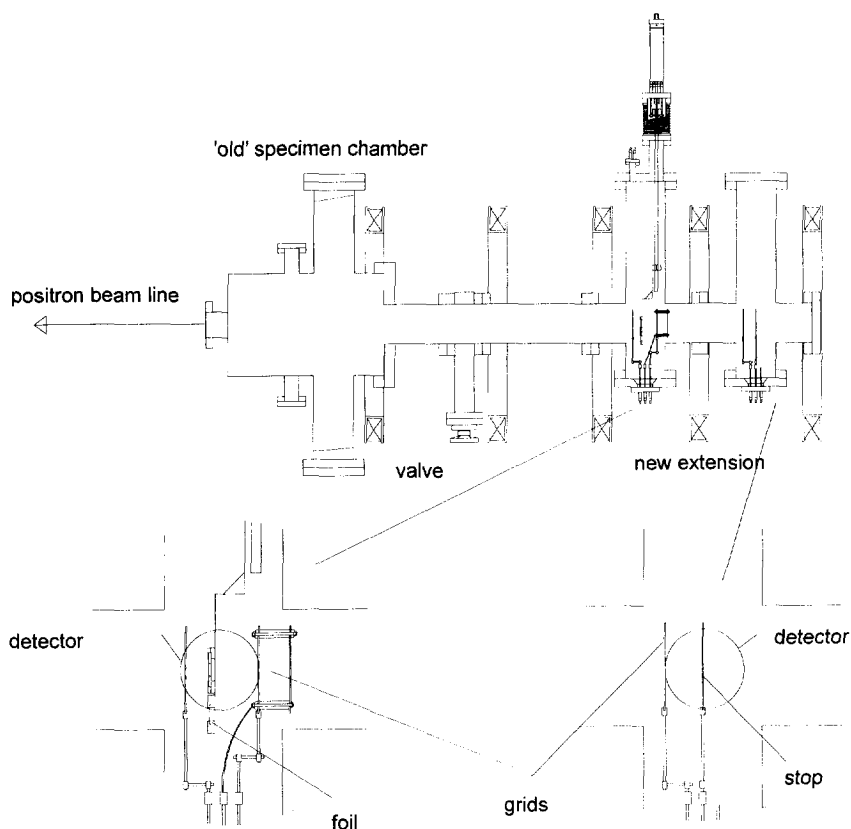
Figure 3.3   Setup of the positron re-emission measurements. Two extra vacuum chambers have been used, one for the foil, and one for measuring the re-emitted positrons. (drawing by K.J. Roos)

3.3.3 Mounting of the foils

The remoderation foil is a 100 nm thick tungsten foil, with a diameter of about 10 mm. This thin foil is put on a 7 μm thick carrier foil with a hole of 4 mm diameter, also made of tungsten.

Figure 3.4 shows the foils clamped on the holder. The holder and clamps have been made of non magnetic stainless steel. By using for one of the
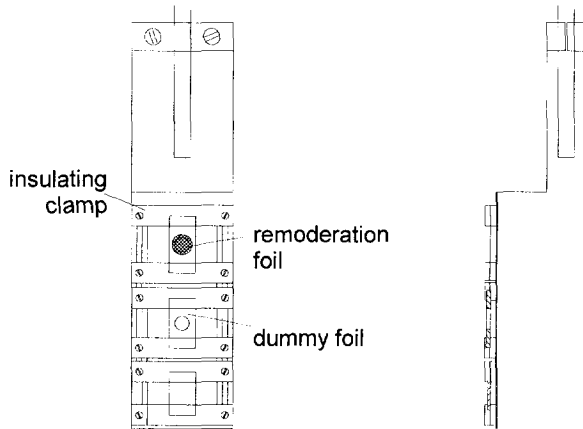
Figure 3.4   Holder of both the remoderation foil as well as the dummy foil with the
              hole in it. (drawing by K.J. Roos)

clamps a ceramic material, it is possible to heat the foil by resistance heating.
The dummy foil has also been put on the holder, it has a hole of the same
size as the hole over which the 100 nm foil was stretched.

3.3.4 Foil treatments

It was seen that the two most important factors for a good re-emission yield
are the absence of defects in the remoderator, to reduce the positron trapping
rate κ and the quality of the vacuum to enhance the branching ratio for free
positrons ε_{e+}. By heating the foils to temperatures at two third of their
melting point, the defects become mobile and can diffuse out of the material.
The branching ratio ε_{e+} can be improved by cleaning the surface. Gas
treatments at different temperatures can desorb unwanted adhesives from the
surface.

The way Chen et al.[2] did their heat treatment consisted of a first heating of
the foils to 1800°C under high vacuum ($\approx 10^{-9}$ mbar). The foils were placed
between a folded 95% transmission W mesh. This mesh was also used as the
sample heater. By this first procedure possible trapping centers were
removed, essential for a long positron diffusion length. The surface of the
tungsten was cleaned by a series of heat treatments. Carbon is believed to be

the most important contaminant for lowering the positron emission, so heating in oxygen followed by an annealing procedure was found to be effective in reducing these and other contaminants. After a vacuum pressure was reached of better than 10^{-9} mbar, the foils were treated first by heating in oxygen ($\approx 10^{-7}$ mbar) at 700-800°C for 40 minutes and then in vacuum ($\approx 10^{-9}$ mbar) at 2000°C for 1 minute. This procedure was repeated ($\approx$3 or 4 cycles) until the foils showed good positron re-emission properties.

Poulsen et al.[3] used a CW-Nd:YAG laser to perform the heating. The procedure they used was adapted from the procedure of Chen et al. The first step is a short laser pulse to heat the foil to 1200°C to clean the surface, followed by an anneal for 20 minutes at 1200°C in an oxygen environment (10^{-6} mbar). The last step in this procedure is to heat the foil to 2000°C in vacuum (10^{-9} mbar).

3.4 Preliminary results
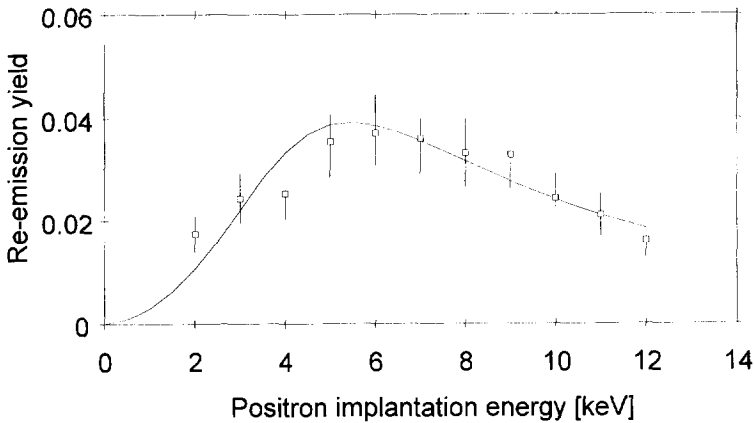
Figure 3.5   The first results of the re-emission setup for a foil with no heat treatment. The measurement has been fitted with the model of Chen et al.

The first results of our measurement setup are for an untreated foil respectively a foil heated to 1500 K in a poor vacuum of 10^{-7} mbar. In Figure 3.5 the results for the non-treated foil is shown with a fit according to Chen et al. It can be seen that the maximum is at an energy of 5 keV and

that the re-emission yield is 4% corresponding to an ε_{e+} of 0.126. The diffusion length in the foil has been taken the same as the value of Chen et al., viz. 138 nm.
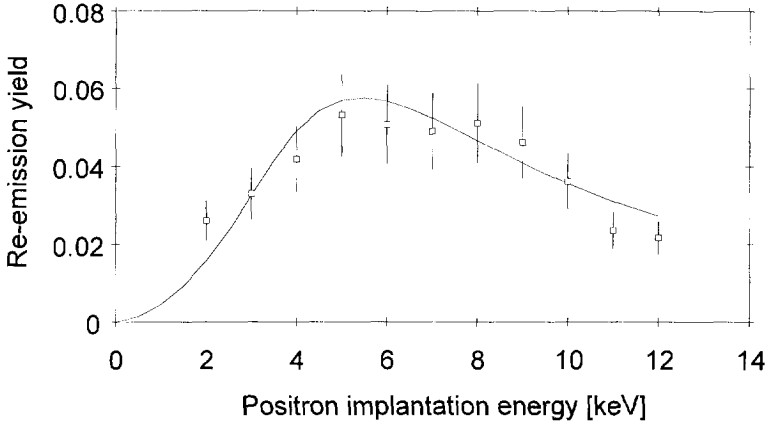
Figure 3.6   Results of the re-emission setup for a foil with one heating to 1500 K. The measurement has also been fitted with the model of Chen et al.

In Figure 3.6 the re-emission as a function of the implantation energy is shown for the foil that was heated to about 1500 K. With the same parameters as the untreated foil it was possible to fit the measurements. The branching ratio has increased from 0.12 to 0.18 resulting in a re-emission yield of nearly 6% at an energy of 5 keV.

3.5 Discussion and conclusions

With the facility built at the VEP, it is possible to measure the transmission of slow positrons through thin foils. The preliminary results for mono-crystalline tungsten are for untreated foils of 100 nm thickness a 4% re-emission yield. Heating the same foil to 1500 K in a poor vacuum of 10^{-7} mbar, resulted in an enhancement of the yield to 6%.

From theory it is possible to calculate the re-emission yield of thin foils. The new parameterization of Ghosh using Monte Carlo calculations does not give accurate answers. The problem here might be the fact that the material

dependent constants were calculated for thick crystals. To make the parameters fit better, Monte Carlo calculations must be performed on thin foils. The fits of Chen et al. were the result of fitting to the measurements they performed on thin tungsten foils. The parameterization used by them, can be used to fit the measurements performed at the VEP-facility. For the measurements to fit, a diffusion length of 138 nm has been used.

To enhance the re-emission yields, better heat treatments in a cleaner system must be performed. With the present setup it is possible to heat the foils to higher temperatures in a vacuum of 10^{-10} mbar. It is also possible to remove possible contaminants from the surface by flushing the foil with oxygen. At this moment a method to heat and clean the foils inside a beam has not been found. The major problem that still exists is the poor vacuum at the re-emission setup.

References

1.   A.P. Mills Jr., Appl. Phys. **23**, 189, (1980)

2.   D.M. Chen, K.G. Lynn, R. Pareja, and B. Nielsen, Phys. Rev. B **31**, 4123, (1985)

3.   M.R. Poulsen, M. Charlton, J. Chevallier, B.I. Deutch, F.M. Jacobsen, and G. Laricchia, in *Positron Annihilation*, Proc. of the 8th Int. Conf. on Positron Annihilation, eds. L. Dorikens-Vanpraet, M.Dorikens, and D. Segers, (World Scientific, Singapore, 1989), p. 597

4.   G. Mertler, M. Rey, and K. Reichelt, Nucl. Instr. & Meth. **192**, 535, (1982)

5.   V.J. Ghosh, Appl. Surf. Sci. **85**, 187, (1995)

6.   V.J. Ghosh, D.O. Welch, and K.G. Lynn, Proceedings of the 5th International Workshop os Slow-Positron Beams and Techniques for Solids and Surfaces, eds E.H. Ottewitte, and A.H. Weiss, (AIP, New York, 1994), p. 37

7.   A.P. Mills Jr., in *Proceedings of the 85th Summer School of Physics on Positron Solid State Physics*, eds. W. Brandt, and A Dupasquier, (1982), p. 432

8.   A. Vehanen, and J. Mäkinen, Appl. Phys. A **36**, 2902, (1985)

4 Calculation of the number of remoderation steps

Summary

A method to calculate the number of remoderation steps is given. It is possible to calculate with simple assumptions the number of remoderation steps necessary for a positron micro beam. With this method it is possible to calculate the positron current that eventually will be in the positron probe. The numbers that should be known are the positron re-emission yield for different energies, the final energy of the positrons and optical parameters of the probe forming system. Guesses of the aberrations of the remoderation section have to be made within not too high precision. Both with the forward re-emission results of Poulsen et al. as with the backward results of Chen et al., the number of remoderation steps found for the positron beam in the SEM with a spot size of 100 nm, and an energy of 20 keV is three.

4.1 Introduction

To do positron analysis, it is important to have a large positron current in the used probe. The brightness (B), as it is used here, also called reduced brightness or brightness per volt, determines the number of positrons that can be focused in a spot of a certain size. In Chapter 1 a definition was already given, here it is defined as:

$$B = \frac{I}{\frac{\pi}{4}d^2 \pi \alpha^2 E} \ .$$

$$(4.1)$$

in which I is the positron current, d is the diameter of the spot, α is the half opening angle of the beam, and E is the energy of the positrons in the beam. The brightness of the beam is a conserved quantity, i.e. it is not possible to change the brightness of a beam by conservative fields, or in other words by magnifying or accelerating the beam.

The total spot size (d_p) of the positron beam can most easily be found by quadratic addition of the most important contributions: the geometrical spot (d_g) and the spot due to spherical aberration (d_s), as in

$$d_p^2 = d_g^2 + d_s^2 \ . \tag{4.2}$$

Both contributions can be written as a function of the opening angle at the image. The geometrical spot size can be written in terms of brightness and the spherical aberration spot equals $0.5\ C_s\alpha^3$, where C_s is the coefficient for spherical aberration related to the image side[1]. Rewriting Eq. (4.2) yields the total probe size as function of the opening angle

$$d_p^2 = \frac{4I}{\pi^2\alpha^2 BE} + \frac{1}{4}C_s^2\alpha^6 \ . \tag{4.3}$$

By optimizing the opening angle it can be found that the maximum current in the probe is proportional to the brightness of the beam and the energy of the positrons:

$$I_p = \frac{3\pi^2}{16}BE\frac{d_p^{\frac{8}{3}}}{C_s^{\frac{2}{3}}} \ . \tag{4.4}$$

In Chapter 2 it has been found that the brightness after the first remoderation step is equal to 2.6×10^{-6} A/m^{2}sr eV. With the spherical aberration coefficient of the objective lens of the SEM, equal to 2.95 cm, it can be found that the number of positrons in a probe of 100 nm is equal to 1 positron per second for an energy of 20 keV. Since the other parameters in this equation are more or less fixed, only brightness enhancement can give a larger positron current.

As described in the previous chapters, Mills[2] has described a method to enhance the brightness of positron beams. A mono-energetic positron beam is focused onto a mono-crystalline foil. If this foil has a negative work function for positrons, the positrons that approach the surface, can be re-emitted. The number of positrons that is re-emitted depends on the energy of the incoming positrons. This has already been discussed in the previous chapter.

A positron beam can be brightness enhanced by having a focused primary beam on a foil with negative work function. The brightness of this beam is given by Eq.(4.1). When the beam leaves the crystal, the spot diameter will marginally have been enlarged. The only two parameters that really change are the number of positrons, and the product of energy and half opening angle of the positrons, that is the transverse energy. The energy of the incoming beam is of the order of a few keV, where the work function is of the order of a few eV. The opening angle of the incoming beam is limited by the spherical aberration of the focusing lens. The opening angle (α_{rem}) of the re-emitted positron beam is given by:

$$\alpha_{rem} = \sqrt{\frac{E_T}{\phi^+}} \quad , \tag{4.5}$$

in which E_T is the transverse component of the energy and ϕ^+ is the work function of the remoderator material for positrons. In the case that the emitting material can be regarded as a good single crystal the transverse energy can be assumed[3] to be equal to kT. For having not to severe demands on the foil an extra factor of 2 has been used for E_T. Possible problems with the opening angle are that the the foil is not flat, and that the work function is smaller than the used one. With a value of 0.025 eV for kT and 2 eV as the work function, the opening angle will be 0.16 rad. Since the opening angle of the incoming beam is determined by spherical aberration, it is limited to a value of the same order of magnitude, as will be shown later. So it can be found that a theoretical brightness enhancement factor of 1000 is possible. But since not all positrons are re-emitted by the remoderator, only a practical brightness enhancement factor of about 300 is possible.

The brightness must be enhanced until the number of positrons in the probe, determined by Eq.(4.4), is equal to the number of positrons remaining in the positron beam after a number of remoderation steps. In other words, no positrons have to be thrown away on apertures, and the only loss in positron current is the loss in the remoderation crystal. It is of no use to go to a higher brightness since it will not give more positrons in the probe.

In this chapter a simple method to calculate the number of remoderation steps is given. The method can be used if a positron beam must be designed, before any optical design has been made. With approximate values for the lens parameters the number of remoderation steps can be calculated. This method is more accurate than the scheme given by Mills[4]. It takes into account that it is more difficult to enhance brightness for a small beam than for a wider beam.

From the definition of brightness of a beam it is possible to deduce the maximum brightness enhancement in one step. To be able to calculate this enhancement, a few numbers must be given. The most important ones are the range of energies in which the positron beam will be operated, and the positron probe size.

First the theory will be given, after which the calculations are done for the Delft micro-beam. The parameters for the Delft beam are a probe size of 100 nm and an energy range from 500 eV to 25 keV. The specimen will be inserted in the specimen chamber of a Philips SEM 535 M of which the spherical aberration of the lenses is one of the parameters in the calculation.

4.2 Theory

To get optimum brightness enhancement the positron beam must be focused to the smallest possible spot size on the remoderation crystal. This focusing must be done by using a lens. The demagnification of the lens can not be too large since for the larger demagnifications the spherical aberration becomes dominant, resulting in an increase of the spot size again and thus a decrease in the current density in the beam, which results in a lower brightness.

It is clear that for the optimum brightness enhancement the spot on the remoderator should be as small as possible, without loosing a single positron between the remoderation foils. The smallest probe size as a function of the demagnification or opening angle can be found by minimizing the spot size given by Eq.(4.2). This yields the minimum half opening angle to be:

$$\alpha_{opt} = \left(\frac{d_p}{C_s}\right)^{\frac{1}{3}} , \tag{4.6}$$

and so

$$d_p = \frac{2}{3}\sqrt{3}\, d_g = \left(\frac{16}{3\pi^2}\frac{I}{BE}\right)^{\frac{3}{8}} C_s^{\frac{1}{4}} . \tag{4.7}$$

When the positron beam is focused on the remoderation foil, the size of the spot from which the positrons are emitted is about the same as the spot size at the front of the remoderation crystal as shown schematically in Figure 4.1.
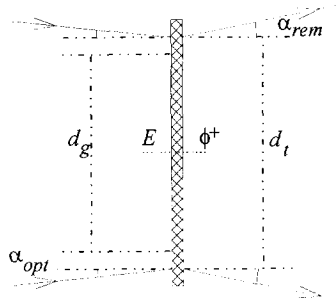
Figure 4.1   Schematic view of the positron beam entering and leaving the remoderation foil.

It is possible to express the new brightness (B_{new}) in terms of the brightness of the incoming beam (B_{in}) by substituting the geometrical spot size d_g of Eq.(4.7) into Eq.(4.1):

$$B_{new} = \frac{\eta(E)\, I_{in}^{\frac{1}{4}} (B_{in} E)^{\frac{3}{4}}}{C_s^{\frac{1}{2}} \frac{\pi^2}{4}\left(\frac{16}{3\pi^2}\right)^{\frac{3}{4}} 2kT} \tag{4.8}$$

In this equation $\eta(E)$ is the fraction of the current I_{in} that is re-emitted. This fraction has been measured by different groups[5,6]. New measurements at the

VEP have been performed and are described in Chapter 3. The results will not yet be used for the remoderation calculations. The re-emitted fraction is a function of the energy of the positrons (E) when they are implanted inside the foil. For the calculations use has been made of the forward re-emission yield measured by Poulsen et al.[6] and of back re-emission yield measured by Chen et al.[5].
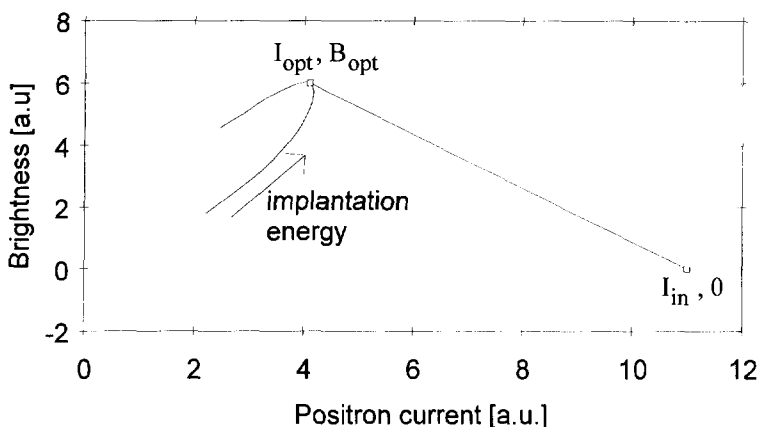
Figure 4.2   Graphical representation of the brightness enhancement merit function. The optimum energy is found where the dotted line is the tangent to the I/B-curve.

To calculate the brightness enhancement, a choice must be made between maximum brightness and maximum number of re-emitted positrons. A merit function has been used in which both the brightness (B_{new}) and the change in positron current $(\Delta I = (1-\eta(E))I_{in})$ is taken into account. The used merit function is given by $B_{new}/\Delta I$. By maximizing this function the optimum implantation energy is found. This maximization can be seen graphically by plotting the brightness versus the current for different implantation energies. The optimum is found at the position where a line from the old current touches the curve as seen in Figure 4.2.

The final brightness is reached after consecutive refocusing of the beam on new remoderators, when the positron beam can be focused into the required spot size in the SEM without loosing positrons on apertures. This optimum must be calculated for all positron beam energies. For lower positron

energies the brightness must be larger because of the larger opening angle of the beam and hence the influence of spherical aberration. So for the lower energies more remoderation steps are necessary in order not to loose positrons on apertures. To optimize for an intermediate energy will give a brightness that is too high for the higher energies where it will give a too low brightness for the lower energies.

The optimum brightness for the positron beam in the SEM is reached when the number of positrons that can be focused in the selected probe is the same as the number of positrons in the beam. The number of positrons in the probe I_{SEM} can be calculated by substituting the spherical aberration coefficient of the SEM, the final beam brightness, the selected probe size and the positron energy in Eq.(4.4). The brightness of the positron beam as it enters the microscope is taken to be the same as the brightness after the last remoderator. In Chapter 7 it will be discussed that the brightness slightly changes in the post remoderation optics. The value of I_{SEM} must be compared with the total number of positrons in the beam (I_{beam}) given by

$$I_{beam} = I_{source} \prod_{i=0}^{n} \eta_i \, , \qquad\qquad (4.9)$$

where I_{source} is the total current from the source, η_i is the efficiency of the ith remoderator, where n is the total number of remoderation steps.

It is clear that the number of positrons in the probe I_{SEM} can never exceed the number of positrons in the beam I_{beam}. During remoderation the positron current in the probe decreases, where the maximum positron current that can be focused in a probe of a certain size increases. Remoderation is useful until the number of positrons in the probe is about the same as the number of positrons in the beam.

It can happen that the number of positrons calculated to be in the probe with Eq.(4.4) is much higher than the beam current calculated with Eq.(4.9). In other words the brightness of the beam is too high. If this might happen, a new choice must be made for the ratio of brightness enhancement and loss of current. The brightness must be less enhanced to gain current in the beam.

Especially in the case of backward remoderation a reduction in implantation energy gives a higher beam current. The same argument can be used if the number of positrons in the probe is just below the number in the beam. By taking a somewhat higher implantation energy the current in the beam will be lower, due to the lower re-emission yield, but since the brightness of the beam is higher an extra remoderation step is not necessary. These small deviations from the optimum enhancement can only be calculated after the aberration figures of the lenses are exactly known.

4.3 Calculation of the number of steps for the Delft positron microbeam

To be able to calculate the number of remoderation steps one needs to know the number of positrons that is re-emitted as a function of the incoming energy. Other important parameters are the optical parameters of the different lenses in the remoderation system and in the SEM. Furthermore the demands on the microbeam must be given. These demands are the probe size, and the positron energy.

In this design the positron energy will be varied between 500 eV and 25 keV. The aimed positron spot size d_p is 100 nm. This spot size includes the spherical aberration and other aberrations in the post remoderation optics. For the remoderation section the spherical aberration coefficients have been estimated to be 5 mm for all sections. The optical parameters of the positron beam are in first approximation determined by the source as seen in Chapter 2 and later determined by the remoderation foils. The starting parameters to do the optical calculations are the starting energy, the opening angle, and spot size. Since the purpose of the remoderation section is to get a smaller spot size, the spot size varies, and will be given for every section.

In Figure 4.3 the results are shown for the calculations for the backward and forward remoderation principle. The number of positrons in the beam after the first remoderation has been estimated in Chapter 2 to be 2×10^9 e$^+$/s. The brightness of the beam is at that position 2.6×10^{-6} A/m^{2}sr eV. The calculations using the backward re-emission numbers as shown in Figure 4.3.a show that a number of 1.3×10^7 positrons per second is possible. The optimum positron implantation energy has been found to be
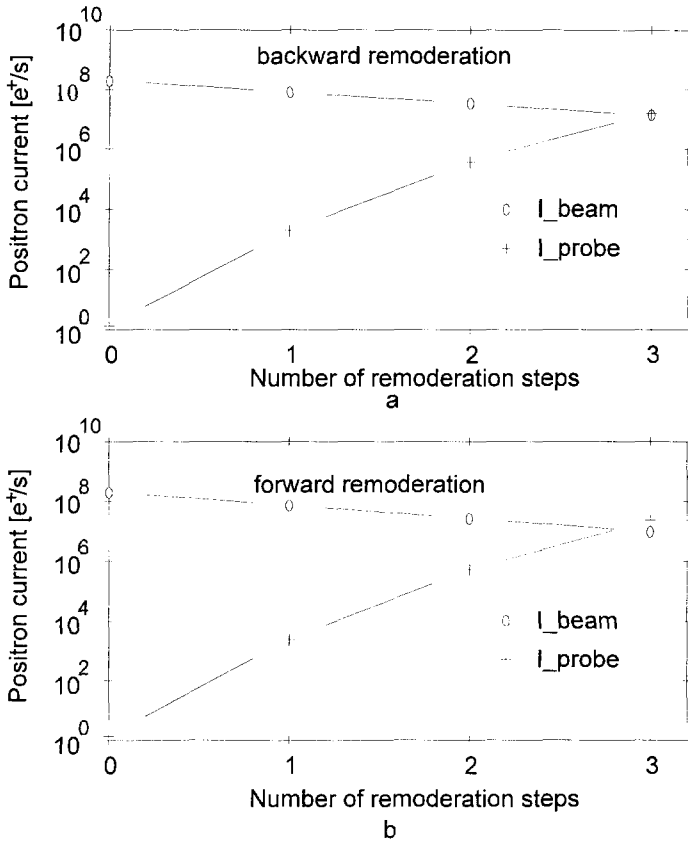
Figure 4.3   Back- and forward re-emission. The current in the beam decreases as a
result of the loss in the foils, the number of positrons in the probe increases
due to the higher brightness.

3000 eV. The total number of positrons per second according to forward
calculations will be 1.0×10^7. Both remoderation principles need three more
remoderation steps. The optimum acceleration voltage, found for forward
remoderation, is equal to 4500 V. The results for the forward remoderation
are shown in Figure 4.3.b.

4.4 Calculation of the final remoderation spot

An important question is what brightness the beam should have after the last remoderator. Or, since all the other terms in the brightness equation are given, what the spot size on this crystal is. This spot size can be calculated since the optical parameters of the post remoderator optics in our case are known.

Since brightness is a conserved quantity, this brightness of the beam must be the same at the specimen in the SEM as when the beam leaves the foil. Since we do not want to loose any particle between the foil and the specimen we can calculate the spot size on the foil using the equation:

$$I_{SEM} = I_{rem}. \tag{4.10}$$

By substituting the probe current given by Eq.(4.4) for I_{SEM} and the beam current given by the brightness of Eq.(4.1) for I_{rem} and using the parameters of the SEM one obtains the spot size on the last remoderator:

$$d_{rem} = \frac{d_{SEM}^{\frac{4}{3}}}{C_{s_{SEM}}^{\frac{1}{3}}} \sqrt{\frac{3}{8} \frac{E_{SEM}}{kT}}. \tag{4.11}$$

With the spherical aberration of the objective lens of the SEM of 2.95 cm, a probe size of 100 nm, and a positron energy of 20 keV, it can be found that the spot size on the last remoderation foil should be 800 nm.

4.5 Discussion and conclusions

With the method described in this chapter it is possible to calculate the number of remoderation steps. This method helps to estimate the number of remoderation steps necessary to reach a given resolution. The method is more important in the case of backward remoderation than in the case of forward re-emission. The reason for this is that in the case of transmission

remoderation, the optimum energy is found close to the maximum re-emission yield. In the case of backward remoderation, the re-emission yield is decreasing continuously with increasing implantation energy, and therefore the optimum energy can not be derived directly without using the derived algorithm.

The influence of the chosen spherical aberration coefficient has not been treated in this chapter. It is possible to calculate the number of steps for a theoretical lens system with no spherical aberration. In that case the optimum demagnification is found where the opening angle becomes exactly $\pi/2$. In that case still two remoderation steps are necessary, at least as long as the SEM is used as the probe forming instrument. For larger spherical aberrations more remoderation steps will be necessary. For too high spherical aberration it might even be impossible to reach the situation where the probe current is equal to the current in the beam.

With the SEM as the probe forming instrument and the nuclear reactor as the positron source, it can be derived that three extra remoderation steps are necessary to enable positron analysis with a sub-micrometer probe size. In this design the result of the four stages of remoderation is a possible spot size of 100 nm with 10^7 positrons per second. Since the number of positrons is almost the same with both methods, the forward remoderation principle has been chosen, since the optics will be less difficult[7,8]. In that case the optimum positron implantation energy will be 4500 eV.

The optimum brightness has been chosen for one single energy. But since the energy of the positrons is changed, the number of positrons in the probe changes as well. The energy can be chosen arbitrarily. In this case the energy is chosen to be 20 keV, the number of positrons as function of the positron energy is shown in Figure 4.4. To get the same amount of annihilation photons in the peak for all energies the measuring time must be adapted to it.

In the figure we can distinguish two regions: region I, in which the positron current changes linearly with the energy, and region II, in which the number of positrons per second is a constant. This break in the figure is at the position where the beam just fills the beam limiting aperture that can be used. Another possibility, is not to use apertures, but to let the probe size vary.
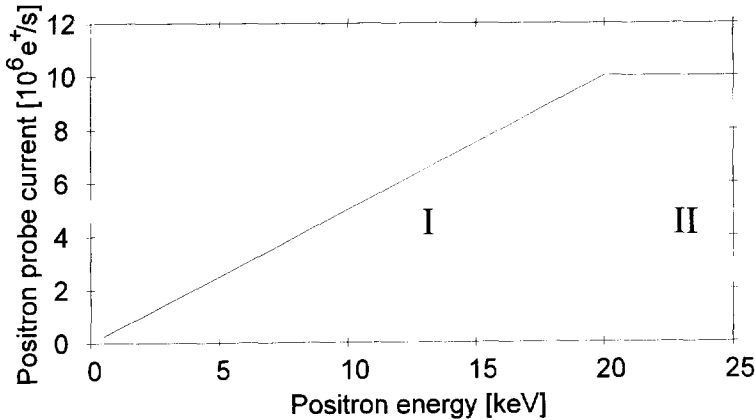
Figure 4.4   Positron current as a function of the positron energy for a constant probe size optimized for an energy of 20 keV.

This would mean that the probe size for the lower energies is larger than the optimized probe size, and obviously the probe size for the higher energies will become smaller.

Further enhancement of the brightness of the positron beam can not be found in the improvement of the lenses of the remoderation section but in the positron source and transport section.

References

1.   L. Reimer in *Scanning Electron Microscopy*, (Springer Verlag, Berlin, 1985)

2.   A.P. Mills Jr., Appl. Phys. **23**, 189, (1980)

3.   G.R. Brandes, K.F. Canter, and A.P. Mills Jr., Phys. Rev. Lett. **61**, 492, (1988)

4.   A.P. Mills Jr. in *Proceedings of the 85th Summer School of Physics on Positron Solid State Physics*, eds. W. Brandt, and A Dupasquier, (1982), p. 432

5.   D.M. Chen, K.G. Lynn, R. Pareja, and B. Nielsen, Phys. Rev. B **31**, 4123, (1985)

6.   M.R. Poulsen, M. Charlton, J. Chevallier, B.I. Deutch, F.M. Jacobsen, and G. Laricchia, *Positron Annihilation*, Proc. of the 8th Int, Conf. on Positron Annihilation, eds. L. Dorikens-Vanpraet, M. Dorikens, and D. Segers, (World Scientific, Singapore, 1989), p. 597

7.   K.F. Canter, G.R. Brandes, T.N. Horskey, P.H. Lippel, and A.P. Mills jr., in *Atomic Physics with Positrons*, eds. J.W. Humberston and E.G.A. Armour, (Plenum, New York, 1987), p. 153

8.   K. Uhlmann, D.T. Britton, and G. Kögel, Optik **98**, 5, (1994)

5 Optical design of the remoderation sections

Summary

In this chapter the calculation of the last three remoderation sections is treated. The spot on the last remoderator is 800 nm. This size is chosen in a way that the spot on the specimen inside the SEM can be 100 nm. The demagnification of the last section is about 14 times. This results in a spot on the one but last remoderator of 12 μm. With a demagnification of 21 times, this results in a spot on the second remoderator of 0.25 mm. The calculation of the second remoderation section has been performed in a design that will not be the definite design. The calculation starts with a total spot of 10 mm, the starting spot on the first remoderator. This means that the positron source should be demagnified 10 times. The spherical aberration is in each section the most important aberration. With a typical system of two lenses it is possible to minimize the contribution of the other geometrical aberrations. This method has been called coma compensation, since coma would be after spherical aberration the most influencing aberration in the remoderation system.

5.1 Introduction

As described in Chapter 2, the positron beam is guided in a hybrid system of electrostatic lenses and magnetic coils out of the reactor. This positron beam has such a low brightness that it is impossible to focus that beam into a spot of 100 nm without loosing too many particles on apertures. Therefore, the brightness of the beam must be enhanced.

The beam design is based upon forward remoderation. The positrons are emitted at the opposite side of the crystal. The advantage of this design is that the secondary beam does not go through the strong lens fields in which the primary beam is focused. The disadvantage is the somewhat lower reported re-emission yield with respect to the yield for backward re-emission. The re-emitted positrons are guided from one remoderator to the next by electrostatic fields. Electrostatic lenses are used to focus the beam to the smallest possible spot sizes. Finally the brightness of the beam will be high enough to get all the remaining positrons in a spot size of 100 nm, the smallest possible spot size usable for defect analysis.

The first remoderation step will take place just outside the blockhouse as described in Chapter 2. After this step the beam will be transported over some distance to get it close to the Philips SEM 535. Just in front of this microscope three more remoderation steps are performed. After the last remoderation step the brightness of the beam will be high enough to get all the remaining positrons in a spot of 100 nm for energies larger than 20 keV. Before the probe can be formed on the specimen, the beam has to be deflected onto the optical axis of the SEM. For this reason a 90°-deflector has been built in the emission chamber of the SEM. The design of this deflector and the transport optics are discussed in Chapter 7.

In the previous chapter it was shown that the spot size on the last remoderation foil must be 800 nm. The spot size on the first remoderation foil is in the order of 10 mm. So the three remoderation sections described in this chapter will have a total demagnification of 12500 times. In Chapter 4 it was also shown that the positron energy must be 4500 eV.

In this chapter the optics for the remoderation system is described. In 5.2 the basic optics necessary for brightness enhancement of the positron beam, are summarized. In the next part the design method is discussed. The fourth section discusses the optical realization of the lenses, starting with the last remoderation section. The mechanical realization of the lenses will be discussed in Chapter 6. This will be in combination with the demands on the vacuum chamber.

5.2 Optics

The best way to realize brightness enhancement is to focus the beam to the smallest possible spot. In a system where spherical aberration is the most important aberration, the brightness enhancement can be calculated quite easily[1]. The total spot size is the sum of the geometrical spot size(d_g) and the aberration disc(d_a) in the plane of best defocus according to:

$$d_p = \sqrt{d_g^2 + d_a^2} \ . \tag{5.1}$$

In the case where only spherical aberration is important d_a equals $0.5C_s\alpha^3$. Now it can be found that the new brightness (B_{new}) can be calculated from the brightness of the incoming beam (B_{in}), as was shown previously in Chapter 4, according to:

$$B_{new} = \frac{\eta(E) I_{in}^{\frac{1}{4}} (B_{in}E)^{\frac{3}{4}}}{C_s^{\frac{1}{2}} \frac{\pi^2}{4} \left(\frac{16}{3\pi^2}\right)^{\frac{3}{4}} 2kT} \ , \tag{5.2}$$

in which η is the fraction of re-emitted positrons, I_{in} is the incident positron current, E is the energy of the primary positrons, C_s is the coefficient for spherical aberration, and T is the temperature of the remoderation crystal. For small beams it can be found that indeed spherical aberration is the most important one. In that case the smallest probe size can be found at a distance $0.75\ C_s\alpha_i^2$ in front of the focus plane. This way not a true image of the source is obtained, but the aim is to get as much current in a spot as small as possible.
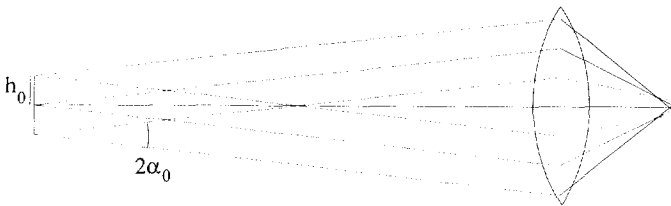

h_0

$2\alpha_0$

Figure 5.1   Remoderation section with only a demagnifying lens

The simplest way to design a lens system for this purpose is by having an accelerating section combined with a demagnifying lens. Important factors are the demagnification and the spherical aberration. A schematic example is

given in Figure 5.1 The parameters of the beam are given by the begin distance to the optical axis h_0 and the initial half opening angle α_0.

If h_0 becomes larger not only spherical aberration but also the other geometrical aberrations are important. In that case, the new brightness can not be found using the above given simple formulae. All geometrical aberrations are the result of rays coming in high in the lens, due to a larger opening angle α_0 and/or a larger object size h_0. The other aberrations are coma, astigmatism and curvature of field, and distortion, of which the aberration disks are respectively given by $MC_{co}\alpha_0^2 h_0$, $MC_{cu+as}\alpha_0 h_0^2$, and $MC_{dist}h_0^3$ and Eq. (5.1) gives:

$$d_p = M\sqrt{d_0^2 + \frac{1}{4}C_s^2\alpha_0^6 + C_{co}^2\alpha_0^4 h_0^2 + C_{cu+as}^2\alpha_0^2 h_0^4 + C_{dist}^2 h_0^6} \quad . \tag{5.3}$$

In this formula, the aberration coefficients (C_x) are all related to the object side of the lenses i.e., the figures are a function of the magnification, the initial opening angle and the size of the object. For the spherical aberration also the coefficient related to the image side has been used so in that case the magnified opening angle and spot size must be used. It can be found that of the other geometrical aberrations coma is the most important. To be able to do efficient remoderation, this aberration must be minimized.
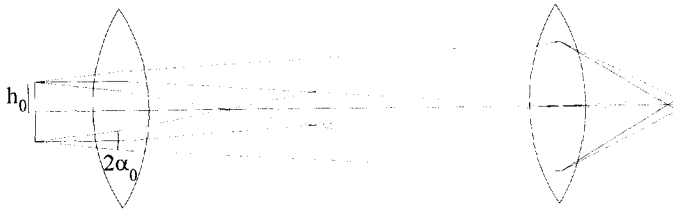

Figure 5.2   Extra lens in the remoderation section causing the rays coming in symmetrically around the optical axis. As a result the geometrical aberrations are lower.

A way to minimize coma is to get a lens in front of the demagnifying lens as shown in Figure 5.2. The lens must have its focal plane in the demagnifying

lens. In this way the rays are going symmetrical through this lens, almost independent of the height of the ray in the object. This coma compensation method works also for the other geometrical aberrations, but since these other aberrations are less important, this technique will be called coma compensation.

5.3 Design method

In this paragraph the design method for the remoderation section is discussed. After the decision to use thin foils for transmission remoderation in combination with electrostatic lenses, a system was designed with optimum optical properties, such as spherical aberration. For having small aberrations, the focal distances of the lenses were kept small. As a result the lens system could be kept short. A logical choice is to have the demagnifying lens close to the demagnified probe. In that case it can be predicted that coma would be an aberration that influences the spot size. For a small diameter beam, the rays come in at a distance of $z_o\alpha_o$ from the axis. In the case of an opening angle of a few milliradians and an object distance of a few millimeters this is in the order of 10 μm. If the size of the object is in the same order of magnitude, the other geometrical aberrations and in particularly coma, become important.

As explained before coma can be minimized by using an extra lens in the system. By optimizing the excitation of the coma compensating lens, a best focus can be found. Since also the spherical aberration may change with a different setting of this electrode, the optimum magnification also changes. The magnification was found by an iterative design process in which systems with different lengths and thus with different magnifications were optimized. In this design the shape of the electrodes has been kept as simple as possible. The distance between the electrodes has been optimized with keeping in mind that too strong electrostatic fields may cause discharges. The bore of the electrodes and the distance between the electrodes determine both the strength of the lens and the spherical aberration. The shape of the electrodes was optimized before the optimum magnification was found. Significantly better lenses could not be obtained, without changing the basic setup after the iterations.

The electrostatic fields of the lenses have been calculated by using the program package ELD[2]. With this program it is possible to calculate two-dimensional electrostatic fields with high accuracy. Through these fields positron trajectories were calculated with the use of a precise ray trace program TRASYS[3]. From these rays it is possible to calculate the aberration figures. These figures were compared with the output of the program LENSPROP[4], which also uses the output of the ELD-program as input. It calculates from the axial field the optical parameters like focal distances, and aberration coefficients of a given lens system.

The different remoderation sections are described in reverse order, starting with the section in which the smallest probe of 0.8 μm is formed, followed by the third section. At the end the second remoderation section will be described. The first remoderation step is already discussed in Chapter 2 as it is not part of the positron microbeam.

5.4 Lens systems

5.4.1 Final remoderation section
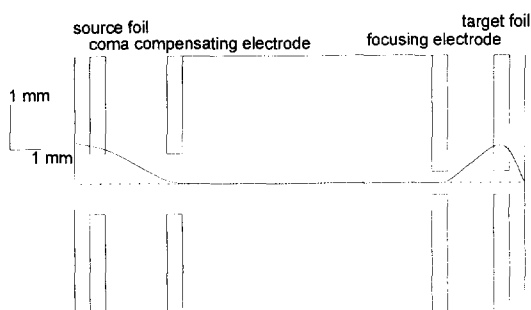
Figure 5.3   Calculated lens design, the figure is not to scale. The total length is 14.6 mm, where the diameter of the smallest holes is 0.5 mm. In the figure the axial potential has been drawn.

In this section the remoderation part is described. The positron beam will have a probe diameter of 0.8 μm. To get the largest demagnification, a lens must be found with C_s as small as possible. Besides this, the coma and other geometrical aberrations must be compensated for. The setup of the lenses can

be seen in Figure 5.3. The setup shows two foils with three electrodes in between. The potential on the middle electrode is in the calculation kept constant on the final potential which is relatively to the source foil -4500 V, giving the optimum implantation energy of 4500 eV as found in Chapter 4. The first electrode with the source foil and the middle electrode form the coma compensating lens. The potential on this electrode has been varied to get optimum coma compensation. The middle electrode with the last electrode and the target foil form the demagnifying lens.

In Figure 5.5 the spot sizes are shown that have been calculated with the aberration coefficients that are shown in Figure 5.4. These coefficients have been calculated with the program LENSPROP. In the figure the aberration coefficients all have their own unit, viz. C_s(spherical aberration): [mm], C_{co}(coma): [no dimension], C_{cu+as}(curvature of field combined with astigmatism): [mm^{-1}], and C_{dist}(distortion): [mm^{-2}]. The optimum potential on the coma compensating electrode is found to be about -440 V relative to the source foil. The potential on the focusing electrode is in that case -403 V. As seen before in the case of a spherical aberration determined system, a defocus can be advantageous. In the calculations of the spot size as shown in Figure 5.5 this defocus is also calculated.
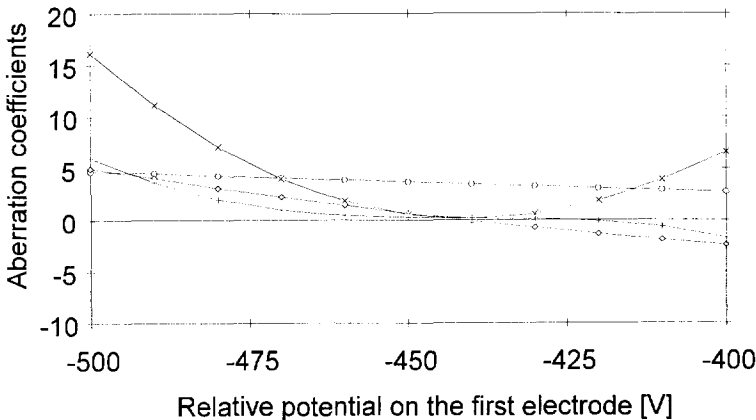

Figure 5.4   Aberration coefficients of the last remoderation section (C_s:□, C_{co}:◊, C_{cu+as}:× and C_{dist}:+) as a function of the potential on the first electrode.
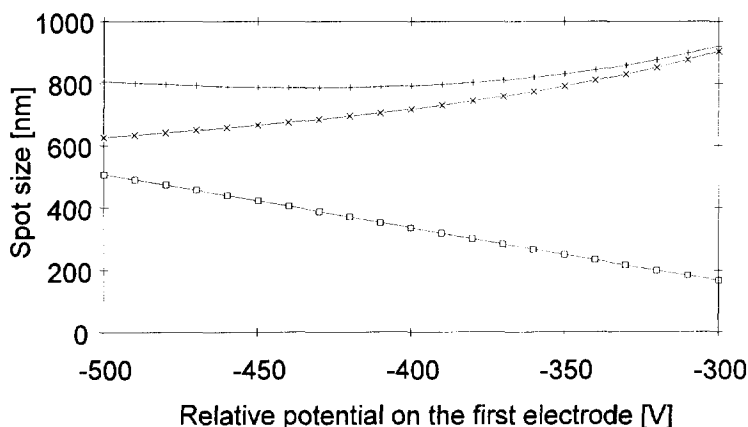
Figure 5.5   Total spot size(+), geometrical spot size(×) and spherical aberration spot size(□) as function of the potential on the first electrode of the last remoderation section.

The spherical aberration coefficient related to the object plane for the combination of the two lenses is 3.523 mm, related to the image plane it is 3.734 mm. From this number it follows, via the optimum opening angle that has been found in Chapter 4, that the demagnification should be 18 times, and so the spot size on the left foil can be 12 μm. With this starting spot size, the resulting spot size is little smaller than the aimed total spot size (d_p) of 800 nm. The resulting spot size of 780 nm consists of two contributions, the demagnified spot (d_g) of 656 nm equal to 12 μm $\times M$ and the spherical aberration disk (d_s) of 405 nm.

With the found values for the potentials on the electrodes, an accurate ray tracing has been performed. Figure 5.6 shows the traces through the lens system that has been drawn in Figure 5.3. The traces come from the outer area of the source foil with five different opening angles viz. 0, $\pm\frac{1}{2}\alpha_0$, and $\pm\alpha_0$, in which α_0 is the maximum opening angle. Also, ray traces coming from the axis are shown.

The result of these calculations are a geometrical spot of 660 nm and a spherical aberration spot of 470 nm, comparable to the results obtained with the LENSPROP program. So it can be concluded that with the given potentials both calculations give a system in which the beam gets its smallest diameter
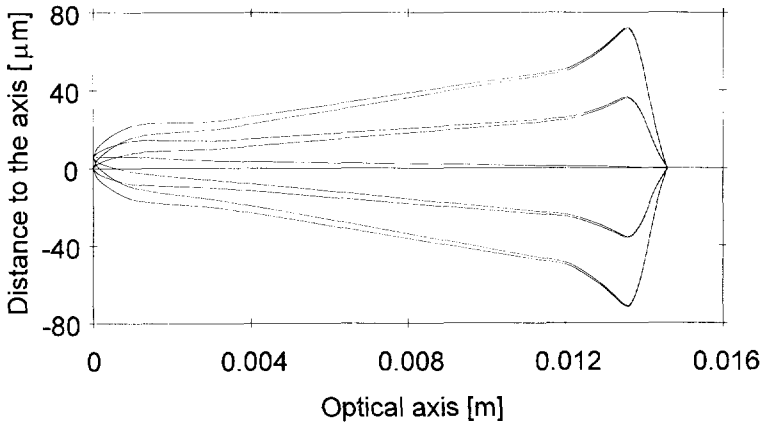
Figure 5.6   Traces through the lens system of Figure 5.3. The traces starting parallel to
               the optical axis cross the optical axis at the second lens.

when the size of the object is the optimized 12 μm. The difference between
the LENSPROP calculation and the ray tracing is the way the two add up.
According to the theory on probe formation described by Barth and Kruit[5] it
can be found that quadratic addition of the two fractions would result in a
total spot of 810 nm with all the positrons in it. According to the ray tracing
the two contributions have to be added linearly resulting in a larger spot size.

After ray tracing of many particles, an impression about the fraction of
positrons in the spot can be obtained. Therefore, ray traces have been
performed with 10000 randomly chosen particles uniformly distributed in
position and opening angle. From the calculated end positions of the rays, a
distribution profile has been calculated that is shown in Figure 5.7. The
figure shows that over 80% of the current is inside a spot of 800 nm. Doing
the calculation in this way gives an error in the profile since the source
profile is not a uniform distribution. But since the beam profile as the beam
emerges from the reactor is not known yet (both distribution of positions and
opening angles), doing calculations with any other profile does not make the
calculation more clear. On the other hand it can be said that in any case the
fraction of positrons inside the spot is at least the found 80%.

As a final check whether the calculations give the optimum results, the
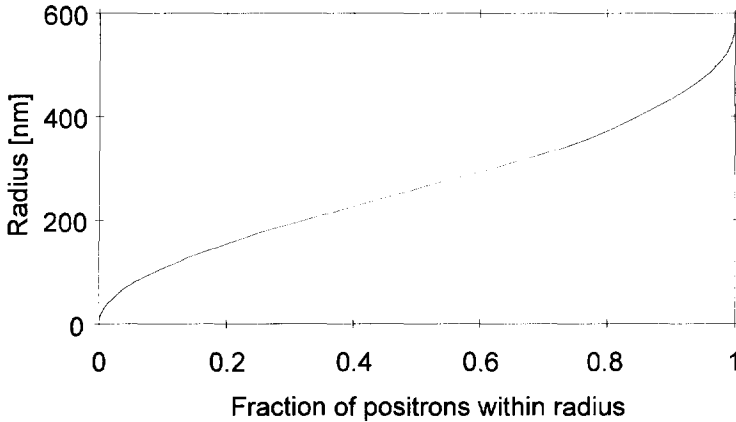calculations have to be checked with the theory described in Chapter 4. In

Figure 5.7   Relative number of positrons that is found inside the radius. At a radius of
              400 nm 15% of the positrons is outside the radius, or 85% is inside this
              radius.

that chapter it was found that the optimum opening angle at the image side
was given by $(d_p/C_s)^{1/3}$. This optimum opening angle must be equal to $\alpha_0 M_\alpha$.
The different values found with LENSPROP are C_s equal to 3.734 mm, and
M_α equal to -0.3755. Combined with a starting opening angle of 0.16 rad,
and a spot size of 800 nm this results in an optimum opening angle of
59.8 mrad and a calculated opening angle of 60.1 mrad. Since the optimum
is not too steep, small deviations, like this one, do not give a different spot
size. The other demand on the optimum is that the total probe size is equal to
$2/3\sqrt{3}$ times the geometrical spot size. The calculated geometrical spot from
LENSPROP is equal to 674 nm, resulting according to the theory in a total
spot of 778 nm, little less than the calculated spot of 786 nm. So to be in the
real optimum the magnification should be little more than the magnification
of the designed lens system.

In this section coma compensation was not necessary, the influence of coma
in a system like this one is small. However, the use of the extra lens is
beneficial, since the acceleration lens in this design was optimized.

5.4.2 Third remoderation section

In the previous section it was shown that the spot size on the third remoderator can be 12 μm. The principle of this remoderation section must be the same, a demagnifying lens in combination with a coma compensating lens. If a lens with the same spherical aberration coefficient can be used, the demagnification can be larger since the final opening angle is proportional to $d_p^{1/3}$. Thus the demagnification can be larger, resulting in a larger brightness enhancement. On the other hand, larger beams require lenses of which the bore is larger, with the result that the spherical aberration will be larger, resulting in a smaller increase in brightness enhancement. The coma compensation in this section is more important since the size of the object is larger.
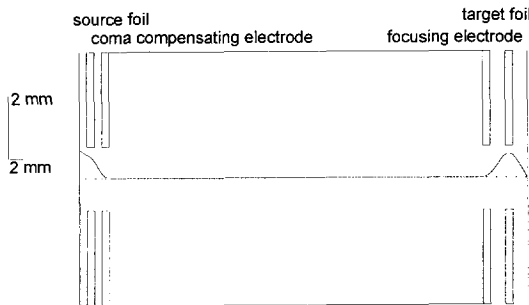
Figure 5.8   Calculated lens design. The figure is not to scale. The total length is 60 mm where the diameter of the holes is 2 mm. In the figure a possible axial potential has been drawn.

The setup of this section is shown in Figure 5.8. Its resemblance with Figure 5.3 is clear, a coma compensating lens together with a demagnifying lens. In the figure a possible axial potential has been shown. The length of this section is a little longer than the previous one, since the demagnification is larger, also the distance between the different electrodes is larger, resulting in a longer focal distance. The electrostatic field of this arrangement has been calculated with the ELD-program package. The obtained field was used to calculate the geometrical aberrations with the program LENSPROP. The results of this calculation are shown in Figure 5.9.

Figure 5.9   Aberration coefficients of the third remoderation section (C_s:□, C_{cc}:◊, C_{cu+as}: × and C_{dist}: +) as a function of the potential on the first electrode.

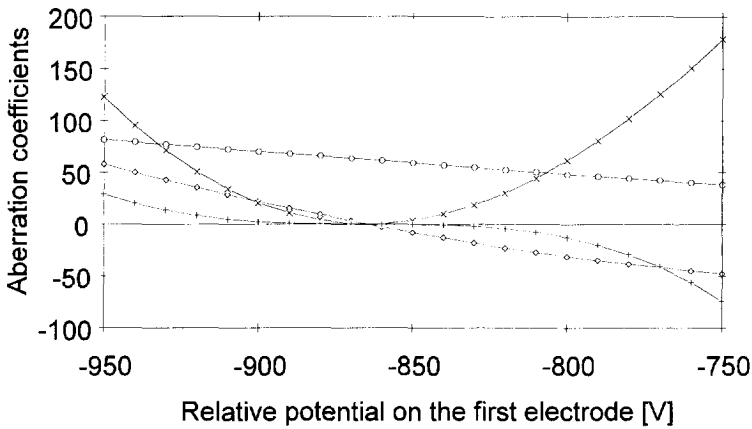It can be seen that it is possible to compensate the geometrical aberrations other than spherical aberration completely. The results of the LENSPROP calculations are that with a relative potential of -870 V on the first electrode a good compensation can be achieved. The potential on the last electrode is here -615 V. Figure 5.10 shows the calculated spot sizes. The demagnification in the optimum setting of the lenses is 23 times, resulting in an object size 0.25 mm. The spherical aberration related to the image side is 23.92 mm. this gives a spherical aberration disk of 5.62 μm. Quadratic addition of the two contributions gives a total spot of the aimed 12 μm.

With the values from the LENSPROP calculations for the potentials on the electrodes, ray tracing was performed. The traces did not show coma compensation. The zero opening rays did not go through the center of the demagnifying lens. By changing the potential on the first electrode to a value of -930 V the coma compensation was complete as the rays in Figure 5.11 show. With -615 V on the last electrode, it is possible to get a 100% spot of 12 μm. The contributions to this spot are a geometrical spot of 9.95 μm and a spherical aberration spot of 1.7 μm.

Figure 5.12 shows the distribution of the positrons over the spot of the third remoderation foil. It can be seen that according to ray tracing, the total
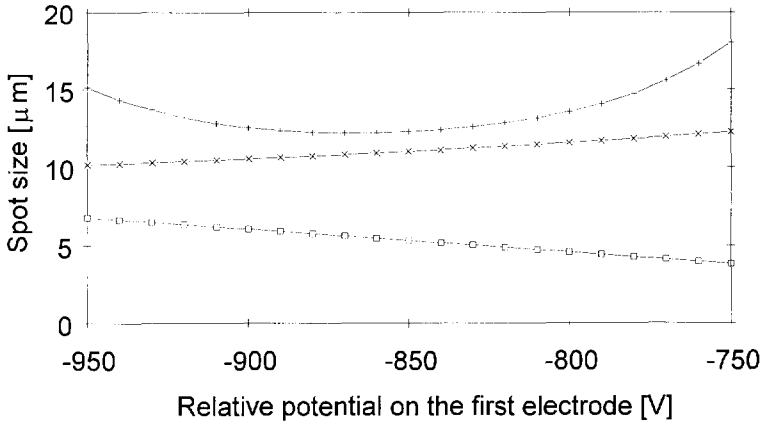
Figure 5.10   Total spot size($+$), geometrical spot size($\times$) and spherical aberration spot size($\square$) as function of the potential on the first electrode of the third remoderation section.
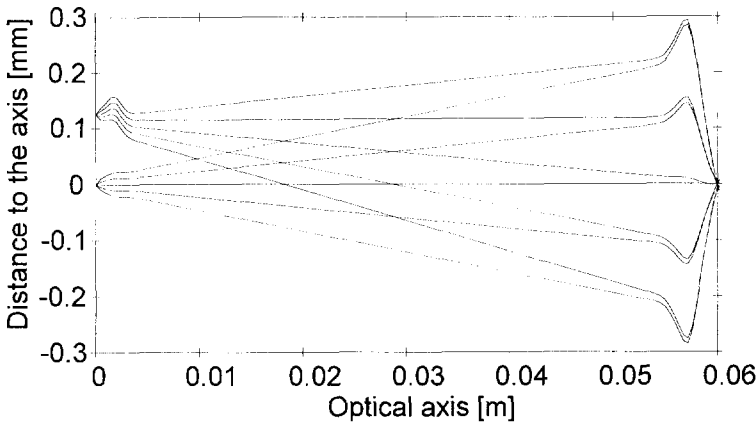
Figure 5.11   Trace through the lens system shown in Figure 5.8. The potentials on the electrodes are different from the with LENSPROP calculated values.

current can be found within a radius of 6 μm.

The conclusion of this part must be that although the two programs give a different result, the positron spot on the remoderator can be kept small enough. The different spot contributions are not optimally chosen in the case of the ray tracing calculations. With the LENSPROP value for C_s the theoretical opening angle is 79.6 mrad. The calculated opening angle is
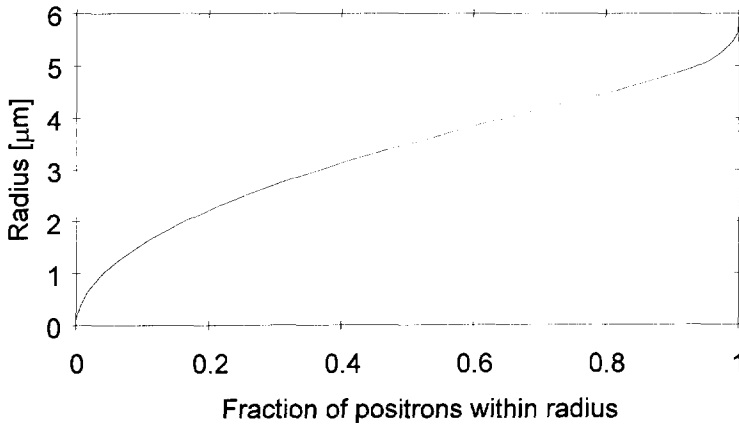
Figure 5.12   Relative number of positrons on the third remoderation foil within a radius.
At a radius of 6 μm 100% of the positrons can be found in this spot.

78 mrad, and is in good agreement with this optimum. Also the opening angle after the ray tracing is in good agreement, the found opening angle is 84 mrad. From these calculations it can not be said what the exact values for the potentials are. Another calculation method[6] or measurements will give the answer to this question.

The difference can be due to the fact that LENSPROP only uses the axial potential for the calculation of the aberration coefficients; small errors in the calculation may give larger errors for the off-axis properties. Condensing of the calculation mesh of the ELD-calculation showed only a small change in the optimum potential on the first electrode, not far enough for agreement with the TRASYS output. Another possibility due to the disagreement can be the parameterization of the fields close to the axis as used by TRASYS. A new parameterization, resulting in high accuracy tracing off-axis, is now being developed[7].

5.4.3 Second remoderation section

Since the positron beam has not been realized yet, it is not possible to design a fully optimized remoderation section. The remoderation section described here is a possibility that can be used in combination with a source of 1 cm

diameter, or with an intermediate image at that position. In that case it must be noted that the calculations performed do start with the kinetic energy of 2 eV, which is the work function of the remoderator. In that case, the positrons in the intermediate image have already been accelerated and thus the opening angle or the intermediate image has been reduced.
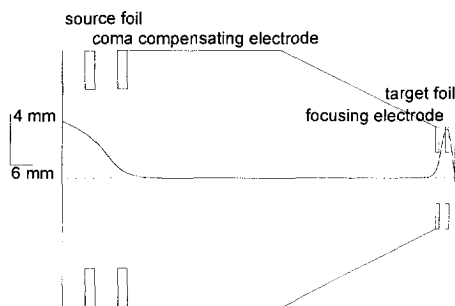
Figure 5.13   Lens design of the second remoderation section. The length of this section is 121 mm. The diameter of the smallest electrodes is 4 mm. In the figure an axial potential has been drawn.

Figure 5.13 shows the configuration that has been used for the calculations. In case of an intermediate image the changes to the design should be to put some more electrodes between the two foils. In that way the positron beam is transported over larger distance without any magnification or demagnification. The figure also shows a calculated axial potential like the other figures with calculated configurations.

Ray tracing through this field has not been done, since the precise configuration is yet not ready and ray tracing with estimations of the starting positions and angles does not give more information than the parameter calculations. An estimate of lens properties has been made with the LENSPROP program. To be able to get a beam with a starting radius of 5 mm through the system large radius electrodes are necessary. As a result the spherical aberration (related to the object side) is again larger. Figure 5.14 shows the values of the different aberrations; the spherical aberration coefficients are scaled a factor of 100. In the optimum, where the other aberrations are nearly zero, the spherical aberration coefficient related to the object side equals 1.3 m.
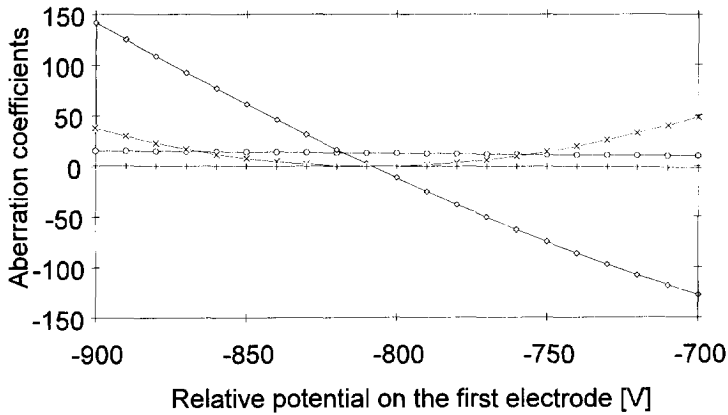
Figure 5.14   Aberration coefficients of the second remoderation section (C_s:□, C_{cu}:◊, C_{cu+as}:× and C_{dist}:+) as a function of the potential on the first electrode.
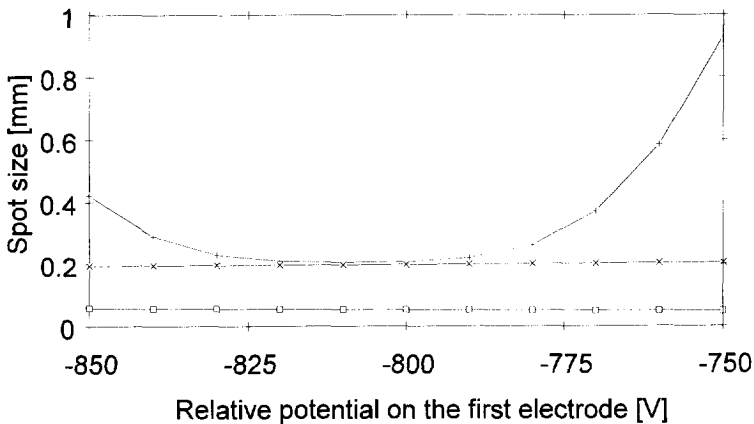
Figure 5.15   Total spot size(+), geometrical spot size(×) and spherical aberration spot size(□) as function of the potential on the first electrode of the second remoderation section.

With these aberration coefficients the different contributions to the total spot size have been calculated. Figure 5.15 shows the two main contributions to the total spot size. The geometrical spot size is equal to about 200 μm and the spherical aberration disk is equal to 54 μm. By quadratic addition of these two contributions, a total spot of 207 μm has been found.

Next to the optimum setting of the first electrode it can be seen that the other geometrical aberrations contribute to the total spot, where in the optimum the spot size is mainly determined by the geometrical spot. In the above described remoderation sections the magnification was optimized to get a partly spherical aberrated spot. In this section this would also cause an increase in the other geometrical aberrations. To be able to correct for a less optimized beam, there is still some room for some aberrations. In the design of the remoderation section only the last electrode and the target foil will be described. The other parts of the beam will take place when experimental results on the optical properties of the beam are known.

5.5 Discussion and conclusions

Table 5.1 Optical parameters of the remoderation sections

		LENSPROP						TRASYS	
	d_0 [μm]	C_s [mm]	C_{co} [ ]	$1/M$	d_p [μm]	d_g [μm]	d_s [μm]	d_g [μm]	d_s [μm]
last	12	3.52	0.0275	17.8	0.78	0.67	0.40	0.66	0.47
third	250	63.4	3.14	23.1	11.5	10.8	5.6	10	1.7
second	10^4	1334	2.52	50.5	207	200	54		
first	10^5			10	10^4				

It has been shown that it is possible to go from a spot with a diameter of 10 mm to a spot smaller then 1 μm in 3 remoderation steps. The most important optical parameters related to the object side of the different remoderation systems are summarized in Table 5.1. With some room for different settings or unwanted errors in practice, it is possible to demagnify the positron beam from 10 mm into a probe of 100 nm within three remoderation steps.

The strong electrostatic immersion lenses give spherical aberration small enough for not having too much difficulty in reaching the smallest necessary spot in three steps. The influence of coma and other geometrical aberrations is more difficult to compensate for in the larger diameter beams. The first remoderation section is not part of the section described here. In this section it must be possible to reach a spot of 10 mm. The transport of the positron beam to the remoderation section is at this moment unknown, a dummy calculation has been given showing that it is possible to demagnify the 10 mm spot into a spot of 0.125 mm. Also in this step it is possible to optimize a configuration of which the geometrical aberrations could be kept to only spherical aberration.

References

1.   L.J. Seijbel, P. Kruit, A. van Veen, and H. Schut, Mat. Sci. Forum **105-110**, 1977, (1990), this thesis Chapter 4

2.   B. Lencova and G. Wisselink, Nucl. Instr. & Meth. A **298**, 56, (1990)

3.   J.E. Barth, B. Lencova, and G. Wisselink, Nucl. Instr. & Meth. A **298**, 263, (1990)

4.   J. Chmelik, Internal report of the Institute of Scientific Instruments of the Czechoslovak Academy of Sciences, 1989, not published

5.   J.E. Barth, and P. Kruit, submitted to Optik

6.   e.g. E. van der Steen, Second order electrode method, version 2.0 Delft Particle Optics Foundation

7.   J. Chmelik, and J.E. Barth, Charged Particle Optics, SPIE **2014**, San Diego (1993), eds. W.B. Thompson, M. Sato, and A.V. Crewe

6 Mechanical design of the remoderation sections

Summary

The construction of the remoderation section is treated in this chapter. Severe demands on the fabrication are necessary to get an accurate system of electrodes and foils. The electrodes should be parallel to each other, and almost perfectly aligned. The construction method that has been chosen for is to string the electrodes on a needle. By putting dummy plates between the electrodes, the parallelism is conserved. Glass bars are molten to the electrodes to make a fixed system. The foils are clamped between stainless steel plates that are also molten to the glass bars. The vacuum chamber is made of mu-metal to minimize the influence of magnetic stray fields.

6.1 Introduction

In the previous chapter we have seen the optical design of the lenses of the remoderation section. The electrodes and foils that are used to form these lenses are in general close to each other. The biggest problem is to insulate one electrode from another. The differences in high tension are of the order of 5000 V. The most important aspects are flashovers across solid insulators. It was found that the breakdown voltage is proportional with the square of the length of the insulator[1]. For 5 kV the length must be in the order of 1 mm, where the distance between the electrodes is in that same order. Another aspect that is important is that the electrodes are parallel to each other, and that the bores of the electrodes are on a straight line.

In the calculations in the previous chapter it was assumed that there are no disturbances in the remoderation system. Stray magnetic field may disturb the action of the lenses in the system. Both DC- and AC-fields can cause these disturbances. This is the most important in the last remoderation section, where the probe size is small and thus the influence is relatively large. To be able to get rid of the stray fields a mu-metal vacuum chamber has been constructed. This chamber also ensures a good vacuum necessary to maintain the re-emission properties of the remoderation foils.

In this chapter first the construction of the lens system is presented, followed by a discussion on the realization of the vacuum chamber. An overview of the

complete vacuum setup of the positron beam will be given in this chapter. The transport lens and the SEM as discussed in the next chapter are also part of this setup.

6.2 Realization of the lens system

6.2.1 Setup of the electrodes

The easiest way to construct the lenses is to enclose the electrodes in glass. The materials used for this are non magnetic. Tantalum plate has been used for the thin electrodes of 0.5 mm, for the other electrodes, non-magnetic stainless steel 316 has been used. To these electrodes molybdenum ears have been spot welded. Molybdenum has been chosen since it has a linear expansion corresponding to the type of glass that has been molten to it. To have the glass fitted to the metal as good as possible, the molybdenum was first cleaned after which the glass was put to it in an oven. To the electrode the ears are spot welded. An example of such an electrode can be seen in Figure 6.1.
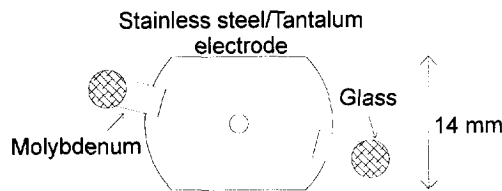
Figure 6.1   Example of a non-magnetic electrode with Mo-ears spot welded to it. On the ears a drop of glass has been put to enable connection to glass bars.

Since the holes in the electrodes become smaller coming from the positron source to the SEM, it is possible to put a needle through all electrodes that fits as closely as possible. The fit for the smallest holes is better than 0.05 mm, so will be the mechanical misalignment. The effect of the misalignment is the largest for the focusing lens of the last remoderation section. This misalignment can be neglected as long the misalignment is less than the filling of the lens. In Chapter 5 it was shown in the ray tracing that the filling of the lens is 80 μm.

The roundness of the holes must be of the order of 0.001 mm. This accuracy

can be reached by spark erosion of the holes. This accuracy enables a mechanical astigmatism that is below the maximum astigmatism allowed. The difference in lens strength is now in that same order. So the unroundness of the probe on the last remoderator is better than 100 nm.
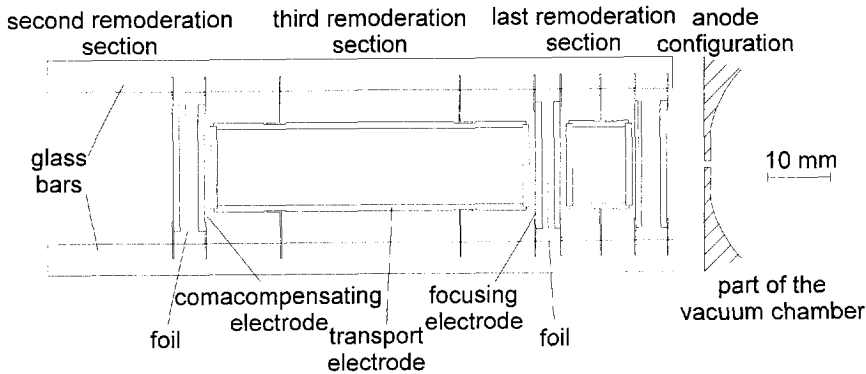
Figure 6.2   Complete electrode setup. The remoderation foils are shown without clamps. The setup consists of two complete and one incomplete remoderation section and the anode section.

In Figure 6.2 the complete setup is shown with all electrodes. The foils are not shown since these will be positioned after the complete setup is made. The figure also shows the anode configuration that will be discussed in Chapter 7. This accelerating section of the positron beam is part of this section since the last foil is part of this lens.

The distance between the electrodes was kept by putting dummy plates between the electrodes. When all the electrodes and dummies were strung on the needle, the glass bars were molten to it, making an unmovable system. After the needle was taken out, the dummy plates were removed. To check whether the system was still in position the needle was put back in position without having to put any force on it. So it can be concluded that during the cooling of the glass bars, there was no tension between the bars and that the system is as good aligned as it was before the glass bars were put on to it.

6.2.2 Mounting of the foils

As described in Chapter 3 of this thesis, the 100 nm thick foils were connected to the lens system via a thicker 7 μm tungsten foil. In the foil a hole has been made that it as small as possible. The size of the hole is determined by three demands. The first one is the size of the positron probe on the thinner foil. Obviously, the hole in the foil must be larger than the probe size. The second demand is that it must be possible to put the hole on the optical axis. It is not necessary to position the center of the hole exactly on the optical axis. The last demand is that the hole must be as small as possible. The smaller the hole is, the stronger the foil is, and the easier it is to fasten it.

For the last remoderation foil the position of the hole is more important where in the second remoderator the size of the hole is more important. In the case of a spot of 1 mm, it is obviously important that the hole is larger than 1 mm. This hole can be positioned easily on the optical axis. For the smallest spot of 800 nm, it is not possible to see where the hole is, if the hole is in the same order of magnitude as the probe size is. In that case the hole must be larger. In general it can be concluded that the order of magnitude of the holes must be 1 mm. For a 1 mm-hole it was found that the foils were strong enough. In fact when during testing, the foil was ripped, only the thicker foil was damaged. The thin foil could be used again by fastening it on a new foil. It must be noted that the hole in that foil must be smaller, due to the fact that it is impossible to disconnect the thin foil from the thick foil after heat treatment and thus only the area of the thin foil that was stretched over the hole could be used.
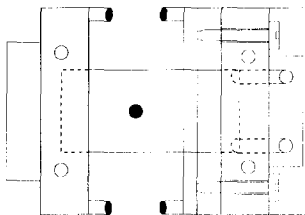
Figure 6.3   Setup of the foil connection. The clamps have been molten to glass bars. By turning the screws, the foil can be stretched.

The thick foil has been clamped between two stainless steel plates. These plates are fastened to the glass bars. Since the two clamps are electrically insulated

from each other, the foils can be heated by letting a high current run through the foils. To heat the foils to a temperature of 2000 K a current of about 20 A is necessary for the used foils. Figure 6.3 shows the foil fastened between the clamps. By turning the screws the two clamps are moved away from each other, and the foil is stretched.
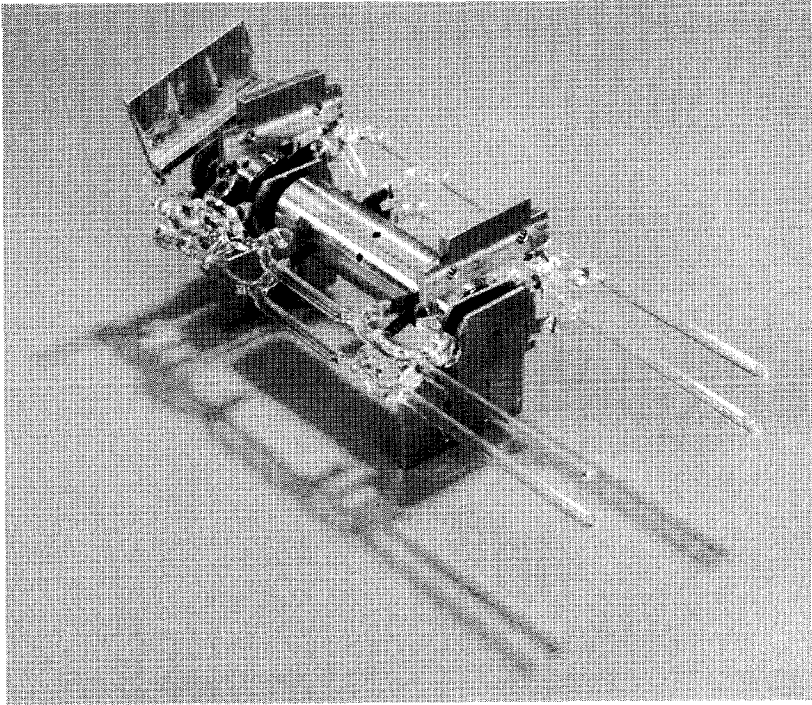
Figure 6.4   Photo of the remoderation sections

The complete setup of the remoderation section is shown in Figure 6.4. Since the glass is molten to it, the straight bars as showed in Figure 6.2 are not as straight anymore. The foil clamps are rotated with respect to each other, which does not effect the position of the foil.

6.3 Vacuum chamber

6.3.1 Vacuum demands
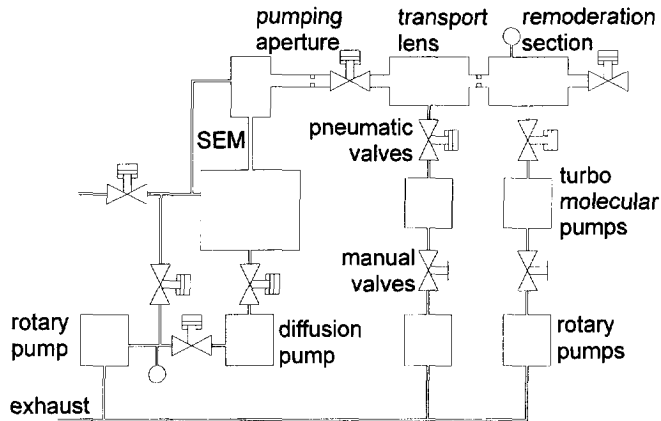
Figure 6.5   Setup of the vacuum system of the positron microbeam.

The foils used for remoderation only have good properties when they are extremely clean. Especially any carbon contaminates on the foils would let the positron emission rate go down drastically. More positronium is formed, and as a result the branching ratio for free positrons is decreased. Therefore, the base pressure in the chamber is in the order of 10^{-10} mbar. To achieve this pressure, the vacuum chamber was constructed according ultra high vacuum standards. The problem in maintaining this pressure is due to the high pressure in the SEM. Therefor, a vacuum system has been designed that enables differential pumping via the transport lens that will be discussed in the next chapter. This pumping scheme of the system is shown in Figure 6.5. The SEM is pumped by an Edwards oil-diffusion pump in combination with an Edwards rotary pump. The ultimate pressure in the SEM is not better than 10^{-6} mbar. The pump connected to the mu-metal chamber is a Balzers TPU 062H with a possible end pressure of 10^{-11} mbar and a pump speed of 53 l/s. The pump connected to the transport optics is an Edwards turbo-molecular pump with a pump speed of 65 l/s. The possible end pressure is 5×10^{-10} mbar. The pumping apertures between the different sections have a diameter of 1 mm, so the pressure in each step can be 100 times lower.

6.3.2 Magnetic field shielding

If no precautions are being made, magnetic stray fields disturb the quality of the remoderation sections. Mainly there are two sorts of fields. The largest is the DC-field, caused by the earth magnetic field. This field causes a deflection of the beam. It is constant and is about 5×10^{-5} T. The AC-field is smaller but causes a spot enlargement. The size of this field is not constant, but it varies in the order of 1×10^{-6} T.

The influence of the DC-field can be a deflection of the beam of about 20 μm. This gives a misalignment of the beam and probably more geometrical aberrations since the beam comes in higher in the lenses. AC-fields can give a spot enlargement. For the last remoderation section and a field of 10^{-6} T this is maximum about 0.4 μm. Since these numbers are too large for the positron beam, the magnetic stray fields have to be screened off. It can be found that the factor of screening (ε) can be found using the formula:

$$\varepsilon = \frac{B_{unscreened}}{B_{screened}} = \mu_r \frac{t}{D} \, , \qquad (6.1)$$

in which t is the thickness of the chamber walls and D the diameter of the chamber. It can be seen that a high μ_r is important. For this reason the vacuum chamber has been constructed out of mu-metal. Mu-metal has a high permeability also for low field strengths.

The magnetic stray field does not stop at the end of the remoderation chamber. From the remoderation chamber the beam will be guided into the magnetic transport lens that will be discussed in the next chapter. To continue the shielding, a fit between the mu-metal chamber and the iron lens has been made. If a magnetic lens is excited, the μr of it is larger, and so ε will be larger, resulting in a smaller stray field in the lens.

6.3.3 Realization of the mu-metal chamber

The resulting mu-metal chamber as shown in Figure 6.6 was constructed at Fisons Instruments inc. In the chamber many aspects can be seen. The strange
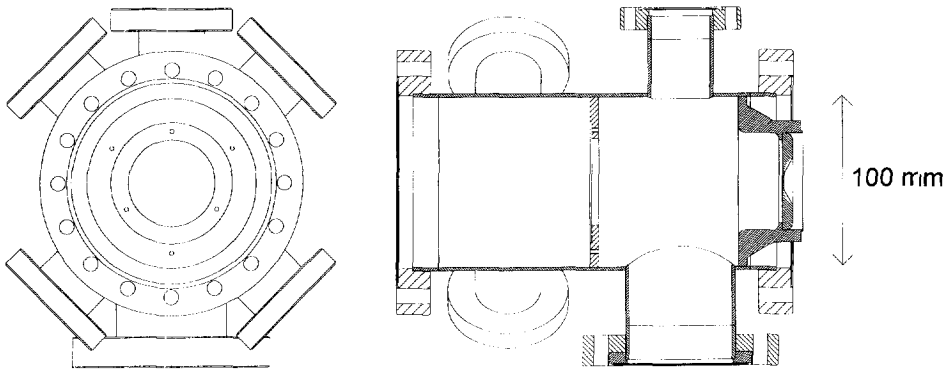
Figure 6.6   Mu-metal chamber, the right side in which the remoderation section is
              installed, and the left side in which the beam enters and the electrical
              connections are. (drawing by O. Wolfs)

nose on it was designed to get a magnetic connection between the remoderation
chamber and the transport lens. The transport lens will be discussed in
Chapter 7. One of the aspects of a magnetic lens is that it shields the beam from
magnetic stray fields as a result of the higher magnetic permeability when the
lens has been switched on. For not letting stray fields leaking in via a slit
between the two parts, a fit between the two parts has been designed. A rim in
the first pole piece of the transport lens fits in the nose of the mu-metal
chamber. This rim also gives a little alignment of the remoderation section and
the post remoderation optics. The two parts are connected to each other with
two CF100 flanges. Care must be taken when screwing these two together.

The thickness of the mu-metal is 2 mm. With a diameter of 100 mm this gives
a shielding factor of $0.02\mu_r$. Since the value of μ_r is not known exactly, just
estimates of the shielding factor can be found. Literature values[2] for the relative
permeability of mu-metal are in the order of 60000. So a shielding of 1200
times is the maximum possible.

Measurements with stray fields of 2×10^{-4} T perpendicular to the optical axis
were performed to measure the shielding factor of the mu-metal chamber.
Therefor a coil was positioned near the tube. The magnetic field inside the
chamber was too low to be measured with the used equipment. So it can be

concluded that the shielding is better than 50 times.

For magnetic fields parallel to the optical axis the shielding was measured to be 10 times. This shielding was measured at a distance of 30 mm below the nose. The magnetic field can enter via the non-magnetic anode. In this measurement the transport lens was not connected to the chamber. When the positron beam is in operation, the shielding of the transport lens will enable a low shielding factor.

In the nose of the chamber a stainless steel insert is put. This insert has a hole of 1 mm in it. This insert is part of the post remoderation optics, and can be compared with the anode in the SEM. From this point on, the positron beam has its final energy. Since the insert is part of the optics, mechanical tolerances of the roundness of the hole are important. The roundness of the hole is manufactured within 0.01 mm accuracy.

In the middle of the chamber a mu-metal plate is put. On this plate the remoderation section is connected. To have the remoderation section not tilted the parallelism between this plate and the insert and the flange must be better than 0.02 mm.

On the chamber six ports have been put. Three of the four CF35 ports on the side where the positrons beam enters the chamber, are used for high tension feed through. The fourth one can be used for a current feed through in the case small deflectors might be necessary. The CF35 port on the other side of the chamber is used for pressure measurements and rest gas analysis. For this purpose a mass spectrometer must be attached to it. This spectrometer must be used when giving the remoderation foils their in situ heat treatment. The CF63 port is used for pumping of the remoderation chamber. Figure 6.7 shows the mu-metal remoderation chamber as it was constructed.

6.4 Discussion and conclusions

The way the electrode setup has been made is chosen for its stability. Another option to make the electrode setup is by separating the electrodes by insulators. This way it might be possible to make a more flexible system, on the other hand
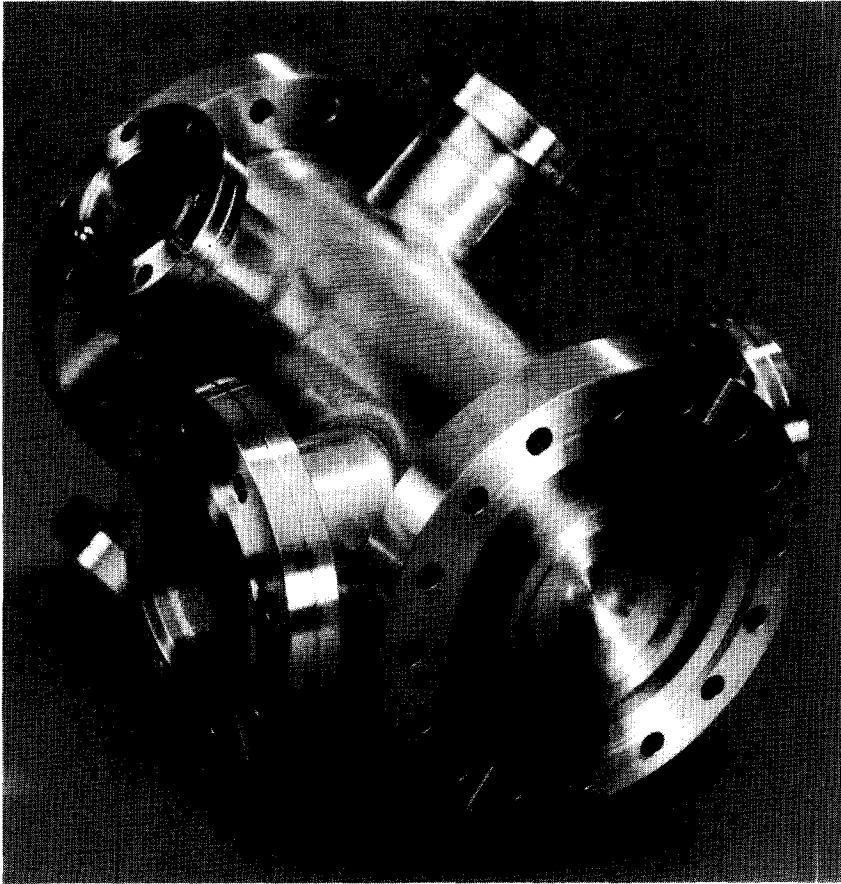
Figure 6.7   Photo of the mu-metal remoderation chamber.

it was expected that the mechanical stability and the alignment are more
difficult. The technique of making the setup is very similar to that of making
CRT-tubes. First tests to see the remoderation section to work can be performed
by using electrons. Secondary electron emission can be used instead of positron
re-emission. The energy of the secondary electrons is comparable to the energy
of the re-emitted positrons where the larger energy spread may give larger spot
sizes due to chromatic aberration. This spot size enlargement is only important
in the last remoderation section.

The vacuum chamber has been constructed of mu-metal. The shielding of it is

necessary to be able to avoid stray magnetic fields. The deflection due to DC-fields can be compensated for by using deflectors, but for the spot enlargement due to the AC-fields, good shielding is necessary and mu-metal can be used for both cases.

References

1.   P.H. Gleichauf, J. of Appl. Phys. **22**, 766, (1951)

2.   R. Boll, in *Weichmagnetische werkstoffe*, (Vacuumschmelze, Hanau, 1990), p. 278

7 Post remoderation optics

Summary

This chapter discusses the optical elements to combine the positron microbeam with the scanning electron microscope(SEM). To position the brightness enhanced positron beam on the optical axis of the SEM a double focusing deflector has been used. A transport lens between the remoderation section and the deflector has to be used to bring the beam in the right position in front of the deflector. The lens system of the microscope has not been changed, but to get the optimum spot size the currents through the lens coils have to be changed. The aberrations of the transport lens, deflector and lenses of the SEM, together with the dispersion of the deflector, cause an increase in opening angle and spot size of the positron beam and thus a decrease in effective brightness. Calculations show that the influence of the deflector can be kept small. The loss in effective brightness of the beam and thus the loss of positrons in the probe is less than a few percent for energies above 1000 eV, and about 28% for the lowest possible energy of 500 eV.

7.1 Introduction

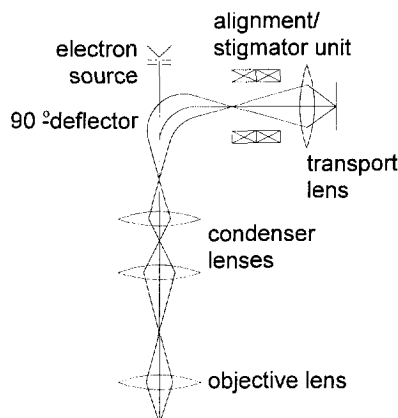Figure 7.1   Schematic overview of the post remoderation optics.In the figure a transport lens is shown, together with a 90°-deflector, and a scanning electron microscope.

In this chapter the optics between the last remoderation foil and the specimen is discussed. This part is schematically given in Figure 7.1 This optics consists of an accelerating lens, transport optics to the 90°-deflector, a 90°-deflector and

the optics in the Philips scanning electron microscope 535-M (SEM). In the next sections these subjects will be discussed in the order in which the positrons will pass these optical elements. Parts of it have also been described elsewhere[1].

From the remoderation section the positron beam must be transported to the deflector. These transport optics can be divided into two parts, the acceleration part and a magnifying part, which in the rest of this chapter will be called the transport lens. In the first section the positrons start with an energy equal to the absolute value of the negative work function of the remoderation foil, and are accelerated to their final energy. This part can be compared with the electron source of the SEM. In the magnifying part the positrons are transported to the optimum position with the optimum magnification.

In the emission chamber of the SEM the beam must be deflected over 90 degrees. It is clear that the shape of the positron probe must be round. To use a stigmatic deflector is advantageous over the use of a non stigmatic deflector in combination with an extra stigmator. It will be shown that in the case of a stigmatic deflector extra demands on the object position of the positron beam are given. Also the image after the deflector is set, resulting in a different position than the position of the image of the electron source, so the settings of the magnetic lenses of the SEM must also change. In the next sections of this chapter calculations on the above mentioned optical elements will be discussed.

In that light it must be seen that two important parameters are as always the brightness and the number of positrons in the beam. When the beam passes the transport optics and the deflector the number of positrons must remain the same, while the change in brightness must be as small as possible. In this part of this thesis we define an effective brightness given by:

$$B_{eff} = \frac{I}{\frac{\pi}{4} d_t^2 \pi \alpha_t^2 E} \, ,$$
(7.1)

in which I is the positron current, $\pi d_t^2/4$ the total spot size, $\pi \alpha_t^2$ the solid angle both including all possible aberrations, and E the energy of the positrons. This brightness determines the maximum number of positrons that can be obtained in a probe of a given size. The advantage of using this definition is that it is

easy to see how many positrons will end up in the probe if all aberrations are taken into account. This brightness is not a conserved quantity as the brightness normally is. Also the brightness is not a constant for all energies, since the aberrations can be different for different energies. As a consequence, the effective brightness has to be calculated after each optical element.

7.2 Transport optics

7.2.1 Demands on the transport optics

A problem in using a SEM is that the pressure inside the SEM is high (10^{-6} mbar) compared to the pressure in the remoderation section (10^{-10} mbar). This problem is solved by differential pumping. A turbo molecular pump has been installed to pump the transport lens to a pressure of about 10^{-8} mbar. Small pumping apertures between the different sections are used to minimize the gas flow from one section to the other. Another problem is that the microscope must be let to air when changing the specimen. Then, the SEM should be separated from the other parts of the beam by closing a valve between the SEM and the transport optics. As a result of the installation of a pump and a valve, the distance between the remoderation section and the SEM is relatively large. Since apart from the accelerating lens, only one other lens is used in the transport section, it must have a large focal length.

It will be shown that it is preferable to have an image of the positron source at a distance of twice the bending radius of the deflector in front of this deflector. It is important that the properties of the beam are optimized with respect to the deflector. This means that the combination of opening angle and spot size must be adjusted. The properties of the remoderated positron beam are a spot size of 800 nm and an opening angle of 0.16 mrad, for an energy of 2 eV, the value of the work function of tungsten, as was seen in Chapter 5. The most important demands on the transport optics are that it will not change the effective brightness and that it positions the positron beam optimally in front of the deflector.

7.2.2 The acceleration section

The acceleration part is an electrostatic lens of which the remoderation foil can be considered as the positron source. The last electrode is at ground potential, an intermediate electrode can be varied to get optimum beam parameters. From this point on, the positron beam has its final energy determined by the voltage on the last foil.

The important parameters for the transport lens are the opening angle and virtual spot size. In the acceleration lens the aberrations should not add up to the total spot size, which would result in a decrease of the effective brightness. A design has been made as already shown in Chapter 6. The last foil is at a distance of 3 mm in front of the electrode, the distance to the 'anode', the electrode at ground potential, is 10 mm.
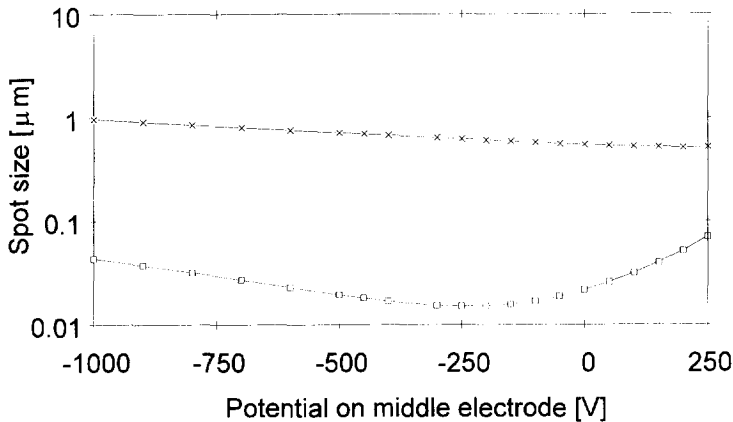
Figure 7.2   Geometrical spot size($\times$) and spherical aberration spot size($\bigcirc$) after the acceleration lens for a positron beam of 500 eV as a function of the potential on the middle electrode.

Calculations with the programs ELD[2], to calculate the electrostatic fields, and LENSPROP[3], to calculate the optical parameters like the magnification and the coefficient for spherical aberration, have been carried out to find the right voltage for the middle electrode. The energy for which the aberrations are the most important is the lowest energy, where the opening angle is the largest, so spherical aberration is the largest. The results of these calculations are shown

in Figure 7.2.

The figure shows that the potential on the middle electrode can be chosen provided that the total spot size (d_t) is completely determined by the demagnified spot (d_g). Because the calculated spot is an intermediate image, the theory on optimum spot sizes as discussed before does not hold. In this case the spherical aberration reduces the current density, and thus the effective brightness, which is an unwanted effect. So in the figure it can be seen that any potential lower than 250 V can be chosen. The position of the lower limit has not been calculated. It should not be too much negative resulting in possible flashovers.

7.2.3 The transport lens

For the magnifying lens is chosen for a magnetic lens with a long focal distance, magnifying about four times. The reason for this magnification will be explained in Section 7.4. In this case it is easier to use a magnetic lens, since magnetic lenses have in general lower aberrations, and the use of high voltages can be avoided. To focus a positron beam with an energy of 25 keV, a voltage difference between the lens electrodes of about 25 kV would be necessary. For the transport of the beam over a long distance a lens is needed with a large focal length. To keep the spherical aberration low for such a lens, the pole pieces of the magnetic lens should be large. As a rule of thumb one can use the following equation:

$$C_s \propto \frac{f^3}{S^2 \cdot D^2} , \qquad (7.2)$$

in which C_s is the coefficient of spherical aberration, f is the focal length of the lens, S the size of the gap between the two pole pieces, and D the bore of the lens. The magnetic lens design program MLD[2] has been used to calculate the magnification, the spherical aberration coefficient and other optical parameters of the transport lens.

To get a magnification of about four times and the image in front of the deflector a lens has been calculated with a focal length of 50 mm. The exact magnification was found to be 3.8 times. It was found that C_s of that lens
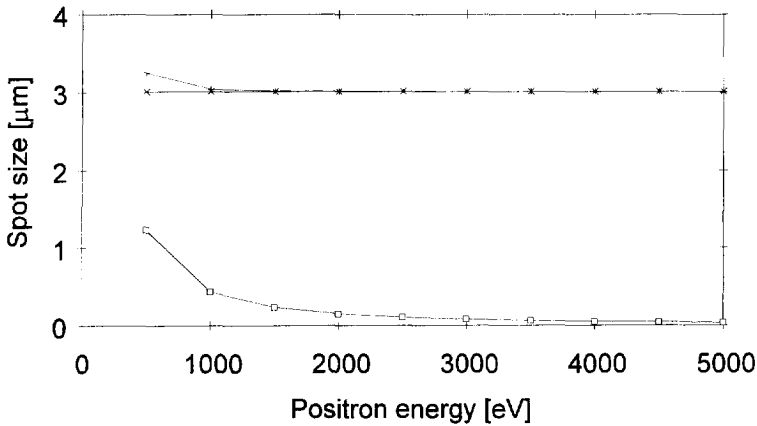
Figure 7.3   total spot size(+), geometrical spot size(×) and spherical aberration spot
              size(□) in front of the deflector as function of the beam energy.

equals 0.34 m, and thus with an opening angle of a few mrad for the lowest
positron energies, the contribution of spherical aberration is about 1.2 μm,
which is small enough compared to the total spot of 3.0 μm diameter. For
higher energies the influence of spherical aberration rapidly decreases. In
Figure 7.3 the total spot size of the positron beam for the lower energies is
plotted. It can be seen that the influence of spherical aberration is small and
negligible for energies above 2000 eV.

7.3 Realization of the transport lens

7.3.1 Lens materials

The transport lens as it has been constructed is shown in Figure 7.4. The
housing of the magnetic lens and the first pole piece, indicated by the coarse
shaded areas, have been constructed of soft iron. The second pole piece,
indicated by the fine shading, is made of nickel iron. Nickel iron has been used
here, since it saturates at higher fluxes, and the flux through this pole piece can
become higher for the higher positron energies. Stainless steel has been used for
the parts in which non-magnetic materials have to be used, for instance to seal
the coils in their housing and for the small liner tube. The tube to the pump is
also made of stainless steel.

100 mm
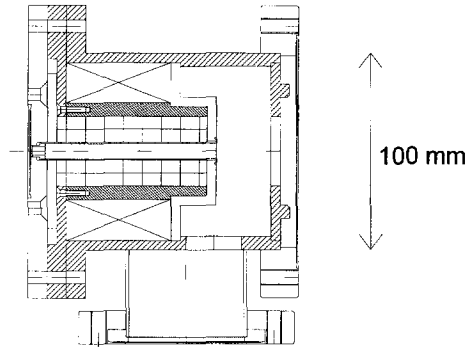
Figure 7.4   Drawing of the transport lens with the pole pieces(shaded area), the lens coil
and the stigmator, alignment unit. At the left side the pumping aperture can be
seen. (drawing by O. Wolfs)

For not having stray fields in the lens, the magnetic circuit should be closed. A
magnetic lens also shields the beam from stray fields. For not having these
unwanted fields between the remoderation chamber and the transport lens, on
the first pole piece a ring of iron has been left that connects magnetically the
mu-metal chamber with the lens.

To be able to correct the positron beam from being astigmatic or misaligned to
the deflector, a complete scan coil/stigmator unit has been taken from a Philips
SEM 500 and inserted in the transport lens. With this transport module it is
possible to get the beam in the right position in front of the deflector. In the
figure this module has been indicated by the square hatching.

7.3.2 Vacuum considerations

To be able to overcome the pressure difference between the remoderation
section and the SEM, the transport lens is closed at both sides except for small
pumping apertures through which the positron beam can pass. Between these
two apertures a turbo molecular pump pumps the lens to the ultimate pressure
that will be in the order of 10^{-8} mbar. To be able to pump the transport lens a
hole has been milled in the outer tube of the magnetic circuit. The effect on the

magnetic field has been kept low enough[4] while some bars inside the pumping hole have been left to minimize influence of the distortion of the field and for shielding against magnetic stray fields that could enter via this pumping hole.
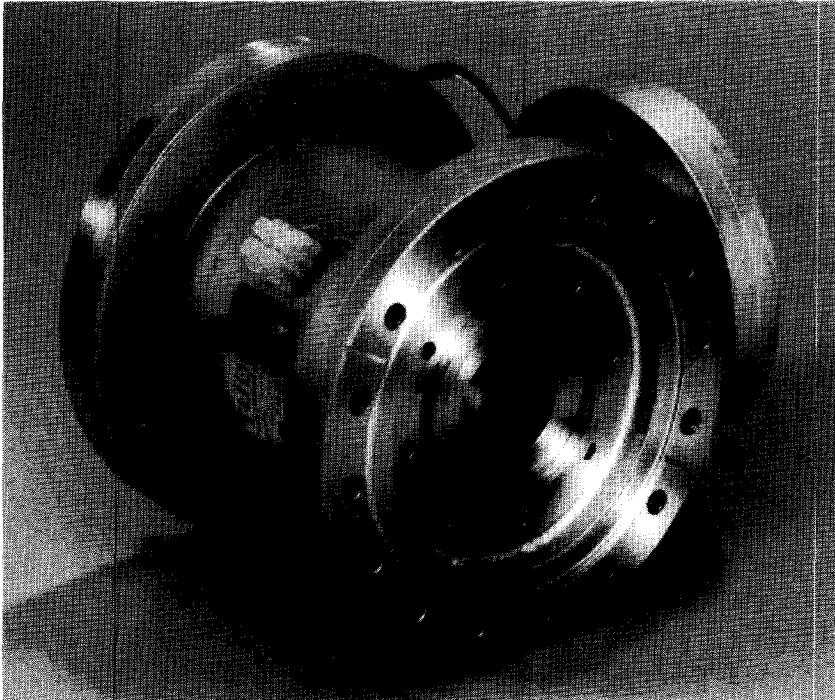
Figure 7.5   Photo of the transport lens.

The vacuum sealing has been done via a CF100 flange with the remoderation section. The right-hand side of the lens can be heated to higher temperatures. These higher temperatures will occur when the remoderation section will be heated to outgas this vacuum chamber. The other side of the transport lens has been sealed by using a Viton® O-ring. This small ring seals the small liner tube. Further down the line a CF-based valve is used to be able to change the specimen without having to let air into the remoderation chamber. The photo shown in Figure 7.5 shows the transport lens as it has been constructed.

7.4 Stigmatic deflection of the positron beam

7.4.1 First order optics

Using simple equations it can be found that the number of ampere turns to deflect a beam of charged particles with a given radius (R) is given by

$$NI = \frac{2G_0}{R\mu_o} \sqrt{\frac{2Em}{q}} \quad . \tag{7.3}$$

In this equation $2G_0$ is the distance between the two pole pieces, μ_0 the magnetic permeability, m and q the mass and the charge of the particle respectively, and E the energy of the particle.

The deflector is supposed to be double focusing i.e., both in the dispersive and in the non-dispersive direction there is a focus. The design follows closely the theory discussed in many textbooks[5,6].

Figure 7.6   Focusing effects in dispersive and non-dispersive direction. a: perpendicular boundaries, b: tilted boundaries

In Figure 7.6 the rays through a single focusing deflector and through a double focusing deflector are schematically given. The deflector acts as a lens in the dispersive direction. To compensate this a quadrupole lens is needed. A quadrupole lens can be obtained by tilting one of the pole piece boundaries over
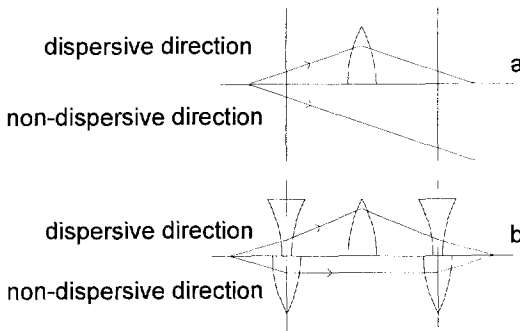
a certain angle. By tilting them both a symmetric lens system has been obtained.

Tilting of the entrance and exit planes gives a quadrupole effect with the focal distances given by:

$$f_{disp} = -\frac{R}{\tan(\varepsilon)} \qquad\qquad (7.4)$$

and

$$f_{nondisp} = \frac{R}{\tan(\varepsilon)} . \qquad\qquad (7.5)$$

In this equation ε is the angle over which the pole boundary is tilted. A logical demand is that after the deflector the beam must still be round. To fulfill this demand, the total lens must be stigmatic, and the magnification in both directions must be the same. This results in an angle ε of 26°34' for both the entrance plane and the exit plane and in an object position at a distance of twice the bending radius in front of the deflector. In this theory the influence of fringing fields is not included. The effect of fringing field is subject of the next section.

7.4.2 Fringing fields

In the previous paragraph it was assumed that the magnetic field is a block field. In practice the fields have long tails called fringing fields. These tails can be cut off by using shunts[6]. A shunt is a part of the magnetic circuit that will cause the magnetic field to go to zero more rapidly, as can be seen in Figure 7.7. In the figure, the constant magnetic field between the two pole pieces can be seen falling off to zero if shunts are used, and falling off less if no shunts are used.

As a result the magnetic potential of the shunt will be zero. With the numbers given by Wollnik[6] it is possible to calculate from the distances of the shunts and the distance between the pole pieces the position where the field can be assumed to be a block field. This position will be called the effective field boundary. In general, this position is outside the pole pieces. Therefore, the real magnet should be shorter than the block field. For the numbers used in this deflector
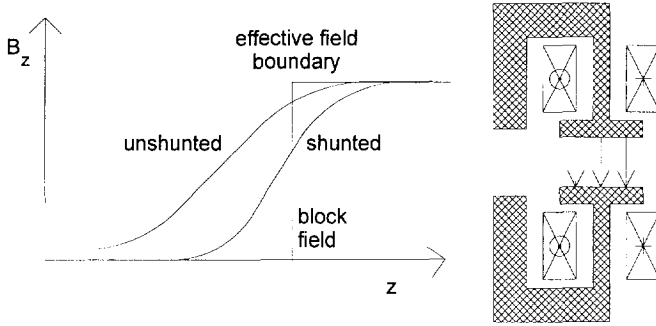
Figure 7.7   Fringing field shunt of a deflector, the beam comes in at the left side, first through a slit, then it travels downwards due to the magnetic field between the pole pieces

i.e., a gap $(2G_0)$ of 2 mm, a distance between the pole pieces and the shunts (D) of 3 mm, and a distance between the shunts $(2G)$ of 2 mm, the effective field boundary is 0.94 mm outside the pole pieces.
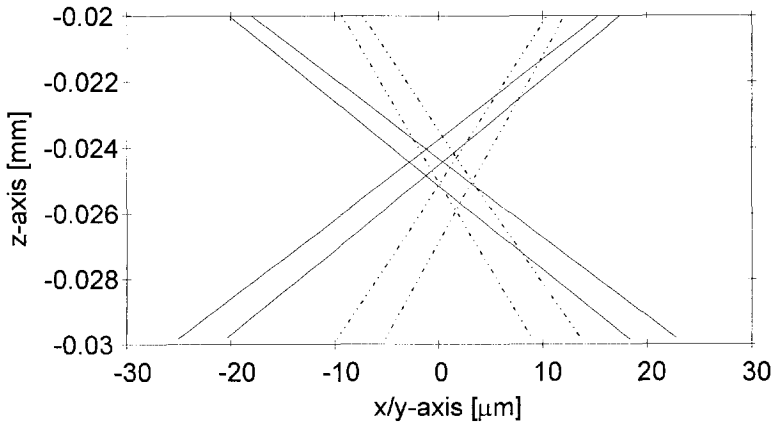
Figure 7.8   Ray traces through a sector magnet with angles tilted over an angle of 29°30' in the dispersive (solid line) and non-dispersive (dashed line) direction.

Another aspect of the use of this fringing field is that the extra quadrupole lens is changed. This change in fringing field was calculated with an adapted version

of the ray tracing program by Bleeker[7]. By calculating rays through magnets with varying tilt angles, it was found that the angle must be 29°30' to obtain the double focusing effect that in the case of a perfect block field should be 26°34'. Figure 7.8 shows the traces through the magnet with the optimized tilted angles. Both in the dispersive direction and in the non-dispersive direction, the positron beam has an intermediate image at a distance of little more than $2R$ below the effective field boundary.

7.4.3 Second order aberrations and dispersion

Like every optical element a deflector has aberrations. For elements with a curved axis the second order aberrations are the most important aberrations. A way to describe the parameters of the beam is by using the matrix notation. With this notation the angle and position of each different ray can be calculated. For many systems the matrix elements can be calculated. From these single rays it is possible to calculate the total spot size and opening angle. The formula for one ray looks like:

$$
\begin{aligned}
x_i = \quad & (x|x)x_o & + \quad & (x|\alpha)\alpha_o & + \quad & (x|\delta)\delta \\
+ \quad & (x|xx)x_o^2 & + \quad & (x|\alpha\alpha)\alpha_o^2 & + \quad & (x|\delta\delta)\delta^2 \\
+ \quad & (x|x\alpha)x_o\alpha_o & + \quad & (x|x\delta)x_o\delta & + \quad & (x|\alpha\delta)\alpha_o\delta \\
+ \quad & (x|yy)y_o^2 & + \quad & (x|\beta\beta)\beta_o^2 & + \quad & (x|y\beta)y_o\beta_o
\end{aligned}
\tag{7.6}
$$

in which x is the coordinate in the dispersive direction normalized to the radius of curvature. For the other direction and both opening angles α and β similar expressions can be derived. The terms between brackets are the coefficients to be found, where the second order terms have to be as small as possible. An overview of all coefficients is given in Table 7.1. These coefficients are calculated from the object plane of the deflector to the image plane.

It can be seen that the most important aberrations for the lower energies are the dispersion and the second order aberrations. Often 90°-deflectors are used as dispersive elements. In this application the dispersive action must be minimized. It can be seen that the spot will be smeared out in the dispersive direction, so

Table 7.1 First and second order coefficients of the 90°-deflector

$(x \mid \ldots)$ terms		$(\alpha \mid \ldots)$ terms		$(y \mid \ldots)$ terms		$(\beta \mid \ldots)$ terms	
x	-1.00	x	-0.75	y	-1.00	y	-0.61
α	0.00	α	-1.00	β	0.00	β	1.00
δ	4.00	δ	1.50	δ	0.00	δ	0.00
xx	-0.75	xx	-0.14	xy	-0.55	xy	-0.01
$x\alpha$	-3.00	$x\alpha$	-0.75	$x\beta$	-5.25	$x\beta$	-2.18
$\alpha\alpha$	-4.00	$\alpha\alpha$	-1.50	αy	-3.64	αy	-0.04
$\delta\delta$	-4.50	$\delta\delta$	-2.06	$\alpha\beta$	-13.0	$\alpha\beta$	-3.39
$x\delta$	3.75	$x\delta$	1.31	δy	1.72	δy	0.63
$\alpha\delta$	8.00	$\alpha\delta$	2.25	$\delta\beta$	11.0	$\delta\beta$	4.96
yy	-1.09	yy	-0.65				
$y\beta$	-3.64	$y\beta$	-2.18				
$\beta\beta$	-6.00	$\beta\beta$	-2.25				

the spot will be an ellipse. The contribution to the spot d_{disp} is given by

$$d_{disp} = R(x \mid \delta) \frac{\delta E}{E} \ . \tag{7.7}$$

In this equation δE is the spread in energy and equal to $kT + \Delta V$, with kT the thermal energy, and ΔV the instability of the high tension power supply of the last remoderator, R is the radius of curvature, and $(x \mid \delta)$ the dispersion coefficient that can be found in Table 7.1. The most effective way to avoid dispersion is to use a monochromatic beam, and a deflector with a small radius. A positron beam in general can be very monochromatic since the energy difference is only due to thermal vibrations. To make the second parameter, the radius of curvature, as small as possible has its limits in the practicality of its design. As can easily be seen by using Eq.(7.3), a small radius will demand a high magnetic field with possible saturation of the magnetic material.

Compared to the dispersion the second order aberration, given by:

$$d_{\alpha^2} = R(x \mid \alpha\alpha)\alpha^2 \; , \tag{7.8}$$

is small. For the higher energies these aberrations are not important. Dispersion is low since the relative energy spread is low for the higher energies, and the second order aberrations are low since for higher energies the opening angle is much smaller. Apart from the aberrations in position there are also second order aberrations in the opening angle. In the case of this beam these aberrations are not important, and become less important with higher energy. The aberrations that are a function of the object size, are in general a few orders lower and thus do not play a role in microbeams.

7.4.4 Calculation of the effective brightness

The magnification of the transport lens is chosen to be in the order of four times. From the previous arguments it could be concluded that the magnification should be large. If the magnification of the beam would be approximately 75 times, the second order aberrations in angle and in position would be equal to each other, and thus resulting in a minimum aberration disk. Since this would give some practical problems, and to avoid complexity, there has been chosen to use one lens, the magnification was chosen to be in a more practical value. The outcome of calculations was the value of 3.8. This value was taken to be able to minimize the aberrations of the deflector. This magnification can not be changed since the position of the intermediate image in front of the deflector is fixed. With this number the spot size and opening angle of the beam entering the deflector can be calculated.

In our design the bending radius of the deflector equals 8 mm. This value was chosen from both practical view and optical view. In the emission chamber of the SEM there is only room for a small deflector, and a small radius minimizes the aberrations. On the other hand the construction of the deflector becomes more difficult for smaller pole pieces. Also, the saturation of the magnetic material becomes more important due to the higher field. In this case it must be seen that the saturation will not occur in the pole pieces but in the smaller core inside the coil. The magnetic field necessary to bend a positron beam with an energy of 25 keV equals 0.067 T for a radius of 8 mm. With a 12 times larger

pole piece than the core, it can be seen that the maximum magnetic field in the
core, equal to 0.80 T, is lower than the saturation value of nickel iron.
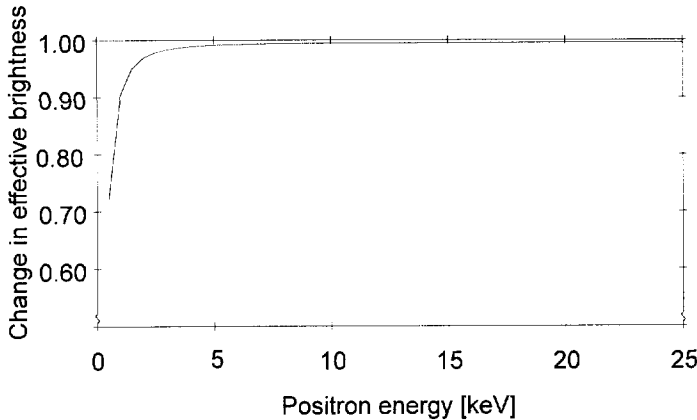

Figure 7.9   Change in effective brightness as function of the positron energy. For the
              lower energies there is a loss in brightness of about 20%.

The second order aberration is in the design with R equal to 8 mm and M equal
to 3.8 equal to $R(x|\alpha\alpha)\alpha^2 + R(x|\beta\beta)\beta^2 = 0.4$ μm, which is much smaller then the
3.5 μm of the unperturbed spot. With a δE of 50 meV, $\alpha_{disp} = 0.15$ mrad which
is smaller than the unperturbed opening angle. The size of the dispersion spot
$(x|\delta)\delta E/E$ will be 3.2 μm which is almost equal to the 3.5 μm diameter of the
unperturbed spot and therefore the largest aberration. These aberrations are only
important for the lower energies. The examples given above are for the lowest
positron energy of 500 eV. Figure 7.9 shows the change in effective brightness
as a result of the 90°deflector. It can be seen that only for the very low energies
there will be a significant change.

7.5 Realization of the deflector

Figure 7.10 shows a drawing of the deflector as it was made. The basic parts
of the deflector have been made from nickel iron. The two coils wound over the
magnetic cores both have 90 turns. For not having to pump the air between the
windings of the coils, the coils are placed in a vacuum tight chamber sealed with
a Viton[®] o-ring. On the other side the vacuum is kept by using non-magnetic
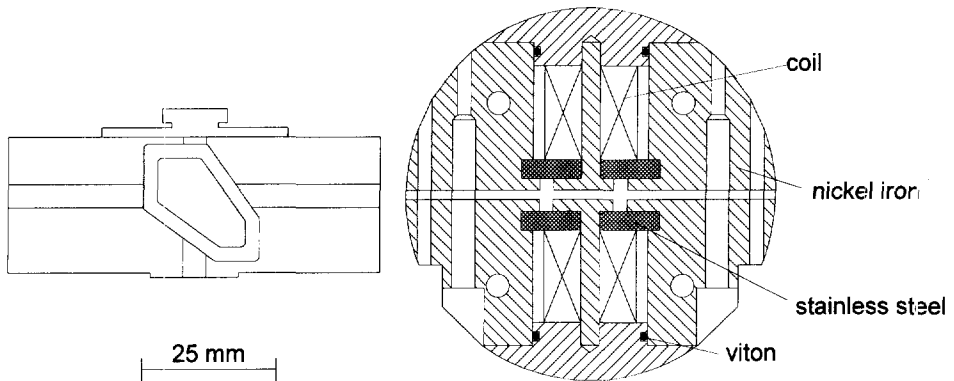
Figure 7.10   Drawing of the 90°-deflector

stainless steel as an intermediate material between the pole pieces and the shunts. The distance between the two pole pieces is 2 mm, which is also the distance between the shunts. The distance from the shunts to the pole pieces is 3 mm.

The deflector was made according the following procedure. First the nickel iron pole pieces and shunts and the stainless steel intermediates were roughly milled to its measures. Then the parts were put together by soldering the stainless steel intermediates between the nickel iron parts. By using a high temperature soldering material, the nickel iron got a heat treatment. The temperature was raised in a vacuum oven to 1150°C at which the solder melts and flows between the three parts. By cooling down slowly (100°C per hour), the material becomes both mechanically and magnetically soft. After the soldering, the pole pieces and shunts were milled to their exact measures.

In the previous section it was already shown that the magnetic field between the two pole pieces is equal to 0.067 T. To get this magnetic field between the two pole pieces the number of ampere turns was found to be 106 according to Eq.(7.3) for a positron beam with an energy of 25 keV. As stated before, the distance between the pole pieces $(2G_0)$ is equal to 2 mm, where the bending radius (R) is equal to 8 mm.

In the coil of the deflector heat is dissipated when the deflector is switched on.

The heat dissipation for a coil with given dimensions can be derived and is:

$$P = (NI)^2 \, \frac{\rho\pi}{vh} \, \frac{R_2 + R_1}{R_2 - R_1} \, . \tag{7.9}$$

In this equation ρ is the specific resistivity of the windings, v is the fill factor, a measure for the way the coil is wound, h is the length of the coil, and R_1 and R_2 are respectively the inner and outer diameter of the coil. By using behind both pole pieces a coil, the heat dissipation was reduced to 0.0186 W per coil.
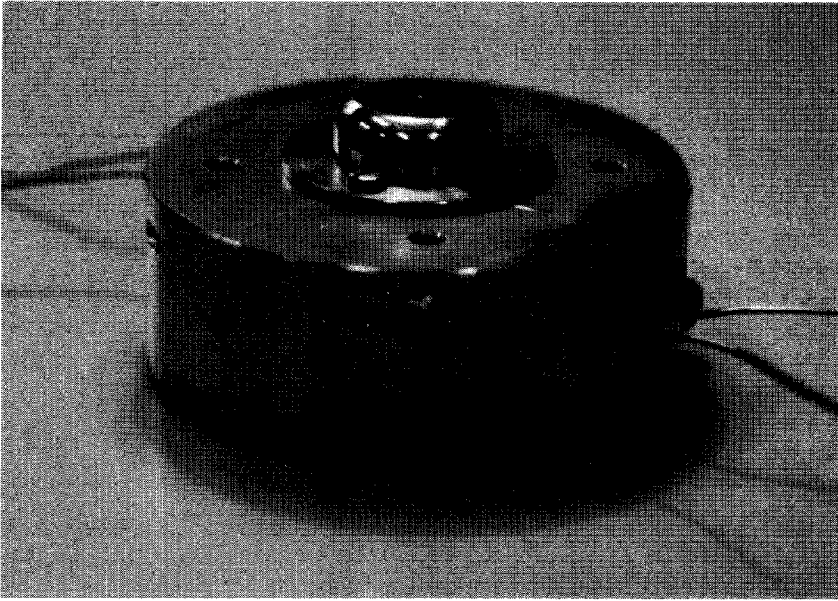
Figure 7.11   Photo of the deflector. On top of the deflector the anode has been positioned.

With a height of 25 mm, the deflector has been designed to be the holder of the original anode. To be able to fit the deflector in the emission chamber, the emission chamber has been milled from a diameter of 60 mm to 100 mm. In the bottom of the emission chamber a circle shaped fitting has been made. A pin in the bottom of this emission chamber makes it impossible to the deflector to rotate. Figure 7.11 shows a photograph of the deflector as it has been constructed.

7.6 Microscope optics

7.6.1 Introduction to SEM-optics
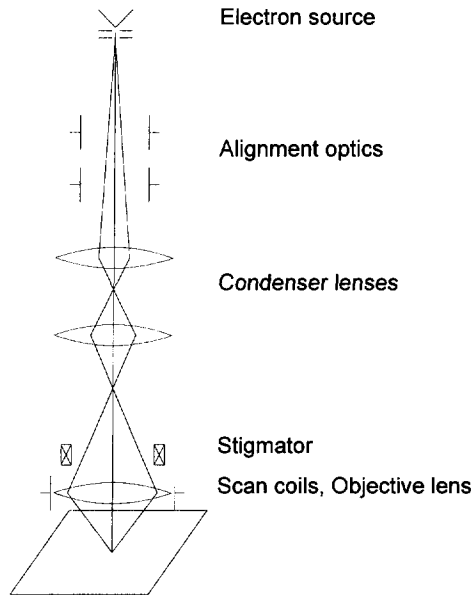
Figure 7.12   Schematic overview of the SEM. The SEM consists of, from top to bottom, an electron source, alignment optics, a double condenser lens, a stigmator, scan coils, and the objective lens.

As shown in Figure 7.12, the optics of a SEM consists of gun alignment coils, a double condenser lens, an objective lens, a stigmator, and scan coils. To minimize aberrations and prevent image shifts, the electron beam and positron beam must pass the lenses in the SEM exactly through the middle of these lenses. To compensate for mechanical misalignment, magnetic coils are used to shift and tilt the beam to the optical axis. Both the positron beam and the electron beam have to be demagnified, the condenser lenses of the SEM enable possible demagnifications of a few times to about 3000 times. The objective lens of the SEM enables a stable focus on the specimen close to the under pole piece of this lens. The scan coils can be used for scanning in video mode, and in slow scan, the options that can be chosen in slow scan are a full frame, and a line. It is also possible to perform a point analysis. In this section the optics of the SEM is discussed from top to bottom with respect to the differences in operation

that may occur when using the positron beam.

7.6.2 Alignment optics

In electron operation the alignment coils are purely shift and tilt coils, they respectively move the beam onto the optical axis and make the beam parallel to the optical axis. Since the positron beam has a different virtual source as the electron beam, the pivot point should move as well. This change in pivot point is made using the software of the automated SEM. In the next chapter this will be discussed.

7.6.3 Spot size selection

The spot size on the specimen is supposed to be 100 nm, although in practice there can be chosen for the constant current option and thus the varying probe size as discussed in Chapter 2. It was shown that the spot size after the deflector is 3 μm. The demagnified spot size will be 87 nm, so the demagnification will be about 35 times. This demagnification is set by the three lenses in the SEM. To be able to calculate the setting of the lenses, the distance of the specimen to the objective lens must be known. This distance can be calculated by measuring the current through the lenses of the SEM in the electron mode. With the known object distance the position of the intermediate images and the final image on the specimen can be calculated. With this now known distances, and the demand on the demagnification, the current through the lenses can be calculated.

Figure 7.13 shows the focal distance of the objective lens as a function of the working distance. The figure shows that although the magnification of the two systems, the strength of the lens is not changed more than by 5 % for the larger working distance and by less than 4 % for the shortest possible working distance. The demagnification of the objective lens in the positron mode is equal to 5.7 times, where the demagnification in the electron mode is equal to 7.8 times. Both demagnifications are calculated for a working distance of 10 mm.

A problem to get the right magnetic field is the hysteresis of the lenses. For a given current through the lens coil, the magnetic field can be different. A way
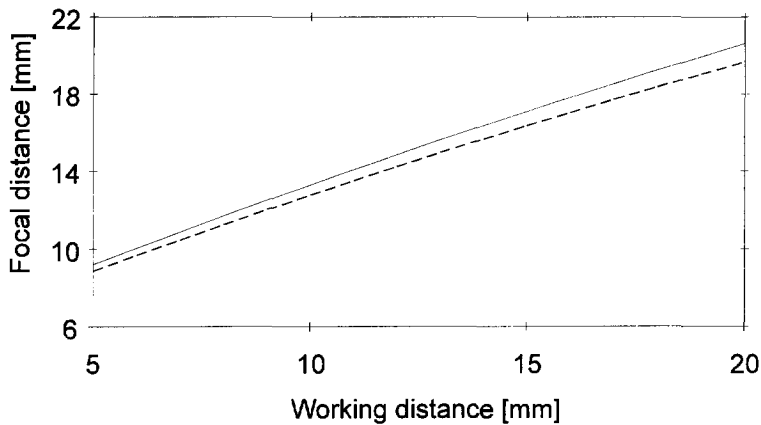
Figure 7.13   Focal distance of the objective lens of the SEM as a function of the distance
                of the specimen to the lower pole piece both for electrons (solid line) and
                positrons (dashed line).

to circumvent hysteresis is to go to saturation of the iron and go from this situation to the wanted magnetic field. A problem with this way is that the currents through the coils should be very high to saturate not only the pole pieces but the total circuit. The current supplies in the microscope can not deliver such high currents. Another way to compensate for hysteresis is to let an ac-current through the lens. The description of the setting of the lenses of the SEM will be discussed in the next chapter.

7.6.4 Stigmation

Since the electron beam has been used at high resolution, the stigmators have to be used. The way a stigmator works is that it compensates for non rotational symmetric fields. In first order the stigmator makes the field round again. The astigmatism of the objective lens is proportional to the square of the magnetic field. The difference between the strength of the objective lens for electrons and positrons was shown in Figure 7.13. The astigmatism changes with the same amount. Since the spot size in positron mode is about 14 times larger, the influence of the slightly wrong setting of the stigmator can be discarded.

7.6.5 Scanning

The way the positron beam will be operated is to make an image with the electron beam, after which the positron beam is focused to an interesting part of the specimen where a depth scan can be performed. So it is important to have the electron beam on the right position. The positrons only have to be focused on that specific region. To determine the lateral resolution of the positron analysis, a line scan can be performed. A full scan may take too long a time since the recording time per point is estimated to be 100 seconds for a beam containing 10^6 positrons per second. For a view of 640×480 pixels this would mean a measuring time of 356 days. A line of 640 pixels will result in a measuring time of about 18 hours. These calculated times are for measuring with only one energy.

7.7 Changes to the SEM

a   b
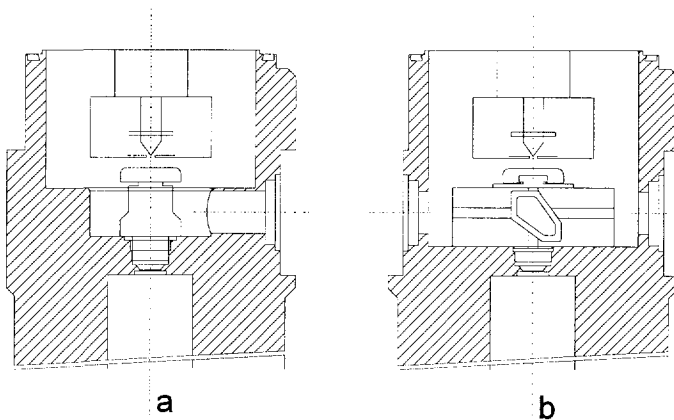
Figure 7.14   Changes to the emission chamber of the SEM. a: the old situation, b: the new milled emission chamber with the deflector in it.

As seen already the changes to the SEM are as few as possible. There are no changes in the optical parts. The only changes to the SEM are an extra port opposite to where the positron beam enters the microscope and an enlargement of the emission chamber. The extra port can be used to detect the positron beam when the deflector has been switched off. Further, the emission chamber was

milled to be able to position the deflector in it. In Figure 7.14 the old and the new emission chamber are shown. In the new situation the anode holder is replaced by the deflector.

The positron beam enters the SEM from the right-hand side. An intermediate image is made inside the shunt configuration. After the deflection over 90 degrees an image is made below the deflector. The intermediate image of the electron beam is made inside the anode.

7.8 Discussion and conclusions

With the designed transport optics and deflector it was shown that it is possible to get a positron beam with variable energy on the optical axis of the SEM. The transport lens magnifies the positron beam to get the aberrations of the deflector small enough, so the loss in brightness could be kept within the limits. The aberrations of the transport lens itself could be kept very low, so the brightness is not changed at all by the lens. The most important aberration of the deflector is the dispersion. This dispersion gives a reduction in effective brightness of a few percent except for the lowest energy of the positrons where the reduction is in the order of 20 percent.

To the SEM the hardware changes were kept as small as possible. The only important hardware change has been the milling of the emission chamber to make room for the deflector. The other changes are only changes to the electronics of the SEM. These changes will be discussed in the next chapter.

References
1.   R.F.J. Neelissen, masters thesis Delft University of Technology, (1993), unpublished

2.   B. Lencová, and G. Wisselink, Nucl. Instr. & Meth. in Phys. Res. A **298**, 56, (1990)

3.   J. Chmelik, Internal report of the Institute of Scientific Instruments of the Czechoslovak Academy of Sciences, (1989), unpublished

4.   M. Lenc, and B. Lencova, private communication

5.   H.A. Enge, in *Focusing of charged particles II*, ed. A. Septier, (Academic Press, Orlando, 1967), p. 203

6.   H. Wollnik, in *Optics of charged particles*, (Academic Press, Orlando, 1987)

7.   A.J. Bleeker, Internal report, Department of Applied Physics, (1991), unpublished

8 Computer control of the positron microbeam

Summary

This chapter discusses the computer control of the positron microbeam as it is inserted into the scanning electron microscope. The computer control can be split into two parts, the first part being the positron beam transport and the remoderation section, and the second part being the post remoderation optics and the scanning electron microscope. The first part can easily be automated since the beam properties do not change. The only thing that changes is the base potential of the total beam. For the post remoderation optics the settings are more important, since the energy and working distance may change. The computer control may be more complicated but the settings of the optical parts can sometimes be found by using simple scaling formulae. When switching from electrons to positrons, the settings of the lenses can be calculated out of the accurately measured settings of the SEM. The problems that were encountered were mainly in the second part of the beam. The first part could be designed in an optimum way to automate, this also holds for the transport lens. The computer control of the SEM is more complex since the SEM was already partly automated. The changes to the SEM have been kept as few as possible. The problem of hysteresis of the magnetic lenses and the remanence of the 90°-deflector has been solved by applying reverse currents through the coils until the remanence of the magnetic material is small enough.

8.1 Introduction

In this chapter the computer control of most of the parts that are used to handle the positron beam is discussed. The positron beam must be highly automated, since manual operation is almost impossible due to the low intensity of the beam and thus to the long time it will take to make an analysis of the used setting. The first part of the positron beam is the easiest part to control since the settings of the lenses do not change with the final energy of the positrons. The only thing that changes is the base potential of the beam. This potential is determined by the final energy of the positron beam. This first part will be discussed in section 8.2.

The computer control of the SEM is more complicated, since the settings of all the optical parts are changing with energy of the positrons and the settings do differ from the settings used when the electron beam is switched on. Another aspect on these parts is that they are partly magnetic. Since magnetic lenses do not always give the same magnetic field for the same current due to

hysteresis, a solution has to be found to circumvent this effect. This effect is also visible in a different shape in the remanence of the magnetic material of the 90°-deflector. The magnetic field of this deflector must be as small as possible (at best 0) when the electron beam is used. It will be shown that the problem of the lenses and the deflector can be solved in the same way.

Another problem with using the SEM as the probe forming system is its changing free working distance. For every specimen, the distance to the objective lens is different. This distance can be calculated from the settings of the SEM for the electrons. With this number it is than possible to focus the positron beam on the specimen.

The computer control of the post remoderation optics will be discussed in two sections. The transport optics and the deflector are discussed in section 8.3 and section 8.4 discusses the computer control of the SEM.

8.2 Computer control of the positron beam

8.2.1 Setup of the positron beam

The part of the positron beam that was described in Chapter 2 does not need a complete computer control. As can be seen in Figure 8.1 none of the potential differences changes, only the final beam potential changes, resulting in a constant velocity of the positrons in this part of the beam. Since the effect of the coils is proportional with the velocity of the positrons, and the velocity of the positrons in that part of the beam never changes, the current through the Helmholtz coils does not have to be changed at all.

8.2.2 Control of the remoderation section

The computer control of the remoderation section is thus the easiest part of the computer control. In the whole system there is only one potential that has to be set by computer. The potential differences on the different electrodes are being set once. Thus it is not necessary to have a complete computer control. The different tensions to the electrodes can be given by using a
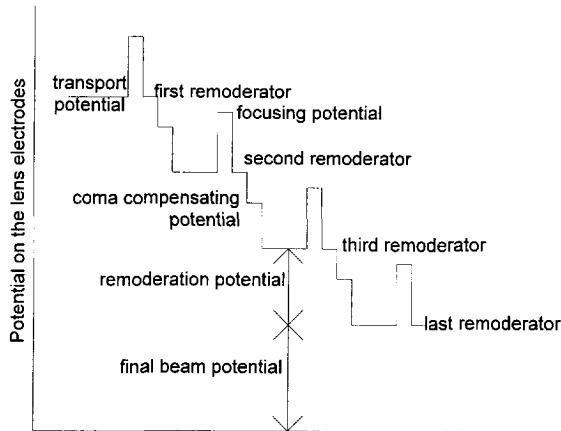
Figure 8.1   Potentials on the different electrodes in the positron beam. The differences
between the electrodes do not change, only the final beam potential changes.

system of resistors.

One aspect that is important for the remoderation section is the stability of
the power supplies. In the remoderation section three different types of
potentials can be distinguished, viz. the accelerating potential, the potential
on the coma compensating electrodes, and the potential on the focusing
electrodes. All these electrodes have their different demands.

In Chapter 5 it was shown that the potential on the coma compensating
electrodes does not have to be set accurately. The spot size as function of this
potential gives a minimum where the spot size hardly changes over a region
of several volts, and the potential on the focusing electrode does not change
with a change in this potential. A more strict demand is the potential
difference between the target foils and the focusing electrodes. A change of
about 10 V is necessary to get the optimum defocus of $C_s\alpha^2$, so a change in
potential of 10 V might give a $\sqrt{4.75}$ times larger spot.

8.3 Computer control of the post remoderation optics

8.3.1 Control of the transport optics and 90°-deflector

The transport optics consists of a coil, a stigmator set and an alignment unit. For all these parts only current sources are necessary. The maximum current through the lens coil is about 0.5 A. For changing energy the current through the coils changes with the square root of the energy (E) as in:

$$I = C\sqrt{E} \ , \tag{8.1}$$

with a constant C that is a function of the optical element. For the transport lens this constant is equal to 1.83×10^{-3} A/eV$^{1/2}$. The currents through the other coils are in the order of tens to hundreds of mA. The current through all these coils must be set only when the beam has been disassembled. To enable automatic changing of these currents, a circuit has been designed in which the reference voltage of the SEM gives the proportionality with this energy. This reference voltage will be discussed in section 8.4.2.

The only variable in the deflector is the current that goes through the coils. If the magnetic field does not saturate with higher currents, the needed current (I) can be found by using Eq.(8.1). For the deflector described in Chapter 7 it follows that the constant must be equal to 3.73×10^{-3} A/eV$^{1/2}$. Again use can be made of the reference voltage of the SEM.

The way the deflector is controlled is by having a stable and accurate power supply that can be computer controlled. The setting of the supply is calculated by a computer program. The other possibility to have the current set via a hardware connection between the power supply and the high voltage supply of the last remoderator is possible, but more complex.

Might the setting in practice be more difficult, e.g. due to saturation of the magnetic material, the settings for different energies can be stored in the pc. In that case the system becomes less variable, and it would be better to work with preselected energies. Calculations on the magnetic materials did not show any influence of saturation.

8.3.2 Demagnetization of magnetic optical elements

When the electron beam passes the deflector it should not experience a force due to the magnetic field. To demagnetize this deflector a simple combination of electronics and software has been designed. The best way to demagnetize is by applying a slowly decreasing AC-current through the coils of the deflector as already discussed in Chapter 7. The disadvantage in using an AC-source is that instead of one supply two supplies are necessary. To overcome this problem, there is chosen for a double switch that can be operated via the PC. With this switch it is possible to change the direction of the current. Within discrete steps the current is lowered according to:

$$I(n) = (-1)^n I_{max} \left(\frac{I_{min}}{I_{max}} \right)^{\frac{n-1}{k-1}} , \qquad (8.2)$$

in which I_{max} is the maximum used current, I_{min} is the minimum current low enough for having no disturbance of the remanence, and n is the step number that varies from 1 to k, the total number of steps. Figure 8.2 shows a possible demagnetization curve for the deflector with a maximum current of 1 A. The current drops logarithmically to $1 \mu A$.

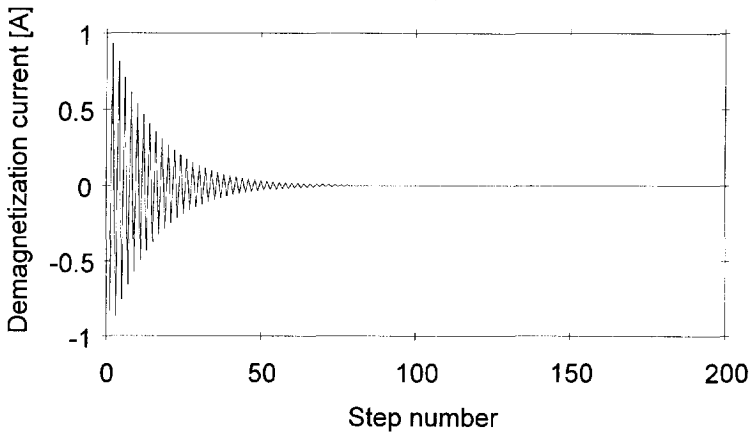Figure 8.2   Demagnetization current with $I_{max} = 1$ A, $I_{min} = 10^{-6}$ A, and $k = 200$ steps.

This solution can also be used for the problem of hysteresis in the magnetic lenses. Normally the lenses of the SEM show hysteresis, but the user sets the magnetic field of the lenses by looking at the image. In the automatic mode of the apparatus, the image can not be evaluated, and thus the only remaining way of setting the lenses is by setting the current in an accurate way. Hysteresis is both determined by the current through the lens and the history of the magnetic material. Measurements have shown that hysteresis can give a 'defocus' of 2 mA. By demagnetizing the lenses, the initial magnetization curve of the magnetic material is used and so the magnetic field is only determined by the current through the lens coil.

8.4 Computer control of the scanning electron microscope

8.4.1 Introduction to the scanning microscope

In this part the control of the SEM via a pc is described. A more detailed overview is given by Schroten[1]. The parts of the SEM that have to be controlled are the beam alignment module, the three lenses, the scan coils, and the stigmator unit. If the 90°-deflector has been positioned accurately enough in the emission chamber of the SEM and the deflection is exactly 90 degrees, the alignment coils do not have to be used. But for the electron beam it is known that these coils have to be used. So when switching from electrons to positrons the current through these coils has to be switched off. If the positioning of the deflector is not that accurate, the coils have to be used.

There are three lenses in the SEM, two condenser lenses and one objective lens. The two condenser lenses use the same coil so there are only two currents that have to be controlled. The accuracy with which these currents can be set is quite high. So chosen is to use the accurate and stable current sources of the SEM and not to choose for an external source that can be controlled by computer directly. To be able to control the objective lens, the electronics of the SEM has been adjusted. The setting of the condenser lens was already under computer control via the computer interface of the SEM. Via this interface the SEM can be connected to the RS 232 port of a simple

PC. In Chapter 7 it was shown that the change in objective lens setting is small. On the other hand the change in the condenser lenses is big.

In principle the scan coils do not have to be controlled by computer. It is already possible to set the magnification of the SEM. This magnification is nothing else than the field of view since the magnification is the size of the field of view divided by the size of the screen. The scan mode can be chosen via the computer interface. Possible choices are TV-mode, slow scan, line scan and point analysis. For this last option will be chosen in the case of positron analysis. The positron analysis will be done by changing the energy of the positrons in one position on the specimen that was preselected with the electron beam. A simple line scan may also be done for instance to get information on the used probe size.

Since the settings of the lenses all change with the energy of the positrons or electrons, it is easier to change the high tension than to change the current through that optical part. For this reason the knob on the desk of the SEM has been equipped with a step motor. Behind this knob there are two different potentiometers: one to set the high tension on the electron source, the other to set a reference voltage for lens control. This reference voltage is proportional to the square root of the high tension; it is used to change the current through the coils when the energy is changed without having to change all other settings. The step motor is controlled via a card in the PC.

8.4.2 Changes to the microscope electronics

In the previous section the different parts of the SEM have been discussed shortly. This section will discuss the hardware of the computer control more thoroughly. After a short discussion of the used communication ways the following will be discussed: high tension, condenser lens, objective lens, alignment coils, stigmators, and scan coils. In general first the old situation is discussed followed by the changes to that part. Figure 8.3 shows the changes in the setup of the control; the "old" communication ways are not shown.
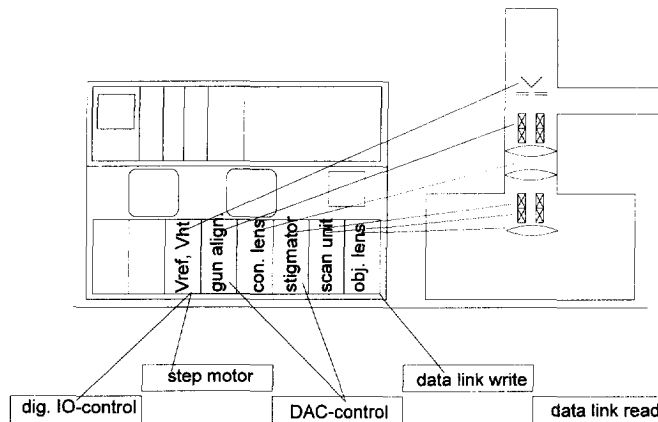
Figure 8.3   Overview of the new communication channels. New are the writing via the
              data link to the objective lens, the DAC-communication with gun alignment
              and stigmator, and the step motor.

ways of communication

All different parts of the SEM are connected with each other via the data
link. Many of the settings of the SEM are stored in one or more addresses on
this data link. To communicate with the outside world the SEM has been
equipped with a computer interface. Via the RS 232 port of a PC it is
possible to change data on the data link of the SEM. The control of the SEM
would be easy if all the parameters were on this data link and could be
changed. Unfortunately the high tension setting is not available on the data
link. The value of the read out on the display is available, but this is by far
not accurate enough. Another example is the setting of the objective lens.
The setting can be read in 16 bit accuracy, but it is not possible to change
these values. Parts that can be read and written are e.g. the scan mode, the
magnification and the current through the condenser lens.

To overcome the problems of not being able to write on the data link,
changes to the electronics have been made. To be able to control the high
tension and reference voltage, the high tension knob has been equipped with
a step motor, connected with a special card in the PC. By changing the
electronics of the objective lens, and adding a new address on the data link, it
is possible to control the objective lens with the highest accuracy. By
installing a multi IO-card in the PC, many parts can be controlled.

The communication with the data link of the microscope via the RS 232 port of the PC is the most difficult part of the complete computer control. On the data link the data is sent continuously. Both the address and the data meant for that address is on the same time on the data link. A unit that needs that data waits until its address is passed on the data link. Set with a clock pulse, it reads its data when it passes. The time one address is active lasts for 32 μs. Since there are 128 different addresses on the data link, the addresses can be read or written every 4.1 ms. The problem with the program that must be written to exchange data with the data link is the timing.

The step motor is a bipolar motor. The advantage of this type of motor is that its momentum is quite high and that it has a high efficiency. The control of this step motor is done via a single PC-bus add-on card, designed by ELV GmbH[2]. Since the used step motor needs higher currents than the card can provide, small changes to the electronics have been made. These changes are the use of high power transistors and high power diodes.

The multi IO-board consists of six 12-bit DA-converters that can be set individually to any of the following ranges: 0 to 5V, 0 to 10V, -5 to 5V, -10 to 10V, or 4 to 20mA. In addition to the analog output the card provides 16 channels of digital output and 16 channels of input. The six 12-bit DA-converters are used to set the current through the alignment coils and the stigmator. The digital output of this card is used for the HT-range selector and can be used for current direction switching of the magnetic lenses and deflector as described in section 8.3.2. The digital input channels are only used for checking whether the microscope has been set to computer control, since this has to be done manually.

Furthermore, it must be noticed that some functions on the desk of the SEM will loose their function if the SEM has been set to computer operation. Only the high tension and the objective lens can be changed by hand in automatic mode. As a consequence of this, the electron beam must be used in automatic mode when preselecting areas before the positron analysis, since it is not possible to read all the data accurate enough from the data link or the data can be disturbed when switching on the computer control.

high tension

The high tension can be set by a ten-turn potentiometer in combination with a range selector. The knob on the desk of the SEM serves two potentiometers. One for the real high tension and one for the reference voltage. This reference voltage is in this case more important since this voltage is used to set the currents through the optical elements. With this reference the settings of the lenses are not changed when the energy of the particles is changed.
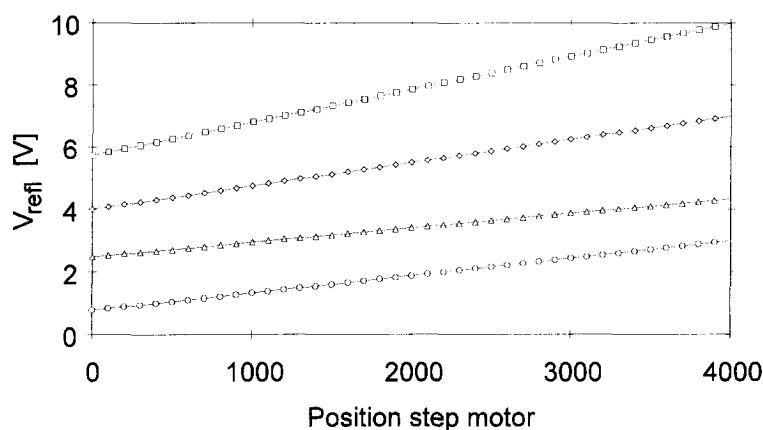

Figure 8.4   Reference voltage as function of the position of the step motor for four voltage ranges (□:10-30 kV, ◇:5-15 kV, ▵:2-6 kV, ○:0.2-3 kV).

The step motor used to set the reference voltage needs 4002 steps to turn the potentiometers from their minimum value to their maximum. Figure 8.4 shows the measured reference voltage as function of the position of the step motor for the four energy ranges. These ranges go from 0.2 to 3 keV, from 2 to 6 keV, from 5 to 15 keV, and from 10 to 30 keV. These ranges can be selected via a digital output on a multi IO-card installed in the PC, and a decoder installed in the high tension module.

condenser lens

The condenser lens is used in electron mode to select the spot size. In general only the spot size selector is used, the potentiometer, to change the current through this lens semi-continuously, is not used. Behind this potentiometer there is an AD-convertor, so only discrete steps in condenser current can be made.

The condenser lens can be set via the computer interface. The current through this lens can be parameterized with three independent parameters: the high voltage, or the reference voltage or the position of the step motor in combination with the range switch, the stepped spot size selector, and the quasi-continuous spot selector. The function that describes the current through the condenser lens is given by:

$$I_{cond} = (V_{refL}A + C)d_{qc} + V_{refL}B + D \ , \tag{8.3}$$

in which d_{qc} is the setting of the quasi continuous spot selector, and A, B, C, and D are fitted constants that are a function of the stepped spot size selector and of the selected energy range, i.e. only for the lowest energy range the constants are slightly different. Note further that the stepped spot size selector only has the possible values 2,3..7, and so there are $4 \times 6 \times 2 = 48$ constants that describe the condenser lens current.

objective lens
The objective lens is used to focus the electron beam on the specimen. In Chapter 7 it was shown that the setting of this lens for positrons could be calculated given the focusing of the electron beam. The objective lens is controlled by a pulse generating knob, together with a counter. The pulses or steps in current are weighted by the step size switch with seven positions. These factors are 1024, 256, 64, 16, 8, 4, and 2.

Since it is not possible to write on the addresses on the data link used by the objective lens, two new addresses have been created on the data link. Now the pulses, normally coming from the pulse knob, can be generated by the PC and be put on one of the addresses. The other address is used to give the weight factor of the steps.

The function that describes the current through the objective lens is given by:

$$I_{obj} = (V_{refL}A + C)d_{obj} + V_{refL}B + D \ , \tag{8.4}$$

in which A, B, C, and D are again the fitted constants that are only a function of the selected energy range.

When setting the current through the condenser lens, the setting of the objective lens changes automatically. So it must be remembered that the order in which the different parts are set is first the condenser lens and then the objective lens. It must also be remembered that it is easier to do positron analysis with increasing energy. This will overcome the problem of hysteresis; the lower energy positrons need lower magnetic fields, and this field will follow in that case the initial magnetization curve.

alignment coils

In electron mode the alignment coils are used to position the electron beam exactly on the optical axis of the SEM. By a right choice of the relative excitation of the different coils, the potentiometers on the front of the SEM give an absolute gun tilt or shift in one of the two opposite directions.

When the switch on the front of the SEM is set to computer control, the gun tilt and shift knobs do not work anymore. The current through the alignment coils now can only be operated by computer control. The four independent coils can be set by four of the six analogue outputs of the multi IO-board.

The software to set the alignment coils now sets the pivot point for the positron beam. The positron beam has the first intermediate image at a distance at 16 mm below the deflector, while the electron beam has its first intermediate image in the anode. So for the two different beams it is not easy to make an electronic circuit that changes from one pivot point to the other. So chosen is to make the software in a way that by applying the right voltages to the different parts of the alignment circuit one gets automatically a change in pivot point.

stigmators

Two potentiometers are used to set the current through the stigmator coils, together with the automatic stigmator push button. Astigmatism is found when the magnetic field is not axially symmetric. Stigmators compensate for this not being round in first order. Since the positron beam will not follow the same path as the electron beam, the effect of astigmatism for positrons will be different from the effect for the electrons. But since the positron beam will be 20 times larger the relative influence of the astigmatism to positron spot will be much smaller. The automatic stigmator with which the

SEM has been equipped must not be used in the computer control mode, since it changes the current through the stigmator coils in a non-controllable way.

To control the stigmator current, the other two analogue output channels of the IO-board are used. The stigmator current is not expected to change when switching from electrons to positrons, but it must be set when preselecting the position on which the analysis will be performed. The electronics of the stigmator coils are comparable to the electronics of the alignment coils, and so is the change in electronics. If it might be necessary to alter the stigmator setting, it can be done by storing the settings in the pc after calibration measurements.

scan unit
The only optical element of the SEM that did not have to be automated is the scan unit. The scan unit is used to select the scan mode, and the magnification. The settings of this unit can all be changed via the computer interface. For positron analysis only the point or line analysis will be selected.

If the positron current is large enough, and the computer control of the total beam will work properly it might be possible to do line scans or even make full positron images. In that case it must be noticed that the positrons will scan the specimen from the lower right to the upper left corner. This problem can be solved by reversing the current through the scan coils.

8.4.3 Software for microscope control

The software to operate the SEM has been written in Turbo Pascal Version 7.0 of Borland International, Inc. The program has been set up in different units, with each unit used for a different optical function. A special unit contains procedures that read the settings from a file that consists of the data acquired with the electron beam, like the stigmator settings and the free working distance. At this moment an interface to the microscope user has not been written, but possible users can make their own programs by simply using the procedures for the different optical elements.

A unit not to be used by the microscope user is the communication unit. Each optical element unit uses this unit to enable communication via all possible ways, like the RS232-port and the data link with the microscope. Communication via the RS 232 port is the most complex one. A special unit has been written to enable communication via this port[3] with the data link.
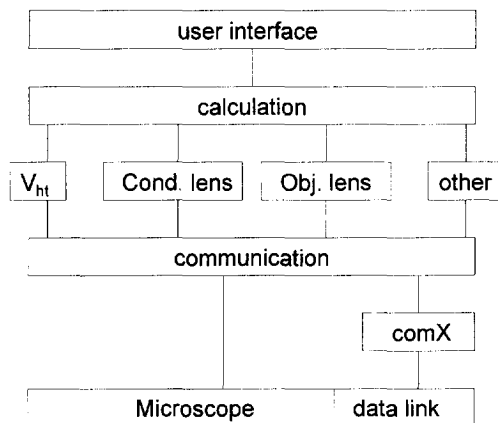

Figure 8.5   Computer control scheme in which all communication channels are shown. A special comX unit is used for communication via the data link.

Figure 8.5 shows the setup of the computer control. The user communicates with the SEM via a user interface that controls the optical elements of the microscope. The settings of these elements are put in the SEM via a special communication unit that for the data link uses a special unit comX.

8.5 Discussion and conclusions

In this chapter it was discussed that the computer control of the first part of the positron beam is not too complex. This is in contrast to the post remoderation part. The settings of this part of the positron beam do change for different positron energies, and for different working distances. The focusing must be done by computer, since the positron current is too low to be able to see whether the positron beam had been focused. Several possibilities for the computer control can be chosen. The solution for each different element is optimized. Considerations in the design were the

minimization of the number of parameters to be set, minimization of changes in the hardware of the microscope. Where the number of parameters can not be minimized, it is possible to store settings in the pc.

The changes to the SEM were also for the electronics kept small. Although it might be easier to install computer controlled power supplies, the solution chosen for is to use the stable and precise power supplies that are present in the SEM The most important change is the change in the control of the objective lens. A small electronic circuit has been added, to be able to set the current of the objective lens via the data link. Other changes are the addition of a switch in the stigmator and alignment circuits to enable control over these coils via an analogue output of a multi IO-card in the PC. The third change is the addition of a step motor on the high tension knob. Although it is possible by changing the electronics as it was done to the objective lens, it is easier to control it via the installed step motor. The step motor reproduces better than 10 ppm. The high tension and the reference voltages to the lenses now can be controlled. The position of the step motor gives the computer the reference voltages with high accuracies.

At this stage the different units have been tested. The most important part of the program is the communication between the SEM and the computer. At this moment the communication works well, but for a different PC it might be necessary to change the delay time between writing to different addresses. The settings of the lenses can be found by using the computer. How the computer control will work for the positron beam must be subject of later testing.

References
1.   E. Schroten, masters thesis Delft University of Technology, (1992), unpublished

2.   Elektuur **6-92**, 80, (1992)

3.   C.F. de Pierre, ComX, routines to enable communications via a serial interface, (1990), unpublished

An Instrument for Positron Micro-analysis: Summary

Positron beams can be used for defect analysis in different materials. With its positive charge the positron is very sensitive for small changes in the electron density. By energy variation, depth information can be obtained. The problem in using most positron beams is that it can not give information on 3-dimensional material structures. Only by means of a small probe it is possible to obtain information in the lateral direction. This thesis describes the design of an intense positron microbeam ($\sim 10^6 e^+$/s) with a probe size of 100 nm.

The positron microbeam will be one of the facilities of the intense positron beam being built at the Interfaculty Reactor Institute of the Delft University of Technology. In Chapter 2 an overview of this beam is given. Via the neutron capture reaction: $^{63}Cu + n \rightarrow ^{64}Cu$ and the decay reaction $^{64}Cu \rightarrow ^{64}Ni + e^+$ it is possible to generate positrons. Through a hybrid system of electrostatic lenses and magnetic coils the positrons are guided out of the nuclear reactor. The expected current at the end of the coils is of the order of 10^9 positrons per second, the brightness is at that position smaller than $10^{-7}A\ sr^{-1}m^{-2}eV^{-1}$. After brightness enhancement the beam is deflected onto the optical axis of a scanning electron microscope.

The brightness of positron beams can be enhanced by repeated remoderation as proposed by Mills (Appl. Phys. **23**, 189, 1980). A positron beam is focused on a crystal. If the crystal has a negative work function for positrons part of the implanted positrons can be re-emitted from the surface. The energy of the emitted positron is then equal to the absolute value of the work function. If a thin foil is used as the remoderation crystal, it is possible to use positrons that are re-emitted in the forward direction.

One of the most important parameters for remoderation is the re-emission yield. In Chapter 3 a setup to measure the forward re-emission yield is described. Preliminary measurements show that 6% of the implanted positrons are re-emitted. This low number is due to the fact that the measurements were performed in a poor vacuum of 10^{-7} mbar. Cleaning of the foils in a UHV-system must give an enhancement of the re-emission yield.

Since there are two possible options for remoderation, a choice between these options must be made. In Chapter 4 it is argued that the best way to perform brightness enhancement is forward remoderation. By means of a simple but novel model in which the limitations of the focusing lenses must be estimated it was found that three remoderation steps are necessary to reduce the beam from the reactor to the optimized brightness-current combination.

In Chapter 5 the optics needed for the remoderation section are treated. In each remoderation step two lenses are needed. One strong lens to demagnify the beam as far as possible, and one lens with its focal plane inside the demagnifying lens. This last lens is needed to reduce the off-axial geometric aberrations. Starting with a spot of 10 mm, the spot will be demagnified to a spot smaller than 1 μm in the last remoderation section.

The system of electrodes is put together by welding glass bars to all the electrodes giving good insulation between the different electrodes. To reduce the mechanical aberrations as astigmatism, strict tolerances are needed. By estimating the consequences of inaccurate fabrication of the electrodes, the tolerances could be calculated and are of the order of 5 μm for the roundness of the smallest holes and 0.01 mm for the misalignment. By using a needle fitted through the holes of all electrodes, a well-aligned system could be obtained. The design is described in Chapter 6.

In Chapter 7 all optics to get the bright positron beam on the specimen is discussed. To get the positron beam on the optical axis of the electron microscope, an intermediate lens and 90°-deflector have been constructed. No mechanical changes to the lenses of the microscope were necessary. However, to get the positron beam focused on the specimen, the settings of the lenses must be changed, since they differ from the settings needed to focus the electron beam. Since it is not possible to focus the positron beam manually, the microscope must operate under computer control. A description of the control is given in Chapter 8.

With the instrument described in this thesis it should be possible to obtain a positron micro-beam of 0.1 μm diameter with a current of over 10^6 e$^+$/s at a variable energy between 0.5 and 25 keV. This beam is suited to detect defects by positron micro-analysis.

Een Instrument voor Positronen Micro-analyse: Samenvatting

Positronenbundels kunnen worden gebruikt voor onderzoek naar defecten in verschillende materialen. Door de positieve lading is het positron zeer gevoelig voor kleine veranderingen in de elektronendichtheid. Het manco bij de huidige techniek is dat het niet mogelijk is om de defecten in 3-dimensionale structuren te observeren. Door middel van variatie van de energie van de geïmplanteerde positronen is het slechts mogelijk om informatie te verkrijgen over de diepte waarop de defecten voorkomen. Laterale informatie kan slechts dan verkregen worden wanneer de positronen gefocusseerd worden in een smalle bundel. Dit proefschrift beschrijft het onderzoek dat leidde naar de constructie van een intense positronen-microbundel ($10^6 e^+$/s) met een bundeldiameter van 100 nm.

De positronen-microbundel is één van de faciliteiten die gekoppeld worden aan de intense positronenbundel die gebouwd wordt bij het Interfacultair Reactor Instituut. Een beschrijving van deze bundel wordt gegeven in hoofdstuk 2. Via de neutron vangst reactie $^{63}Cu + n \rightarrow ^{64}Cu$ en de vervalreactie $^{64}Cu \rightarrow ^{64}Ni + e^+$ kunnen positronen worden gegenereerd. Door een stelsel van elektrostatische lenzen en magnetische spoelen wordt de gegenereerde positronenbundel uit de reactor geleid. De bundel heeft na het verlaten van de reactor een intensiteit van 10^9 positronen per seconde, waarbij de helderheid van de bundel kleiner is dan $10^{-7} A \, sr^{-1} m^{-2} eV^{-1}$. De positronenbundel wordt vervolgens in helderheid verhoogd, waarna het door een 90°-afbuiger op de optische as van een raster elektronenmicroscoop wordt gebracht.

De helderheid van positronenbundels kan worden verhoogd door middel van het door Mills (Appl. Phys. **23**, 189, 1980) bedachte scenario van herhaalde remoderatie. Het principe hiervan is dat de bundel wordt gefocusseerd op een éénkristal. Bij kristallen met een negatieve werkfunctie voor positronen kan een deel van de positronen worden gereëmitteerd met een kinetische energie gelijk aan de absolute waarde van de werkfunctie. Het emitterend oppervlak kan zowel de voorzijde zijn waaraan de positronen werden geïmplanteerd alsook in het geval van dunne folies de achterzijde.

In hoofdstuk 3 wordt een methode beschreven om reëmissie van dunne folies te meten. Eerste metingen tonen aan dat 6% van de positronen worden

gereëmitteerd. De oorzaak van dit lage aantal is het slechte vacuüm van 10^{-7} mbar waarin de folies te vuil zijn om een groot deel van de naar het oppervlak gediffundeerde positronen te emitteren. Verbeteringen van het vacuüm en aan het schoonmaken van folies moet een verhoging geven van de reëmissie.

In hoofdstuk 4 wordt met behulp van een eenvoudig doch origineel model beargumenteerd dat de eenvoudigste methode voor helderheidsverhoging remoderatie in voorwaartse richting door dunne folies is. Schattingen van de beperkende factoren van de lens geven aan dat drie remoderatiestappen nodig zijn om te komen tot een optimale helderheid stroom combinatie.

De optiek voor deze drie stappen wordt beschreven in hoofdstuk 5. Door middel van sterke elektrostatische lenzen is het mogelijk een bundel met een begindiameter van 10 mm terug te brengen tot een diameter kleiner dan 1 μm. Naast een verkleinende lens wordt er in iedere remoderatiestap een extra lens geïntroduceerd. Doordat deze extra lens zijn brandvlak heeft binnen de verkleinende lens, worden de geometrische aberraties die het gevolg zijn van de uitgebreidheid van het af te beelden voorwerp geminimaliseerd.

Het totaal van elektrodes is verbonden met elkaar door het aansmelten van glazen staafjes. Daar mechanische afwijkingen kunnen zorgen voor extra aberraties dienen de toleranties streng te zijn. Door te schatten wat de gevolgen van onrondheid van elektrodes en het niet goed gealigneerd zijn van de elektrodes zijn kon de onrondheid van de gaten bepaald worden op maximaal 5 μm, en de verschuiving bepaald worden op maximaal 0.01 mm. Een beschrijving van het ontwerp wordt gegeven in hoofdstuk 6.

In hoofdstuk 7 wordt de optiek beschreven die nodig is om de heldere positronenbundel te focusseren op een preparaat in de elektronenmicroscoop. Voor dit doel zijn een magnetische lens en een 90°-afbuiger vervaardigd. Aan de lenzen van de microscoop zijn geen veranderingen toegebracht. Echter de instellingen van deze lenzen zijn niet gelijk aan de instelling voor elektronen. Omdat het met behulp van positronen niet mogelijk is om met behulp van het oog te controleren of de microscoop gefocusseerd staat, is

geautomatiseerde besturing noodzakelijk. De beschrijving van deze besturing staat in hoofdstuk 8.

Met behulp van de onderdelen beschreven in dit proefschrift is het mogelijk een positronen-microbundel te construeren met een bundeldiameter van 100 nm en een intensiteit van meer dan 10^6 positronen per seconde. Deze bundel zal geschikt zijn voor defectonderzoek door middel van positronen micro-analyse.

Tot slot

Op deze plaats wil ik allen die mij behulpzaam waren bij het realiseren van dit proefschrift bedanken. Natuurlijk zijn dat alle leden van de vakgroep deeltjesoptica en de afdeling reactorfysica die het werken een stuk plezieriger maakten. In het bijzonder wil ik Pieter en Tom bedanken. Zij waren het die het project begonnen, waardoor ik mee kon doen aan één van de betere positronenprojecten. Jim wil ik bedanken voor het mij onderwijzen van de deeltjesoptiek, ook zijn interesse in mijn optische problemen waardeer ik zeer. De studenten Egbert en Roeland zijn verantwoordelijk voor een deel van het onderzoek zoals beschreven in de respectievelijke hoofdstukken 8 en 7. Hun bijdrage is duidelijk te vinden in het eindprodukt. Zonder ondersteuning is het werk van een promovendus onmogelijk. Hoewel het werk dat Astrid voor mij gedaan heeft niet zichtbaar is in dit proefschrift, dient de ondersteuning die ik van haar gekregen heb zeker niet onderschat te worden. Erik, Peter, Jan, Jacques, Karl en Bob waren als technici ieder op hun terrein mij altijd behulpzaam. Daarnaast was het onontbeerlijk de medewerking te hebben van de ondersteunende diensten. Medewerkers van de instrumentmakerijen van TN en IRI bedank ik dan ook hartelijk. In het bijzonder wil ik Bram Huis voor de snelle klussen, Aad Dijkshoorn voor het glaswerk en Otto Wolfs voor de tekeningen bedanken. Tot slot wil ik natuurlijk Lia bedanken, haar steun was gedurende de afgelopen periode onvervangbaar.

Curriculum Vitae

Léon Seijbel is geboren op 9 juni 1966 te Middelburg. Na het behalen van het Atheneum B diploma in juni 1984 ging hij materiaalkunde studeren aan de Technische Hogeschool Delft, later TU Delft. In 1990 studeerde hij af in de fundamentele materiaalkunde in de sectie materiaalfysica op het gebied van thermische desorptie spectrometrie. Op 1 september van dat jaar begon hij zijn promotieonderzoek als onderzoeker in opleiding bij de vakgroep Deeltjesoptica van de faculteit der Technische Natuurkunde en de afdeling Reactorfysica van het Interfacultair Reactor Instituut, beide aan de TU Delft. Dat onderzoek resulteerde in het voor u liggende proefschrift.